63-3-3

DASA 1357 (II)

403 054

403054

CATALOGED BY ASTIA
AS AD No.

UNDERGROUND EFFECTS OF NUCLEAR WEAPONS IN THE CLOSE-IN REGION

G. F. McDonough, Jr.

FINAL REPORT

Contract No. DA-49-146-XZ-073

15 March 1963

Volume II of IV Volumes

Engineering Division
E. H. PLESSET ASSOCIATES, INC.
Santa Monica, California

Prepared for

Headquarters
Defense Atomic Support Agency
Washington 25, D. C.
Task No. 13.092

ASTIA
RECEIVED
MAY 8 1963
TISIA

Best
Available
Copy

DASA 1357 (II)

UNDERGROUND EFFECTS OF NUCLEAR WEAPONS IN THE CLOSE-IN REGION

G. F. McDonough, Jr.

FINAL REPORT

Contract No. DA-49-146-XZ-073

15 March 1963

Volume II of IV Volumes

Engineering Division
E. H. PLESSET ASSOCIATES, INC.
Santa Monica, California

Prepared for

Headquarters
Defense Atomic Support Agency
Washington 25, D. C.
Task No. 13.092

TABLE OF CONTENTS

	Page
CHAPTER IV - Directly-Transmitted Ground Phenomena, Elastic Analysis	1
A. Introduction	1
1. Statement of Problem and Objectives	1
2. Methods of Analysis and Results	3
3. Starting Conditions	4
B. Effects of the Equation of State	5
C. Theoretical Solution for Infinite Space	12
D. Solutions by Digital Simulation	26
E. Significance of Results and Conclusions	30
1. Discussion of Results	30
2. Decay of Peak Radial Pressures, Velocities, and Accelerations	32
3. Specific Conclusions	33
F. Special Cases	34
1. Non-Homogeneity and Stratifications	34
2. Spherical Problems in Bilinear Solids	35
G. Recommendations for Further Studies	41
CHAPTER V - Directly-Transmitted Ground Phenomena, Elasto-Plastic Analysis	103
A. Introduction	103
B. Statement of Problem	105
C. Formulation	107
D. Pilot Problem	118
E. Conclusions and Recommendations	122

TABLE OF CONTENTS (Continued)

	Page
CHAPTER VI - Combined Effects	133
A. State of the Art, Directly-Transmitted Effects	
1. Hydrodynamic Analysis	133
2. Elastic Analysis (Newmark)	134
3. Elasto-Plastic Analysis (Brooks)	136
B. Proposed Methods for Combining Effects	137

CHAPTER IV

DIRECTLY-TRANSMITTED GROUND PHENOMENA

ELASTIC ANALYSIS

A. INTRODUCTION

This chapter consists of the report by N. M. Newmark and Associates of the results of a subcontract study under Contract DA-49-146-XZ-073. Only minor editorial changes have been made to fit this study into the format of the overall final report under this contract. The report was prepared by N. M. Newmark and A. Ang with the assistance of J. P. Murtha (who contributed the section on the equation-of-state effects), A. R. Robinson (who contributed the analytical solution of the spherical problem), and S. Sutcliffe (who contributed the section on the spherical solid with bilinear behavior). Computer programming for these studies was done by J. W. Melin, G. N. Harper, and J. Rainer.

1. Statement of Problem and Objectives

The prediction of close range ground motions and pressures resulting from nuclear explosions involves a wide range of material properties, ranging from that of a purely liquid state to that which is essentially of the original solid state. The transition between these two states of the material is gradual and probably no definable interface exists between any two intermediate states.

For purposes of studying the effects of ground shocks, the total earth motions generated by a nuclear blast are usually divided into those that are caused by stress waves which are directly transmitted through the earth material from the

energy released directly into the earth by a blast, and those that are induced by stress waves which are initiated from the earth surface by the expanding air shocks.

Based on a hydrodynamic model, Brode and Bjork* have successfully performed numerical calculations for a simulated two megaton burst in tuff, a soft rock material. Brode and Bjork pointed out that their calculations for the low pressure ranges, less than 8 kilobars, are not strictly valid since in these pressure ranges, the effects of the plastic and elastic properties of the solid material become significant.

Using the results of Brode and Bjork in the transition pressure range, (assumed to be at a radial distance of 660 feet from the center of a 2 megaton burst), as a starting condition, directly induced ground motions for a half-space solid were determined numerically on the assumption that the material beyond the region of the crater is homogeneous, isotropic and linearly elastic. Such an assumption, of course, is not realistic since a plastic region would precede the elastic region; however, the use of this assumption was dictated by available means for obtaining approximate answers. Results of an approximate study of the effect of the equation of state indicated that no significant error in the applied pressures is involved by neglecting a plastic region between the liquid and the elastic regions. Aside from the half-space solid, the simpler problem of an infinite space subjected to an explosive pressure applied in a spherical cavity was solved.

In this study, no consideration of the effects of the expanding air blast pressures on the surface was included although this can be considered without much

*Brode, H. L. and Bjork, R. L., "Cratering From A Megaton Surface Explosion", RM-2600, The RAND Corp., June 30, 1960

difficulty. The solution of one of the half-space problems involves a situation which is essentially similar to that of the actual air blast.

The specific problems of which solutions are presented here are outlined below:

Problem 1—A full-space with a spherical hole subjected to a uniformly distributed pressure (see Figure 98a).

Problem 2—A half-space with a stress-free semi-spherical cavity; loads are applied on the horizontal surface which are exactly equal to the negative of the tangential stresses from Problem 1, referred to as "correction" loading (as shown in Figure 98b). Results from this problem are referred to in this report as "correction" stresses, velocities, or accelerations.

Problem 3—A half-space with a semi-spherical cavity subjected to a uniformly distributed blast pressure applied directly on the boundary of the cavity (see Figure 98c).

Problem 4—The same as Problem 3, except that the applied pressure is uniformly distributed only over the lower half of the semi-spherical surface of the cavity; the pressures on the upper half of the cavity are distributed as $p_o \sin 2\phi$ (as shown in Figure 98d).

2. Methods of Analysis and Results

Problem 1 was formulated analytically and calculations for the radial and tangential stresses were performed. Additional results were also obtained by an alternate analytical procedure for the infinite space subjected to an exponentially decaying pressure-time curve (see Appendix I). Solutions for stresses in Problem 1 obtained with

the use of a spherically symmetric discrete model were in very good agreement with the corresponding analytical solutions.

Results for the half-space solids, Problems 2, 3 and 4, were obtained exclusively by the technique of digital simulation. Although no analytical solutions are available for direct verification of these results, there are a number of limiting conditions which all the solutions satisfied, thus indicating the correctness of the solutions. Furthermore, the mathematical consistencies of the models provide a basis for ascertaining the correctness of the solutions if the numerical results are reasonable from an intuitive standpoint.

All calculations were performed on large high-speed digital computers. In addition, whenever the discrete models are involved, the problems were simulated directly on the computers.

All results are presented graphically. For the full-space solid, time functions of the radial and tangential stresses, and of the particle displacements, velocities, and accelerations at points of varying radial distances from the burst are given. Analytically determined solutions are given only for the radial and tangential stresses. For the half-space solids, the radial and tangential stresses, and the radial particle motions are plotted against time. These were presented for points along lines with different angular positions from the horizontal. The solutions for the half-spaces include other stresses (shear and circumferential) and the tangential accelerations, velocities, and displacements; however, these are not presented here.

3. Starting Conditions

The original data from the calculations of Brode and Bjork, previously mentioned, were presented in the form of contours connecting points of equal pressure,

velocity or density at specified times. From these contours, pressure-time relationships were reproduced and presented in a form that is more meaningful for further study and analysis. These pressure-time relationships at radial distances of 330, 495, and 660 feet from the point of burst, are presented in Figures 99 through 101. Corresponding relationships for the particle velocities were also reproduced but are not presented here.

The problem considered in this study involve a full space with a spherical hole, or a half-space with a semi-spherical cavity on the surface. The radius of the cavity in all cases is 660 feet from the center of a two-megaton burst.

The pressure-time relationship of the applied pressure is shown in Figure 102, which represent the pressure-time curve from the calculations of Brode and Bjork at 660 feet directly below the burst. The decay portion of this curve is extrapolated by inference from available measured data. In the solutions by digital simulation, this pressure is actually applied at a radial distance of 645 feet from the point of burst, and not at 660 feet, for convenience in treatment of the lumped-mass model. There is therefore a slight discrepancy between the analytical and the lumped-mass solutions; this is not of significance in the results.

The velocities at the surface of the cavity, which were also calculated by Brode and Bjork, were not considered in this study,

B. EFFECTS OF THE EQUATION OF STATE

In the present study of the stress field outside the crater region, the pressure-time relations at some radius as obtained from the hydrodynamic model of Brode and Bjork are used as the boundary stresses applied to an elastic solid. Theoretically, the pressures derived from the hydrodynamic model results should be adjusted in order to provide a consistent boundary condition. The need for this

adjustment results from two factors: namely, (1) the wave propagation velocity in the elastic solid will be less than that in the fluid model, and (2) the particle velocity at the boundary between the fluid and solid regions should be the same in both media. That these two conditions are not automatically satisfied is the result of omitting the plastic or transition region which in the real situation, separates the hydrodynamic and elastic regions. It is apparent that any procedure adopted to adjust these pressures can only be an approximation. In the subsequent discussion it is shown that the necessary adjustment appears to be small and may be neglected without serious error.

If the mathematical model is assumed to consist of compressible fluid and elastic solid regions, a wave propagating through the fluid could be partially reflected at the boundary separating the two regions. The relations which must be satisfied by the incident fluid pressure and particle velocity, p and $\dot{u}_f$, and the transmitted stress and particle velocity, σ and $\dot{u}$, are as follows:

$$p + \Delta p = \sigma \tag{1a}$$

$$\dot{u}_f - \Delta\dot{u}_f = \dot{u} \tag{1b}$$

where Δp and $\Delta\dot{u}_f$ are changes in the fluid quantities resulting from the reflection. The relationships between stress and particle velocity in both the incident fluid and solid waves are time dependent; however, at the front of an ideal wave the following relations* exist

$$\dot{u} = \frac{\sigma}{\rho_s c_s} \tag{2a}$$

$$\dot{u}_f = \frac{p}{\rho_f c_f} \tag{2b}$$

* Force equal change in momentum per unit time.

where ρ and c are density and wave velocity, respectively, and the subscripts refer to the solid, s, and fluid, f. Although the fluid pressure pulse shapes calculated by Brode and Bjork are not truly ideal, Equation (2b) is approximately correct for the initial part of the pulse. The application of Equation (2b) implies a value of the parameter $p/\dot{u}_f$ which is not time dependent for a given radius. The following table summarizes the values of this parameter for the pressure-time and velocity-time pulses in the fluid at a range of 200 meters:

Time m sec	p kilobars	$\frac{p}{\dot{u}_f}$ (kilobar-sec)/kilometer
58	3.4	45.4
65	5.0	48.6
74	4.5	45.0
82	3.0	32.0
85	2.4	31.5

These data indicate that the assumption of a constant value for $p/\dot{u}_f$ is reasonable, at least for the principal part of the pressure pulse.

If it is assumed that a relation similar to Equation (2b) is valid for the reflected pressure and velocity, i.e.,

$$\dot{u}_{fr} = \frac{p_r}{\rho_f c_f} \tag{3}$$

the relation between the incident and transmitted stresses is as follows:

$$\sigma = \frac{2p}{1 + \psi} \tag{4}$$

where $\psi = \frac{\rho_f c_f}{\rho_s c_s}$

In Equation (4) σ represents the transmitted stress that is developed when a plane wave impinges on the boundary between two different media. As such, it would be correct at least at the shock front.

Since Equation (4) represents an acoustic reflection, it is desirable to calculate the reflection factor for plane, finite amplitude waves in the fluid reflecting from a rigid wall. The equation of state used by Brode and Bjork for tuff is

$$p = (0.425E + 0.113n^{3/2}E) + 5.30n \left(\frac{E}{10^{10}}\right)^{1/2} 10^{10} + \frac{0.707n \left(\frac{E}{10^{10}}\right)^2 10^{10}}{10^5 + (E/10^{10})} \tag{5}$$

where p = pressure in dynes/cm^2

E = specific internal energy in ergs/gm

$n = \frac{\rho}{\rho_o}$: ρ_o = initial density = 1.7 gm/cc

For pressures less than 10 kilobars and n less than about 1.5, Equation (5) may be approximated as

$$p = \sim 5.3 \times 10^{10} n \left(\frac{E}{10^{10}}\right)^{1/2} \tag{6}$$

Combining Equation (6) with the Hugoniot energy equation,

$$\Delta E = \frac{1}{2} (p - p_o) \left(\frac{1}{\rho_o} - \frac{1}{\rho}\right) \quad , \tag{7}$$

results in the following pressure-density relation:

$$p = 8.25 \times 10^{10} \left[\left(\frac{\rho}{\rho_o}\right)^2 - \left(\frac{\rho}{\rho_o}\right)\right] \frac{\text{dynes}}{\text{cm}^2} \tag{8}$$

for the ambient pressure, p_o, equal to zero. As a check on Equation (8), we may calculate the wave velocity, c_o, for waves of small amplitude;

$$c_o = \sqrt{\frac{d_p}{d\rho}} = \sim 7.200 \text{ ft/sec}$$

for very small values of $\frac{\rho}{\rho_o}$. The value of c_o usually quoted for tuff ranges from about 6,000 - 8,000 ft/sec.

When a finite amplitude wave undergoes normal reflection from a rigid boundary, the ratio of the excess pressures behind the reflected and incident waves is given by Cole* as follows

$$\frac{p_r - p_o}{p - p_o} = 1 + \left(\frac{\rho'}{\rho_o}\right) \left\{ \frac{\frac{\rho}{\rho_o} - 1}{\frac{\rho'}{\rho_o} - \frac{\rho}{\rho_o}} \right\} \qquad (9)$$

where ρ' is the density behind the reflected shock front.

The ratio of reflected to incident pressures, p_r/p may be calculated using Equations (8) and (9). For an incident pressure, $p = 9$ kilobars, $p_r/p = 2.2$. For the same incident pressure in water, $p_r/p = 2.9$. Thus the reflection factors for finite amplitude waves in the range of interest do not appear to greatly exceed the acoustic reflection factor, which is 2.0.

Approximate values for the wave velocity in the fluid can be derived in several ways, each of which yields about the same result. Using ideal shock relations and the calculated maximum values of p and $\dot{u}_r$ from Brode and Bjork the following results are obtained:

Range Meters	$f_f = \frac{p}{\rho_o \dot{u}}$ ft/sec
150	8,650
200	8,100
250	8,030

*Cole, R.H., "Underwater Explosions", Princeton University Press, Princeton, New Jersey, 1948.

Thus at a range of 200 meters the appropriate value of $\psi = 8{,}100/7{,}200 = 1.12$ and from Equation (4) $\sigma = 0.945\ p$. This reduction in the fluid pressure is sufficiently small that it may be neglected. Thus the applied stress for the elastic solid may be taken as the fluid pressure at the radius of the boundary.

The applicability of the results of Brode and Bjork as boundary conditions for subsequent calculations in media other than tuff depends upon several factors including the effect of differences in the equation of state between any other material and that assumed for tuff. Of particular importance is the effect of the equation of state on the pressure-time variation from point to point. Unfortunately, no calculations are available for any other rock or soil material. A qualitative estimate of the effect of material properties can be made by comparing the peak overpressure-distance relation for water and a gas with the results for tuff.

The variation of peak pressure with vertical distance below ground zero is given for tuff in Figure 103 along with similar results for water and an ideal gas with $\gamma = 3$. The RAND Corporation calculations for tuff were terminated at a peak pressure of about 5 kilobars. At these lower pressures, the peak pressure varies approximately as the inverse three-halves power of radial distance, while at higher pressures, not shown in the figure, the peak pressure variation is approximately like the inverse cube of the distance. The dashed lines in the figure are extrapolations of available data.

The ideal gas solution was also obtained by Brode and Bjork using the hydrodynamic model. Here the peak pressure varies as approximately the inverse cube of the distance for all the ranges calculated. A comparison of the tuff and ideal gas

calculations indicates that for a given range the peak pressures between the two materials differ by less than a factor of about three.

The relationship for water shown in Figure 103 was derived from the peak water overpressure-distance data for a deep underwater explosion*. In deriving the relation for water it was assumed that the weapon yield was 1200 KT or twice the total energy assigned to the rock half-space at time zero by Brode and Bjork. The peak water pressure varies approximately as the inverse of the distance for pressures of about 0.1 kilobar. As in the previous case, less than a factor of three separates the curves for the tuff and water for peak pressures ranging from about 0.1 to 10 kilobars.

On the basis of these comparisons it seems reasonable to expect that differences in the equation of state for various rocks and soils would not cause differences in the peak pressures found using the hydrodynamic model of more than an order of magnitude and perhaps much less. This observation, along with the preceding discussion of the boundary conditions for the elastic model suggest an approximate method of extending the RAND Corporation calculations to materials other than tuff. Since the peak pressure-distance data do not appear to be too sensitive to significant variations in the equation of state, it may be assumed that the tuff results of Brode and Bjork are applicable to other types of rock and perhaps soil materials. Equation (4) may be used to adjust the pressure input for the elastic body to compensate for the differences in density and wave velocity between tuff and a given material. It should be emphasized that this procedure is recommended here because no close-in calculations are available for materials other than tuff. When such calculations have been made, another procedure should be devised.

*Glasstone, Samuel, The Effects of Nuclear Weapons, U. S. Atomic Energy Commission, April, 1962

In all of the problems, the material of the solid is assumed to be linearly elastic. Values of the elastic constants of the solid are assumed to be approximately those of materials similar to tuff, a material in which the calculations of Brode and Bjork apply. These values were determined or inferred from available field data, and are as follows:

Lame's constants: $\lambda = 3.9 \times 10^5$ psi

$\mu = 3.5 \times 10^5$ psi

Dilatational wave velocity, $c = 6{,}000$ fps.

These values correspond to a Young's modulus of 8.8×10^5 psi and Poisson's ratio of $\nu = 0.265$.

C. THEORETICAL SOLUTION FOR INFINITE SPACE

Consider an infinite homogeneous, isotropic elastic space with a spherical cavity of radius a. Let the cavity be loaded by a normal stress σ_{rr} (θ, ϕ, t), where θ and ϕ are angles locating a point on the surface of the sphere. The stresses will usually be compressive; however, the ordinary sign convention of the theory of elasticity, tensile stresses positive, will be used for convenience. In what follows, no distinction is made between the initial and final configurations of the medium, so that the ordinary theory of elasticity applies.

For a radially symmetric load, it is apparent that the only displacement is the radial displacement u. There are only three non-zero stress components, σ_{rr}, $\sigma_{\theta\theta}$ and $\sigma_{\phi\phi}$. For small displacements the acceleration in the radial direction is $a_r = \ddot{u}$, the strain $\epsilon_r = \frac{\partial u}{\partial r}$, $\epsilon_\theta = \epsilon_\phi = \frac{u}{r}$. The equation of motion in the radial direction is

$$\frac{1}{r^2}\frac{\partial}{\partial r}(r^2\sigma_{rr}) - \frac{\sigma_{\theta\theta}+\sigma_{\phi\phi}}{r} = \rho a_r$$

or

$$\frac{\partial \sigma_{rr}}{\partial r} + \frac{2\sigma_{rr} - \sigma_{\theta\theta} - \sigma_{\phi\phi}}{r} = \rho \ddot{u}_r \tag{10}$$

Expressing the stresses in terms of the strains, we have

$$\sigma_{rr} = \lambda\Delta + 2\mu\epsilon_r = \lambda\left(\frac{\partial u}{\partial r} + \frac{2u}{r}\right) + 2\mu\frac{\partial u}{\partial r}$$

$$\sigma_{\theta\theta} = \sigma_{\phi\phi} = \lambda\Delta + 2\mu\epsilon_\theta = \lambda\left(\frac{\partial u}{\partial r} + \frac{2u}{r}\right) + 2\mu\frac{u}{r}$$

The equation of motion, Equation (10), becomes

$$(\lambda + 2\mu)\frac{\partial^2 u}{\partial r^2} + 2(\lambda + 2\mu)\frac{1}{r}\frac{\partial u}{\partial r} - 2(\lambda + 2\mu)\frac{u}{r^2} = \rho\ddot{u}$$

or

$$\frac{\partial^2 u}{\partial r^2} + \frac{2}{r}\frac{\partial u}{\partial r} - \frac{2u}{r^2} = \left(\frac{\rho}{\lambda + 2\mu}\right)\ddot{u} = \frac{1}{c_p^2}\ddot{u} \tag{11}$$

Now we introduce the displacement potential ϕ such that $u = \frac{\partial \phi}{\partial r}$. The left side of Equation (11) becomes

$$\frac{\partial^3\phi}{\partial r^3} + \frac{2}{r}\frac{\partial^2\phi}{\partial r^2} - \frac{2}{r^2}\frac{\partial\phi}{\partial r} = \frac{\partial}{\partial r}\left(\frac{\partial^2\phi}{\partial r^2} + \frac{2}{r}\frac{\partial\phi}{\partial r}\right)$$

The right side is just

$$\frac{1}{c_p^2}\frac{\partial}{\partial r}\left(\frac{\partial^2\phi}{\partial t^2}\right),$$

so that the equation of motion is satisfied if

$$\frac{\partial^2\phi}{\partial r^2} + \frac{2}{r}\frac{\partial\phi}{\partial r} = \frac{1}{c_p^2}\frac{\partial^2\phi}{\partial t^2} \tag{12}$$

The general solution of this partial differential equation may be obtained by noting that if we set $\phi = \frac{1}{r}\psi$,

$$\frac{\partial\phi}{\partial r} = \frac{1}{r}\frac{\partial\psi}{\partial r} - \frac{\psi}{r^2} \quad ;$$

$$\frac{\partial^2 \phi}{\partial r^2} = \frac{1}{r}\frac{\partial^2 \psi}{\partial r^2} - \frac{2}{r^2}\frac{\partial \psi}{\partial r} + \frac{2}{r^3}\psi$$

The left side of Equation (12), is then equal to $\frac{1}{r}\frac{\partial^2 \psi}{\partial r^2}$, so that the scalar wave Eq. 12 becomes $\frac{1}{r}\frac{\partial^2 \psi}{\partial r^2} = \frac{1}{rc_p^2}\frac{\partial^2 \psi}{\partial t^2}$,

The general solution of which for outgoing disturbances is

$$\psi = F(r - c_p t). \quad \text{Here, } c_p = \left(\frac{\lambda + 2\mu}{\rho}\right)^{1/2}$$

is the P-wave velocity. The displacement potential is now of the form

$$\phi = \frac{1}{r} F(r - c_p t)$$

Straight-forward computation yields the following quantities:

$$u = \frac{\partial \phi}{\partial r} = \frac{1}{r} F'(r - c_p t) - \frac{1}{r^2} F(r - c_p t)$$

$$\epsilon_r = \frac{\partial u}{\partial r} = \frac{1}{r} F'' - \frac{2}{r^2} F' + \frac{2}{r^3} F$$

$$\sigma_{rr} = \frac{\lambda + 2\mu}{r} F''(r - c_p t) - \frac{4\mu}{r^2} F'(r - c_p t) + \frac{4\mu}{r^3} F(r - c_p t)$$

$$\sigma_{\theta\theta} = \sigma_{\phi\phi} = \frac{\lambda}{r} F'' - \frac{4\mu}{r^2} F' + \frac{4\mu}{r^3} F$$

The maximum stress difference is

$$\sigma_{rr} - \sigma_{\theta\theta} = 2\mu\left(\frac{1}{r} F'' - \frac{3}{r^2} F' + \frac{3}{r^3} F\right)$$

It can be seen that knowledge of stress at the boundary $r = a$ gives us a differential equation of the form

$$AF''(\xi) - BF'(\xi) + CF(\xi) = f(\xi)$$

where f is a known function and A, B, C are positive constants. From the form of the argument $\xi = r - c_p t$, it follows that ξ becomes smaller as t increases, r remaining constant. When the disturbance starting at $r = a$ at time zero reaches the point r, we have $r - c_p t = a$. For values of $\xi > a$ the function F and all its derivatives

vanish. We may have a stress discontinuity when the disturbance begins, but no displacement discontinuity. Suitable initial conditions for the problem are

$$F'(a) = F(a) = 0$$

The apparent negative damping indicated by the negative coefficient of the F' term in the differential equation for F is explainable if one remembers that ξ will become smaller as t increases. In time, the solution damps out for a limited disturbance, as it should.

If we no longer restrict the pressures on the spherical cavity to be radially symmetric, the problem becomes somewhat more complicated. It is possible, however, to solve this dynamic elasticity problem in such a manner that, as before, only the solution of ordinary differential equations is required in the numerical evaluation. This procedure avoids the difficult and tedious computation of values of a Fourier integral, the unfortunate feature of the classical approach. Of course, in the problem as given the stresses on the "top half" of the spherical cavity are at our disposal. If we choose the stresses to be antisymmetric with respect to the surface (the plane z = 0), this plane will be loaded by only shearing tractions. If, on the other hand, we choose a symmetric distribution, the plane is loaded by only normal tractions. In either case, these loads must be removed by other methods.

The derivation will be given in general terms and then specialized for two cases. The first of these will be the radially symmetric case already treated; the second will be the lowest mode of the antisymmetric case. In what follows, Cartesian Tensor notation will be used throughout the computations. A sum over n will be

meant only if the sum sign occurs explicitly.

If u_i is the displacement vector, the Navier equations of elasticity read

$$(\lambda + \mu) \frac{\partial \Delta}{\partial x_i} + \mu \frac{\partial^2 u_i}{\partial x_j \partial x_j} = \rho \frac{\partial^2 u_i}{\partial t^2}$$

where Δ, the dilatation is $\frac{\partial u_j}{\partial x_j}$. We first express the displacement vector as the sum of two vectors, the first corresponding to no rotation, the second to no dilatation.

$$u_i = \frac{\partial \phi}{\partial x_i} + \epsilon_{ijk} \frac{\partial \psi_k}{\partial x_j}$$

where ϵ_{ijk} is the alternator. Substituting into the equations of motion, we have

$$\left[\lambda + \mu\right] \frac{\partial}{\partial x_i} (\nabla^2 \phi) + \mu \left[\frac{\partial}{\partial x_i} (\nabla^2 \phi) + \epsilon_{ijk} \frac{\partial}{\partial x_j} (\nabla^2 \psi_k)\right] = \rho \left[\frac{\partial}{\partial x_i} (\frac{\partial^2 \phi}{\partial t^2}) + \epsilon_{ijk} \frac{\partial}{\partial x_j} (\frac{\partial^2 \psi_k}{\partial t^2})\right]$$

These three equations are satisfied if $(\lambda + 2\mu)\nabla^2 \phi = \rho \ddot{\phi}$ and $\mu \nabla^2 \psi_k = \rho \ddot{\psi}_k$. The constants, $(\frac{\lambda + 2\mu}{\rho})^{1/2} = c_p$ and $(\frac{\mu}{\rho})^{1/2} = c_s$, are the propagation velocities of P and S waves, respectively. We see that the problem has been reduced to solving a scalar and a vector wave equation.

Consider first the scalar wave equation. A convenient way of solving this equation in a form suitable for use when spherical boundaries are involved is to note that the relevant solutions of the "homogeneous" equation $\nabla^2 \phi = 0$ is $\phi = K^n$, where K^n is a solid spherical harmonic of order n. Three properties of the solid spherical harmonics will be used. The third one will not be needed until almost the end of the computations.

1. $\nabla^2 K^n = 0$ or $\dfrac{\partial^2 K^n}{\partial x_i \partial x_i} = 0$

2. K^n is homogeneous of order n in x_1, x_2, and x_3 so that by Euler's theorem on homogeneous functions, $x_i \dfrac{\partial K^n}{\partial x_i} = nK^n$.

3. The K^n are orthogonal over the unit sphere. Over a sphere of radius a we have

$$\int_{s_a} K^n K^m ds = 0, \quad m \neq n$$

$$\int_{s_a} K^n K^m ds = \frac{4\pi}{2n+1} a^{2n+2}, \quad m = n$$

We now use the idea of variation of parameters and seek a solution of the equation

$$\nabla^2 \phi = \frac{1}{c_p^2} \ddot{\phi}$$

in the form $f_n(r, t) K^n$, where $r^2 = x_i x_i$. We shall find the restrictions on the functions f_n by substituting this solution into the wave equation for ϕ. For this purpose we require $\dfrac{\partial \phi}{\partial x_i}$ and $\dfrac{\partial^2 \phi}{\partial x_i \partial x_i}$:

$$\frac{\partial \phi}{\partial x_i} = \frac{\partial f_n}{\partial r} \frac{x_i}{r} K^n + f_n \frac{\partial K^n}{\partial x_i}$$

$$\frac{\partial^2 \phi}{\partial x_i \partial x_i} = \frac{\partial^2 f_n}{\partial r^2} \frac{x_i}{r} \frac{x_i}{r} K^n + \frac{\delta_{ii}}{r} \frac{\partial f_n}{\partial r} K^n - \frac{\partial f_n}{\partial r} \frac{x_i}{r^2} \frac{x_i}{r} K^n$$

$$+ 2 \frac{\partial f_n}{\partial r} \left(\frac{x_i}{r}\right) \frac{\partial K^n}{\partial x_i} + f_n \frac{\partial^2 K^n}{\partial x_i \partial x_i}$$

where δ_{ij} is the Kronecker Delta, zero if $i \neq j$, 1 if $i = j$ ($\delta_{ii} = 3$). Using the properties of the K^n, we have

$$\nabla^2 \phi = K^n \left[\frac{\partial^2 f_n}{\partial r^2} + \frac{2(1+n)}{r} \frac{\partial f_n}{\partial r} \right] .$$

The wave equation now becomes

$$K^n \left[\frac{\partial^2 f_n}{\partial r^2} + \frac{2(1+n)}{r} \frac{\partial f_n}{\partial r} \right] = \frac{1}{c_p^2} K^n \frac{\partial^2 f_n}{\partial t^2} ,$$

and is satisfied provided that

$$\frac{\partial^2 f_n}{\partial r^2} + \frac{2(1+n)}{r} \frac{\partial f_n}{\partial r} = \frac{1}{c_p^2} \frac{\partial^2 f_n}{\partial t^2} . \tag{13}$$

Equation (13) is a linear hyperbolic partial differential equation in the two variables r and t of a form whose general solution is known. For n = 0 we find

$$\frac{\partial^2 f_o}{\partial r^2} + \frac{2}{r} \frac{\partial f_o}{\partial r} = \frac{1}{c_p^2} \frac{\partial f_o^2}{\partial t^2}$$

the solution of which is

$$f_o = \frac{1}{r} F(r - c_p t) + \frac{1}{r} F_1(r + c_p t).$$

We shall only retain the first term, which represents an outward moving disturbance. It may be verified that if f_n is a solution of Equation (13), then $\frac{1}{r} \frac{\partial}{\partial r} (f_n)$ is a solution of Equation (13) for n replaced by n + 1. It follows that the part of the general solution of Equation (13) we are seeking is

$$f_n (r, t) = \left(\frac{1}{r} \frac{\partial}{\partial r}\right)^n \frac{1}{r} F(r - c_p t) \tag{14}$$

We now turn to an examination of the vector wave equation $\nabla^2 \psi_k = \frac{1}{c_s^2} \ddot{\psi}_k$. As before, we first consider solutions of the equation $\nabla^2 \psi_k = 0$ and then multiply by $g_n(r, t)$. The choice of solution is governed by the condition that, for a loading of the sphere symmetric about the x_3 axis, the displacements lie in the

planes of the meridians. As will be seen later, a convenient form of the solution is the one shown below:

$$\psi_k = g_n(r, t)\ \epsilon_{ijk}\, x_i \frac{\partial K^n}{\partial x_j}$$

where K^n is a solid spherical harmonic of order n. We prove first that

$$\nabla^2\left(\epsilon_{ijk}\, x_i \frac{\partial K^n}{\partial x_j}\right) = 0.$$

That is $$\frac{\partial}{\partial x_\ell}\left(\epsilon_{ijk}\, x_i \frac{\partial K^n}{\partial x_j}\right) = \epsilon_{ijk}\left(\delta_{i\ell} \frac{\partial K^n}{\partial x_j} + x_i \frac{\partial^2 K^n}{\partial x_\ell\ x_j}\right),$$

and

$$\frac{\partial^2}{\partial x_\ell\, \partial x_\ell}\left(\epsilon_{ijk}\, x_i \frac{\partial K^n}{\partial x_j}\right) = \epsilon_{ijk}\left(\frac{\partial^2 K^n}{\partial x_j \partial x_i} + \delta_{i\ell} \frac{\partial^2 K^n}{\partial x_j\, \partial x_\ell} + x_i \frac{\partial^3 K^n}{\partial x_j\, \partial x_\ell\, \partial x_\ell}\right) = 0.$$

Furthermore, it is easy to see that $\epsilon_{ijk}\, x_i \frac{\partial K^n}{\partial x_j}$ is homogeneous of degree n in x_1, x_2 and x_3. It follows immediately that g_n satisfy equations similar to Equation (13).

$$\frac{\partial^2 g_n}{\partial r^2} + \frac{2(1+n)}{r}\frac{\partial g_n}{\partial r} = \frac{1}{c_s^2}\frac{\partial^2 g_n}{\partial t^2} \tag{15}$$

As before, the solution of interest is

$$g_n(r, t) = \left(\frac{1}{r}\frac{\partial}{\partial r}\right)^n \frac{1}{r}\, G(r - c_s t) \tag{16}$$

For an axially symmetric problem, this is all we need for the vector potential. We may now compute the displacement vector $u_i = \frac{\partial \phi}{\partial x_i} + \epsilon_{ijk}\frac{\partial \psi_k}{\partial x_j}$. Computations will be carried out for a single n. For the final solution, of course, a sum on n will be required. The only part of the computation that is not self explanatory is the use of the identity

$$\epsilon_{ijk}\,\epsilon_{mpk} = (\delta_{im}\,\delta_{jp} - \delta_{ip}\,\delta_{jm})$$

This last relation together with the first two properties of the K^n given above leads to

$$u_i = \left(n \frac{\partial g_n}{\partial r} + \frac{\partial f_n}{\partial r}\right) \frac{x_i}{r} K^n + \left[f_n - (n+1)\, g_n - r \frac{\partial g_n}{\partial r}\right] \frac{\partial K^n}{\partial x_i}$$

The (mathematical)strain components may now be calculated:

$$\epsilon_{ij} = \frac{1}{2}\left(\frac{\partial u_i}{\partial x_j} + \frac{\partial u_j}{\partial x_i}\right) \quad , \quad \Delta = \frac{\partial u_i}{\partial x_i}$$

$$\epsilon_{ij} = \left[n \frac{\partial^2 g_n}{\partial r^2} + \frac{\partial^2 f_n}{\partial r^2}\right] \frac{x_i\, x_j}{r^2} K^n + \left(n \frac{\partial g_n}{\partial r} + \frac{\partial f_n}{\partial r}\right) \left(\frac{\delta_{ij}}{r} - \frac{x_i\, x_j}{r^3}\right) K^n$$

$$+ \frac{1}{2}\left(n \frac{\partial g_n}{\partial r} + \frac{\partial f_n}{\partial r}\right) \left(\frac{x_i}{r} \frac{\partial K^n}{\partial x_j} + \frac{x_j}{r} \frac{\partial K^n}{\partial x_i}\right)$$

$$+ \frac{1}{2}\left[\frac{\partial f_n}{\partial r} - (n+2) \frac{\partial g_n}{\partial r} - r \frac{\partial^2 g_n}{\partial r^2}\right]\left(\frac{x_j}{r} \frac{\partial K^n}{\partial x_i} + \frac{x_i}{r} \frac{\partial K^n}{\partial x_j}\right)$$

$$+ \left[f_n - (n+1)\, g_n - r \frac{\partial g_n}{\partial r}\right] \frac{\partial^2 K^n}{\partial x_i \partial x_j} ,$$

$$\Delta = \frac{1}{c_p^2} \frac{\partial^2 f_n}{\partial t^2} K^n$$

The stress components are found from the strains by applying Hooke's Law for an isotropic solid:

$$\sigma_{ij} = \lambda \Delta\, \delta_{ij} + 2\mu \epsilon_{ij}$$

We are especially interested in the tractions on the surface r = a. The unit normal is just $-\frac{x_i}{r}\Big|_{r=a}$

$$\overset{r}{T}_j = \sigma_{ij} n_i = -\frac{x_i}{r} \sigma_{ij} ,$$

$$\overset{r}{T}_j = -\frac{\lambda}{c_p^2} \frac{\partial^2 f_n}{\partial t^2} \frac{x_j}{r} K^n - 2\mu \left\{\left[n g_n'' + f_n''\right] \frac{x_j}{r} K^n\right.$$

$$+ \frac{1}{2}\left(2f_n' - 2g_n' - r g_n''\right) \left(\frac{n x_j}{r^2} K^n + \frac{\partial K^n}{\partial x_j}\right)$$

$$\left. + \left[f_n - (n+1)\, g_n - r g_n'\right] \frac{(n-1)}{r} \frac{\partial K^n}{\partial x_j}\right\}$$

We see that the traction is in the form

$$\overset{r}{T}_j = N_1^n \frac{x_j}{r} K^n + N_2^n \frac{\partial K^n}{\partial x_j},$$

where

$$N_1^n = -\frac{\lambda}{c_p^2} \ddot{f}_n - 2\mu\,(n g_n'' + f_n'') - 2\mu\,(2f_n' - 2g_n' - r g_n'')\,\frac{n}{r}$$

$$N_2^n = -2\mu\left[\frac{1}{2}(2f_n' - 2g_n' - r g_n'') + \frac{(n-1)}{r}(f_n - (n+1)\,g_n - r g_n')\right] \tag{17}$$

Here primes denote differentiation with respect to r.

The known traction on the boundary is a normal pressure $\sigma_{rr}(\phi, t)\Big|_{r=a}$ in the axially symmetric case. It is convenient to expand the stress in spherical harmonics. (In what follows, the solid harmonics will correspond to surface harmonics of zonal type only by virtue of the axial symmetry). The expansion reads

$$\sigma_{rr}(a, \phi, t) = \sum_n a_n(t) K^n \quad \text{on } r = a.$$

Multiply both sides by K^m and integrate over the sphere of radius a,

$$\int_{s_a} \sigma_{rr}(a, \phi, t)\, K^m\, ds = \sum_n a_n(t) \int_{s_a} K^n K^m\, ds\,.$$

By the orthogonality properties of the K^n we have

$$a_m(t) = \frac{2m+1}{4\pi a^{2m+2}} \int_{s_a} \sigma_{rr} K^m\, ds$$

From Equation (17) we have

$$\sum_n \left(N_1^n \frac{x_j}{r} K^n + N_2^n \frac{\partial K^n}{\partial x_j}\right) = \overset{r}{T}_j = \sigma_{rr}\left(-\frac{x_j}{r}\right) = -\sum_n a_n(t) \frac{x_j}{r} K^n \tag{18}$$

That the vector equation should yield solutions for N_1^n and N_2^n may be seen by noting that $\frac{x_j}{r}$ is a radial vector and $\frac{\partial K^n}{\partial x_j}$ lies in the meridional plane if K^n corresponds

to zonal harmonics. We are then dealing with just two components at each point so that two functions should be determined. We expect that $N_2^n = 0$ since it multiplies the only vector in the equation not in the radial direction. Formal computation gives us this result and assures us that the modes decouple.

Let us multiply Equation (18) by $\frac{x_j}{r} K^m$, sum and integrate over the sphere of radius a:

$$\sum_n \left[N_1^n \int_{s_a} \frac{x_j x_j}{r^2} K^n K^m ds + N_2^n \int_{s_a} \frac{x_j}{r} \frac{\partial K^n}{\partial x_j} K^m ds \right]$$

$$= - \sum_n a_n(t) \int_{s_a} \frac{x_j}{r} \frac{x_j}{r} K^n K^m ds ,$$

or

$$N_1^m \frac{4\pi}{(2m+1)} a^{2m+2} + N_2^m m \frac{4\pi}{(2m+1)} a^{2m+1} = - a_m(t) \frac{4\pi}{(2m+1)} a^{2m+2} \qquad (19)$$

We also multiply Equation (18) through by $\frac{\partial x^m}{\partial x_j}$, sum and integrate over the unit sphere. For this purpose we shall require the surface integral,

$$\int_{s_a} \frac{\partial K^n}{\partial x_j} \frac{\partial K^m}{\partial x_j} ds .$$

We note first that this surface integral is simply related to the integral of the same product over the solid sphere by virtue of the homogeneity of the functions

$$\int_{V_a} \frac{\partial K^n}{\partial x_j} \frac{\partial K^m}{\partial x_j} dV = \int_o^a \left(\frac{r}{a}\right)^{n+m-2} \left(\frac{r}{a}\right)^2 dr \int_{s_a} \frac{\partial K^n}{\partial x_j} \frac{\partial K^m}{\partial x_j} ds$$

$$= \frac{a}{n+m+1} \int_{s_a} \frac{\partial K^n}{\partial x_j} \frac{\partial K^m}{\partial x_j} ds .$$

However, the volume integral can be evaluated by the divergence theorem:

$$\int_{V_a} \frac{\partial K^n}{\partial x_j} \frac{\partial K^m}{\partial x_j} dV = \int_{V_a} \left[\frac{\partial}{\partial x_j} (K^n \frac{\partial K^m}{\partial x_j}) - K^n \frac{\partial^2 K^m}{\partial x_j \partial x_j} \right] dV$$

$$= \int_{V_a} \frac{\partial}{\partial x_j} (K^n \frac{\partial K^m}{\partial x_j}) dV = \int_{s_a} K^n \frac{\partial K^m}{\partial x_j} \frac{x_j}{r} ds$$

$$= \int_{s_a} m K^n K^m ds$$

We see then that

$$\int_{s_a} \frac{\partial K^n}{\partial x_j} \frac{\partial K^m}{\partial x_j} ds = 4\pi m a^{2m}, \quad n = m, \quad 0, \quad n \neq m$$

Using this result, we find

$$N_1^m m \frac{4\pi}{(2m+1)} a^{2m+1} + N_2^m m 4\pi a^{2m} = -a_m(t) \frac{4\pi m}{2m+1} a^{2m+1} \tag{19a}$$

Equations (19) and (19a) may be solved simultaneously to give

$$N_2^m = 0, \qquad N_1^m = -a_m(t)$$

These results, together with Equation (17), provide us with two coupled ordinary differential equations if we recall the forms of the solutions for f and g, Equations (14) and (16).

For n = 0, we have $K^0 = 1$ and

$$-\frac{\lambda}{c_p^2} \frac{\partial^2 f_o}{\partial t^2} - 2\mu f_o'' = -\sigma_{rr}(t) \Big|_{r = a}$$

The N_2^0 equation disappears since $\frac{\partial K^0}{\partial x_j} = 0$.

$$f_o = \frac{1}{r} F(r - c_p t)$$

$$\frac{\partial^2 f_o}{\partial t^2} = c_p^2 \frac{1}{r} F''(r - c_p t)$$

$$\frac{\partial^2 f_o}{\partial r^2} = -\frac{2}{r^2} F' + \frac{1}{r} F'' + \frac{2}{r^3} F$$

This gives us precisely the same σ_{rr} we derived before.

For n = 1, the lowest antisymmetric mode, we have $K^1 = x_3$ (or z). It will be remembered that z = 0 is the plane boundary. We have that

$$\int_{s_a} \sigma_{rr}(\phi,t)\, K' ds = 4\pi a^3 \int_0^{\pi/2} \sigma_{rr}(\phi, t) \sin\phi \cos\phi \, d\phi \quad ,$$

$$a_1(t) = \frac{3}{a_o} \int_0^{\pi/2} \sigma_{rr}(\phi,t) \sin\phi \cos\phi \, d\phi \quad .$$

The solutions for f and g are

$$f = \frac{1}{r}\frac{\partial}{\partial r}\left[\frac{1}{r} F(r - c_p t)\right] \quad ;$$

$$g = \frac{1}{r}\frac{\partial}{\partial r}\ \frac{1}{r}\left[G(r - c_s t)\right] \quad .$$

The differential equations expressing the boundary condition read

$$\sigma_{rr} = \frac{\lambda + 2\mu}{r} F''' - \frac{\lambda + 6\mu}{r^2} F'' + \frac{12\mu}{r^3} F' - \frac{12}{r^4} F - \frac{4\mu}{r^2} G'' + \frac{12\mu}{r^3} G' - \frac{12\mu}{r^4} G$$

$$= + a_1 r \quad \text{at} \quad r = a$$

$$-\frac{2}{r^2} F'' + \frac{6}{r^3} F' - \frac{6}{r^4} F + \frac{1}{r} G''' - \frac{3}{r^2} G'' + \frac{6}{r^3} G' - \frac{6}{r^4} G = 0 \text{ at } r = a \ .$$

Stresses may be expressed in terms of the strains. The most interesting stress components are the shear on z = 0, which must be later removed, and the stress σ_{33} or σ_{zz} directly beneath the center of the sphere.

$$\sigma_{31}\Big|_{z = 0,\ y = 0} = \sigma_{zr} = \frac{2\mu}{r^2} F'' - \frac{6\mu}{r^3} F' + \frac{6\mu}{r^4} F - \frac{\mu}{r} G''' + \frac{3\mu}{r^2} G''$$

$$- \frac{6\mu}{r^3} G' + \frac{6\mu}{r^4} G \ ; \quad (r = x)$$

$$\sigma_{33}\Big|_{x=0,\ y=0} = \sigma_{rr} = \frac{\lambda + 2\mu}{r} F''' - \frac{\lambda + 6\mu}{r^2} F'' + \frac{12\mu}{r^3} F' - \frac{12}{r^4} F - \frac{4\mu}{r^2} G''$$

$$+ \frac{12\mu}{r^3} G' - \frac{12\mu}{r^4} G; \quad (r = z)$$

It is not difficult to see how the ideas of the above derivation may be extended to the case of spherical layering. In all but the outer layer, we should have to allow incoming as well as outgoing waves, that is, solutions of the form $(\frac{1}{r}\frac{\partial}{\partial r})^n \frac{1}{r} F(r + ct)$. If there are s layers, we have s - 1 interfaces where two traction components and two displacement components must match (except when n = 0). At the inner surface, we have two equations, as in the present problem. The total number of (scalar) boundary conditions is then 4s - 2. Counting both incoming and outgoing waves we have four F's and G's in each layer but the outer, and two in the outer. The method will then give 4s - 2 equations in 4s - 2 unknowns. It should be noted that these are coupled ordinary differential equations with given initial values, a type of problem well suited for solution on a digital computer.

The solution to Equation (15) for a radially symmetric load was programmed for the IBM 7090 computer using numerical integration of the displacement potential. Radial and tangential stresses were obtained for two media. The first has $\lambda = 390$ ksi, $\mu = 360$ ksi and a density such that the p - wave velocity, c_p, was 6,000 fps. The corresponding Poisson's ratio is 0.260. The second problem has $\lambda = 590$ ksi, $\mu = 260$ ksi and the same density, so that the p-wave velocity remains equal to 6,000 fps but $\nu = 0.347$.

The radial stress at various depths proved to be independent of Poisson's ratio and thus the radial stresses for both problems are shown in Figure 104. The maximum

tangential stresses are nearly proportional to λ. These are shown for various depths in Figure 105 and 106 for both problems.

D. SOLUTIONS BY DIGITAL SIMULATION

Two discrete models of the lumped mass-spring type were used in the present study. The model used for the solution of Problem 1 is a spherical model, whereas that used in solving Problems 2, 3, and 4 is axially symmetric. The equations of motion of the discrete systems are identically the same as the differential equations of the corresponding solid continua. This is demonstrated in the following discussion for the spherical model. A similar demonstration can be made for the axially symmetric use.

In Figure 107 is shown a typical arrangement of the mass points (0, 1, 2, ...) and the stress points (a, b, c, ...) of the spherical model along the radial lines. The masses of the solid are concentrated at the mass points, while the springs provide the average resistances of the solid. The stresses in the springs are average stresses defined at the stress points.

Applying Newton's second law of motion to a typical mass point "O" the equation of motion of such a mass point in terms of stresses can be derived as follows:

$$\sigma_r^a \, (r_a^2) \, \left(\frac{\Delta\theta}{2}\right)^2 - \sigma_r^b \, (r_b^2) \, \left(\frac{\Delta\theta}{2}\right)^2 - 4\sigma_\theta^c \, \left(\frac{1}{4} r_o \lambda \, \overline{\Delta\theta}^2\right)$$

$$= \frac{1}{4} (r_o \Delta\theta)^2 \lambda \rho \ddot{u}_o$$

where: σ_r^a = average radial stress at stress point "a".

σ_θ^c = average tangential stress at stress point "c".

r_a = radial distance of stress point "a" from the center.

ρ = mass density

$\ddot{u}_o$ = radial acceleration of mass point "0"

λ = grid distance, see Figure 107.

$\Delta\theta$ = incremental angle, see Figure 107.

$r_a = (r_o + \frac{\lambda}{2})$; $r_b = (r_o - \frac{\lambda}{2})$

Simplifying, the above equation becomes,

$$\frac{\sigma_r^a - \sigma_r^b}{\lambda} + \frac{2(\sigma_r^o - \sigma_\theta^o)}{r_o} = \rho \ddot{u}_o$$

which is identically the same as the central finite difference analog of the differential equation,

$$\frac{\partial \sigma_r}{\partial r} + \frac{2(\sigma_r - \sigma_\theta)}{r} = \rho \frac{\partial^2 u}{\partial t^2}$$

This last equation can be recognized to be the differential equation of motion of a spherically symmetric solid.

Problem 1 - Infinite Space

This problem involves an infinite solid space with a spherical hole having a radius of 660 feet and subjected to a uniform blast pressure on the boundary of the hole. Results of the numerical calculations with the spherical model are presented graphically in Figures 108 through 113. Figure 111 shows the pressure-time relationship of the radial stresses for points along a radius, while in Figure 112 are shown the same stresses plotted against the radial distance for the specific times indicated. Similar pressure-time plots for the tangential stresses and the particle accelerations, velocities, and displacements are presented in Figures 108, 109, 110, and 113.

Problem 2 - Half-Space with "Correction" Loading

In Figure 98b is shown a meridional section of a half-space which is subjected to a "correction" loading at a specified time, t_1. This correction loading is exactly equal to the negative of the tangential stresses (see Figure 113). The hemispherical cavity is free of stress in this case.

The stresses and particle motions derived from this problem when superposed with the corresponding stresses and particle motions of Problem 1 represent the solution of the half-space subjected only to a uniformly distributed pressure applied at the boundary of the semi-spherical cavity.

Graphical results representing time variation of stresses and particle velocities are given in Figures 114 through 120. Numerical results for points along the surface and those along lines inclined at 15 degrees and 30 degrees from the horizontal are presented. Beyond the 30 degree line, the results are relatively small and are not presented.

The results from this problem are referred to as "correction" stresses, velocities, or accelerations.

Problem 3 - Half-Space with Uniform Loading

This problem involves a half-space with a semi-spherical cavity with a radius of 660 feet as shown in Figure 98c. A uniformly distributed pressure having a pressure-time relationship as that given in Figure 102 is applied on the entire boundary surface of the semi-spherical cavity.

Plots of the radial particle accelerations and velocities, and the radial and tangential stresses as a function of time are given in Figures 121 through 130. The results for points along lines having different angles of inclination, ϕ, with the horizontal surface are given; specifically, the results for lines with $\phi = 0$, 15, and 30 degrees and for points along the vertical line ($\phi = 90$ degrees) are presented. The results for the points along lines with other angles of inclination ($\phi > 30$ degrees) were not presented since they are almost identical with those of the corresponding points along the vertical line. The results along the vertical lines are also identical with the results for the full-space. This, therefore, means that the full horizontal surface does not significantly affect the results for regions in the neighborhood of the vertical axis.

The results of this problem should be identical with the combined answers of Problems 1 and 2. A close examination of Figures 108 through 130 will reveal that this is indeed the case with the solutions presented here.

Problem 4 - Half-Space with Non-uniform Loading

A meridional section of the half-space of this problem is shown in Figure 98d. The problem is geometrically the same as in Problem 3 except that the distribution of the applied pressure is uniform only on the lower half of the spherical surface, while on the upper half, the pressure distribution varies as $p_o \sin \phi$ for $0 \leq \phi \leq 45$ degrees. Such a pressure distribution closely resembles the corresponding results of Brode and Bjork.

Results presented are for radial and tangential stresses, and for particle displacements, velocities and accelerations as shown in Figures 134 through 153. Other stresses and particle motions were computed but are not presented here. The results are plotted as functions of time for points of increasing radial distances along lines with four different angles of inclination from the horizontal.

The results along the lines with $\phi = 45$ degrees and $\phi = 90$ degrees are very close to each other. From this, it follows that the results in the region between the 45 degree line and the vertical should be almost identical with the corresponding results on the vertical line. It should be pointed out that the results on the vertical line are also identical with those of the full-space, thus indicating that the horizontal boundary of the half-space has negligible influence on the ground motions and pressures in the region close to the vertical.

E. SIGNIFICANCE OF RESULTS AND CONCLUSIONS

1. Discussion of Results

The neglect of a plastic region between the hydrodynamic model and the linearly elastic solid has an insignificant effect on the pressure-time relationship assumed in this study. However, since the study was predicated on the assumption of an elastic solid, and because of the extremely high stresses experienced by the solid, which would invariably cause plastic flow in the regions under consideration, the results can not be strictly applicable to materials which are inherently non-linear or which exhibit elastic properties only at low pressures. The calculated ground motions and stresses, therefore, must be considered in this light in relation to actual earth materials.

Comparing the results of the full-space with the corresponding results of the half-space solutions indicates that the horizontal surface boundary has negligible effect on the conditions in the lower regions of the half-space. This is clearly supported by the almost identical results for points on a diagonal line with those on the vertical line, and also by the closeness of all of these relationships with those of the full space. This fact is also verified by the results of the "correction" solutions which show that the "correction" stresses and velocities decay rapidly as a function of depth. In the regions close to the horizontal boundary, the tangential stresses are significantly affected by the boundary; the peak tangential stresses is increased as can be seen from Figure 127 through 130, with its maximum value somewhere along the line with a 15 degree angle of inclination from the surface. A surface effect gave rise to the tangential stresses in the vicinity of the surface, as shown in Figure 127. The radial stresses, on the other hand, are affected to a much lesser degree by the surface boundary; the magnitude of the radial stresses influenced by the boundary are shown in Figure 116 and 117.

Since an expanding air blast over the surface will induce normal pressures, which are essentially similar to the "correction" loading used in Problem 2 although the air blast will have a different pressure-time relation and higher peak values than those of the correction loading, the effects of an air blast can be expected also to be similar to the effects of the correction loading and would be pronounced only in the regions between the surface and the diagonal. In the lower regions of a half-space, the directly-transmitted effects will predominate.

In all cases, the radial velocity-time curves are similar to the corresponding radial stress-time curves; however, these two functions are not simply related as in the simple one-dimensional case. Both the peak values as well as the rise times of the radial stresses, velocities, and accelerations decay with increasing radial distance. The peak values of the tangential stresses also decreases as a function of the radial distance, in addition to its relations with the angle of inclination with the horizontal surface.

2. Decay of Peak Radial Pressures, Velocities, and Accelerations

The rate of decay of the maximum radial pressures at increasing radial distances are summarized in Figure 133 and 156. These show that along the vertical axis of the half-spaces, the radial pressures decay as the inverse power of about 1.15 of the radial distance, which is precisely at the same rate of decay as the radial stresses in the full-space. At the surface, the radial pressures decay more rapidly and is approximately with an inverse power of 1.40 of the radial distance.

The decay of the peak radial velocities as a function of the radial distance follows the same trend as the radial stresses along lines of the same angles of inclination with the horizontal surface. These are demonstrated in Figures 132 and 155. Significantly, these also show that along the vertical axis of the half-space, the peak velocities decay with the same inverse power of 1.15 as the decay of the peak velocities in the full-space solid.

The maximum accelerations decrease with varying inverse powers of the distance, approaching inverse powers of 1.80 at the surface and 1.50 along the vertical axis

at greater radial distances. At closer distances, the decay tends to be less rapid, as shown in Figures 131 and 154.

It must be pointed out that the rate of decay of the peak values of the stresses, velocities, and accelerations for regions between the vertical axis and the diagonal is about the same as the rate of decay along the vertical axis.

These decay rates are for the elastic condition assumed in the analysis, and may be slower than actual decay rates in real earth materials.

3. Specific Conclusions

The following specific conclusions may be derived from the numerical results presented here:

(1). The region below the diagonal line for the half-space remains essentially the same as a full-space; that is, the horizontal surface boundary has practically no effect on the conditions within this region.

(2). Primary effects of the horizontal boundary are limited to the region above the diagonal line. These effects are most pronounced on the surface and decrease very rapidly at greater depths. Tangential stresses in the shallower region are significantly affected by the boundary, while the radial stresses are affected to a lesser extent.

(3). The effects of normal air blast pressures can be expected also to be limited to the regions above the diagonal.

(4). The decay of the radial pressures with increasing radial distance is less rapid for an elastic solid when compared with the decay in the

hydrodynamic model of Brode and Bjork. Inverse powers of 1.40 to 1.15 of the radial distance (depending on the depth) were determined in the present study as compared with inverse powers of 3 to 1.50 for the hydrodynamic case.

(5). Maximum tangential stresses decrease faster with depth from the horizontal surface than with the radial distance.

(6). The rates of decay of the radial velocities are the same as the decay of the radial pressures. Radial velocity-time curves are similar to the pressure-time curves; however, there is no simple relationship between the velocities and pressures.

(7). The peak values of the radial accelerations tend to decay more rapidly at greater distances, with inverse powers approaching 1.80 of the radial distance at the surface and 1.50 along the vertical axis.

(8). Rise times of the radial pressure pulse decays with increasing radial distance; however, no evaluation of this decay has yet been made in this study.

F. SPECIAL CASES

1. Non-Homogeneity and Stratifications

Certain problems involving solid spaces with a number of layers, each possessing different elastic constants can be treated with the technique of digital simulation used in the present study with slight modifications of the present computer program. The layering, however, must be restricted by the following geometric considerations:

(1). For spherically symmetric problems (involving infinite spaces, for example) the layering must maintain the condition of spherical symmetry; this means that the different layers must be spherically concentric.

(2). For axially-symmetric problems (involving half-spaces), the layering can be of two configurations:

(a) If the loads are applied on a semi-spherical cavity, the layers must also be concentric semi-spheres of given radial thicknesses.

(b) If the loads are applied on the horizontal surface, the layers can be horizontal or spherical.

In addition, the analysis must be based on the assumption that there are not relative motions at the interface of any two adjacent layers.

2. Spherical Problems in Bilinear Solids

At present the literature contains a number of solutions to the problems of plane wave propagation in bilinear media (e.g., Rakhmatulin, K. A., "On the Propagation of Plane Waves in an Elastic Medium with a Nonlinear Stress-Strain Law", Uchenye Zapiski, University of Moscow, Vypusk 152, 1951, pp. 47-55; Akaiak, R., and Weidlinger, P., "Attenuation of Stress Waves in Bilinear Materials", Journal of Engineering Mechanics Division, ASCE V. 87, No. EM3, June 1961; Sutcliffe, S., "Strong Shock Formation in Bilinear Media", to be published in the forthcoming issue of EMD, ASCE).

The study of the same problems in the radially symmetric system is not nearly as complete but can be carried out by similar analyses (e.g., Rakhmatulin, K. A., and Demianov, Yu. A., "Prochnost' pri intensivnykh nagrvzkakh", Fizmatgiz, Moscow

1961). The added complexity of the nonlinearity of the differential equations in the radially symmetric case makes the subject somewhat more difficult, and generally makes approximate analytical techniques necessary.

The differential equation of motion for dilatational waves in a radially symmetric system with linear stress-strain relation is given by

$$\frac{\partial^2 u}{\partial r^2} + \frac{2}{r}\left(\frac{\partial u}{\partial r} - \frac{u}{r}\right) - \frac{1}{c^2}\frac{\partial^2 u}{\partial t^2} = 0 \tag{20}$$

where u is the diaplacement in the r - direction, r and t are space and time coordinates, and $c = \sqrt{\frac{\lambda + 2\mu}{\rho}}$ is the acoustic velocity.

The characteristics of Equation (20) are

$$r \pm ct = R \tag{21a}$$

$$dp \pm \frac{dq}{c} + \frac{2}{r}\left(p - \frac{u}{r}\right) dr = 0 \tag{21b}$$

The principal difficulty encountered in the analysis by characteristics lies in the fact that Equation (21b) is not integrable in a simple form unless the potential ϕ, with $u = \frac{\partial \phi}{\partial r}$, is introduced. Thus, as will be done in this treatment, it is sometimes more convenient to use the general solution to Equation (20) and a polynomial representation.

Let the stress-strain relation for a radially symmetric system be given as in Figure 157a where loading takes place along the line with slope c' and unloading along the line with slope c. Let the radial stress at $r = r_0$ be given by a function of the type shown in Figure 157b. In the (r,t) plane, the solution can be represented as

shown in Figure 157c. Up to $r = r^*$, a strong shock is propagated along the line $r - c't = 0$, and unloading takes place in region I. At $r = r^*$, the discontinuity vanishes, and the elastic loading region II forms, with unloading still in region I.

Let us consider only that portion of the (r,t) plane for $r < r^*$, and make a series representation of the solution in that domain.

Introducing the potential ϕ, with $u = \frac{\partial \phi}{\partial r}$ into Equation (20) yields the general solution in the unloading region

$$\begin{aligned}
\phi &= \frac{1}{r} f(r - ct) + \frac{1}{r} g(r + ct) \\
u &= \frac{1}{r} (f' + g') - \frac{1}{r^2} (f + g) \\
\frac{\partial u}{\partial r} &= \frac{1}{r} (f'' \times g'') - \frac{2}{r^2} (f' + g') + \frac{2}{r^3} (f + g) \\
\frac{\partial u}{\partial t} &= \frac{c}{r} (f'' - g'') = \frac{c}{r^2} (f' - g')
\end{aligned} \tag{22}$$

Along the shock front $r - c't = 0$, impulse-momentum yields

$$c' \Delta u_r + \Delta u_t = 0 \tag{23a}$$

where Δu_r and Δu_t are the discontinuities in strain and particle velocity. Or, since u_r and u_t are zero below $r - c't = 0$, Equation (23a) may be written

$$c' u_r + u_t = 0 \tag{23b}$$

On the t-axis let $\sigma_r = \sigma(r_o, t)$ be given as a function of the type shown in Figure 157b. Then letting $f(r_o - ct) = f_o$ and $g(r_o - ct) = g_o$, we have

$$\sigma(r_o, t) = \frac{\lambda + 2\mu}{r_o} (f_o'' + g_o'') - \frac{4\mu}{r_o^2} (f_o' + g_o') + \frac{4\mu}{r_o^3} (f_o + g_o) \tag{24}$$

On the shock front $r - c't = 0$ Equation (23b) yields

$$c'\left[\frac{1}{r}(f'' + g'') - \frac{2}{r^2}(f' + g') + \frac{2}{r^3}(f + g)\right] +$$

$$c\left[\frac{1}{r}(f'' - g'') - \frac{1}{r^2}(f' - g')\right] = 0 \tag{25}$$

and, since $u = 0$

$$\frac{1}{r}(f' + g') - \frac{1}{r^2}(f + g) = 0 \tag{26}$$

Equation (25) becomes:

$$\left(\frac{c' + c}{r}\right) f''\left[r\left(1 - \frac{C}{C^1}\right)\right] + \left(\frac{C' - C}{r}\right) g''\left[r\left(1 + \frac{C}{C^1}\right)\right] - \frac{C}{r^2} f'\left[r\left(1 - \frac{C}{C^1}\right)\right]$$

$$+ \frac{C}{r^2} g'\left[r\left(1 + \frac{C}{C^1}\right)\right] = 0 \tag{27}$$

Furthermore, at r_o, 0, $u = 0$ and σ_r is discontinuous, thus

$$\frac{1}{r_o} f'(r_o) - \frac{1}{r_o^2} f(r_o) + \frac{1}{r_o} g'(r_o) - \frac{1}{r^2} g(r_o) = 0 \tag{28}$$

Equations (24), (27), and (28) are sufficient for the solution in region I for $r < r^*$.

Let $\sigma(r_o, t)$, f and g be represented by the polynomials as follows:

$$\begin{aligned}
\sigma(r_o, t) &= p_o + p_1 t + p_2 t^2 + p_3 t^3 + \text{———} p_n t^n \\
f(r_o - ct) &= f(\xi) = f_o + f_1 \xi + f_c \xi^2 + \text{———} f_n \xi^n \\
g(r_o + ct) &= g(\eta) = g_o + g_1 \eta + g_2 \eta^2 + \text{———} g_n \eta^n \\
f\left[r\left(1 - \frac{C}{C^1}\right)\right] &- f(\alpha r) = f_o + f_1 \alpha r + f_2 \alpha^2 r^2 + \text{——} f_n \alpha^n r^n \\
g\left[r\left(1 + \frac{C}{C^1}\right)\right] &= g(\beta r) = g_o + g_1 \beta r + g_2 \beta^2 r^2 + \text{———} g_n \beta^n r^n
\end{aligned} \tag{29}$$

Substitution in Equation (27) and equating like powers of r yields:

$$g_1 = \frac{\alpha}{\beta} f_1$$

$$g_2 = -\frac{\alpha^2}{\beta^2} f_2$$

$$g_3 = \left[\frac{C' + \frac{C}{2}}{C^1 - \frac{C}{2}}\right]\frac{\alpha^3}{\beta^3}\left(f_3\right) \tag{30}$$

$$g_n = \left[\frac{C' + \frac{n^2 - 2n}{n^2 - n}}{C' - \frac{n^2 - 2n}{n^2 - n}}\right] \left(\frac{\alpha}{\beta}\right)^n f_n \quad n > 3$$

Equation (28) yields

$$\begin{aligned}
&\frac{1}{r_o}\left[f_1 + 2f_c r_o + 3f_3 r_o^2 + 4f_4 r_o^3 + 5f_5 r_o^4\right] \\
&- \frac{1}{r_o^2}\left[f_o + f_1 r_o + f_c r_o^2 + f_3 r_o^3 + f_4 r_o^4 + f_5 r_o^5\right. \\
&+ \frac{1}{r_o}\left[g_1 + 2g_2 r_o + 3g_3 r_o^2 + 4g_4 r_o^3 + 5g_5 r_o^4\right] \\
&- \frac{1}{r_o^2}\left[g_o + g_1 r_o + g_2 r_o^2 + g_3 r_o^3 + g_4 r_o^4 + g_5 r_o^5\right] = 0
\end{aligned} \tag{31}$$

Equation (24) yields

$$\begin{aligned}
P_o = &\frac{\lambda + 2\mu}{r_o}\left[2f_2 + 6f_3 r_o + 12f_4 r_o^2 + 20f_5 r_o^3 + \text{——}\right] \\
&- \frac{4\mu}{r_o^2}\left[f_1 + 2f_2 r_o + 3f_3 r_o^2 + 4f_4 r_o^3 + \text{————}\right] \\
&+ \frac{4\mu}{r_o^3}\left[f_o + f_1 r_o + f_2 r_o^2 + f_3 r_o^3 + \text{————}\right] \\
&+ \frac{\lambda + 2\mu}{r_o}\left[2g_2 + 6g_3 r_o + 12g_4 r_o^2 + 20g_4 r_o^3 + \text{——}\right]
\end{aligned} \tag{32}$$

$$- \frac{4\mu}{r_o^2}\left[g_1 + 2g_2 r_o + 3g_3 r_o^2 + 4g_4 r_o^3 + \text{———} \right]$$

$$+ \frac{4\mu}{r_o^3} \quad g_o + g_1 r_o + g_2 r_o^2 + g_3 r_o^3 + \text{———} \Big]$$

$$P_1 = \frac{1}{r_o}(\lambda + 2\mu) \left[- 6cf_3 - 24cr_o f_4 - 60cr_o^2 f_5 - \text{———} \right]$$

$$- \frac{4\mu}{r_o^2}\left[- 2cf_2 - 6cr_o f_3 - 12cr_o^2 f_4 - \text{———} \right]$$

$$+ \frac{4\mu}{r_o^3}\left[- cf_1 - 2cr_o f_2 - 3cr_o^2 f_5 - \text{———} \right]$$

$$+ \frac{1}{r_o}(\lambda + 2\mu) \left[6cg_3 + 24cr_o g_4 + 60cr_o^2 g_4 + \text{———} \right]$$

$$- \frac{4\mu}{r_o^2}\left[2cg_2 + 6cr_o g_3 + 12cr_o^2 g_4 + \text{———} \right] \qquad \text{(32) con't.}$$

$$+ \frac{4\mu}{r_o^2}\left[cg_1 + 2cr_o g_2 + 3cr_o^2 g_3 + \text{———} \right]$$

$$P_2 = \frac{1}{r_o}(\lambda + 2\mu) \left[12f_4 c^2 - 60f_5 c^2 r_o + \text{———} \right]$$

$$- \frac{4\mu}{r_o^2}\left[3f_3 c^2 - 12f_4 c^2 r_o^2 + \text{———} \right]$$

$$+ \frac{4\mu}{r_o^3}\left[f_2 c^2 - 3f_3 c^2 r_o^2 + \text{———} \right]$$

$$+ \frac{1}{r_o}(\lambda + 2\mu) \left[12g_4 c^2 + 60g_5 c^2 r_o^2 + \text{———} \right]$$

$$- \frac{4\mu}{r_o^2}\left[3g_3 c^2 + 12g_4 c^2 r_o^2 + \text{———} \right]$$

$$P_3 = \frac{1}{r_o}(\lambda + 2\mu)\left[-20f_5c^3\right] - \frac{4\mu}{r_o^2}\left[-f_4c^3\right] - \frac{4\mu}{r_o^2}\left[-f_3c^3\right]$$

$$+ \frac{1}{r_o}(\lambda + 2\mu)(20g_5c^3) - \frac{4\mu}{r_o^2}\left[g_4c^5\right] + \frac{4\mu}{r_o^2}\left[+g_3c^3\right]$$

Equations (30) through (32), when solved simultaneously, will yield approximate values of f and g for the first five terms, which will probably suffice for at least a rough solution.

The solution can be extended beyond r* by noting that in II σ_r, u = o and r-c't = o, σ_r is continuous across the unloading wave separating I and II, and $\frac{\partial \sigma_r}{\partial t} = 0$ on the unloading wave.

It may be noted here, that the problem could be solved by characteristics, but since the boundary conditions are set on two lines; t = 0, r - c't = 0, it would be necessary to set up a finite grid in the (r, t) plane, which would necessitate the solution of an increasingly larger system of simultaneous equations for each successive time step.

G. RECOMMENDATIONS FOR FURTHER STUDIES

The present study serves to indicate that solutions of a number of difficult problems involving ground shocks are possible with the technique of digital simulation employing the discrete models which were used in performing the numerical solution of the present problems. These models were developed with consideration for handling problems of continuum dynamics involving plastic yielding and irreversible flow, as well as viscous effects. However, the computer programs currently

available are restricted to linearly elastic solids, although the inclusion of viscosity for solving problems of Voigt solids does not involve major difficulty. The handling of nonlinear characteristics will require further research.

Further studies that can be performed with only minor or no modifications of present computer programs are the following:

1. More extensive determination of the stresses and ground motions, including shear stresses, circumferential stresses, principal stresses, and directions of principal planes, and tangential accelerations, velocities, and displacements for elastic half-space solids.
2. Determination of the effects of an expanding air blast on the horizontal surface, or the determination of the combined effects of the direct induced wave and the air blast wave.
3. Effects of elastic layering. The layering must be restricted to those discussed earlier.
4. Effects of linear viscosity.
5. Numerical solution of spherical blast problems in solids with similar behavior.

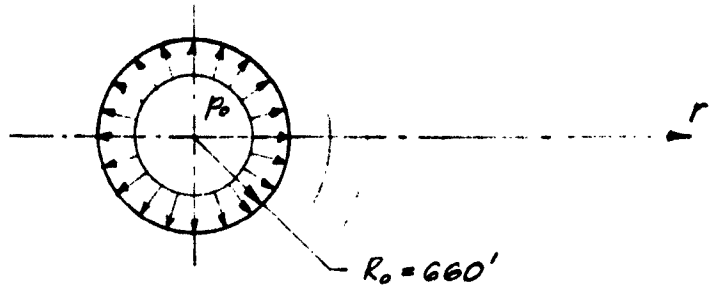

FIG. 98a : FULL SPACE WITH HOLE

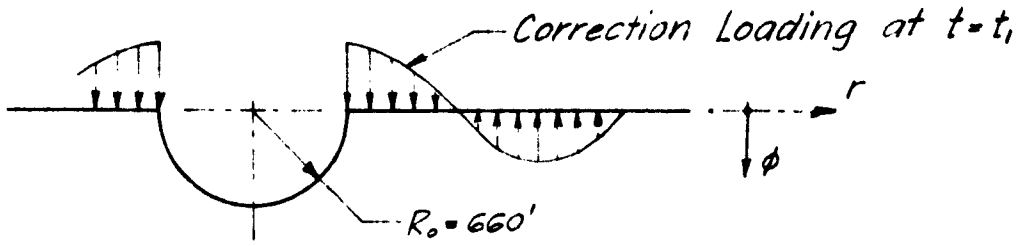

FIG. 98b : HALF SPACE WITH CORRECTION LOADING

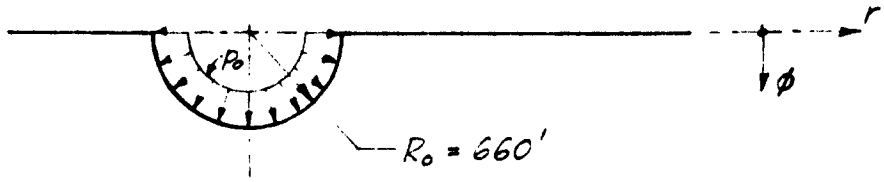

FIG. 98c : PROBLEM 3 - HALF SPACE WITH UNIFORM LOADING

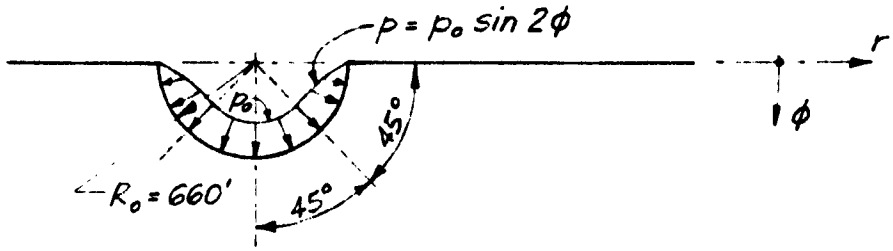

FIG. 98d : PROBLEM 4 - HALF SPACE WITH NON-UNIFORM LOADING

NO. 340R-20 DIETZGEN GRAPH PAPER
20 X 20 PER INCH

EUGENE DIETZGEN CO.
MADE IN U.S.A.

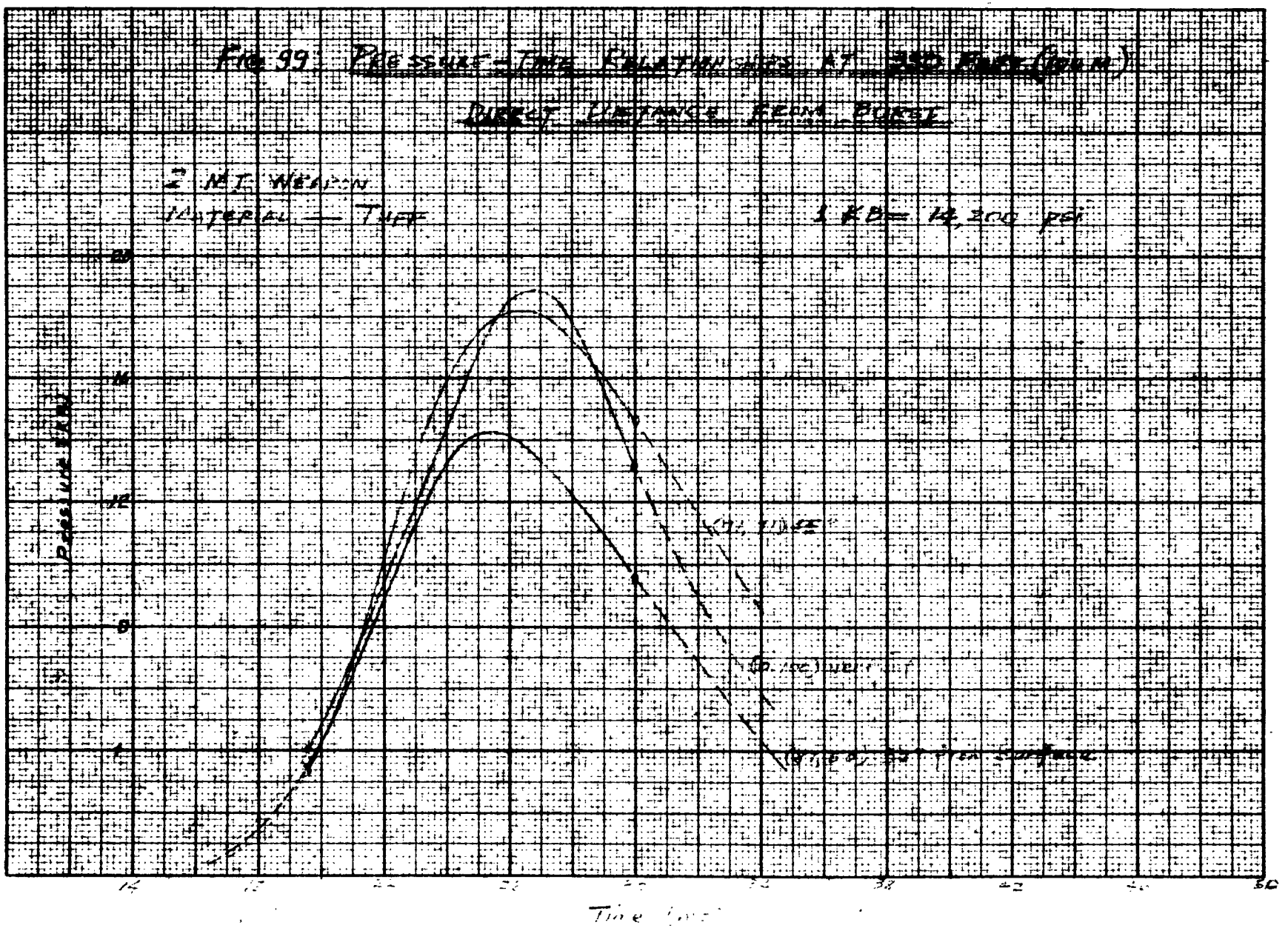

NO. 340R-20 DIETZGEN GRAPH PAPER
20 X 20 PER INCH

EUGENE DIETZGEN CO.
MADE IN U.S.A.

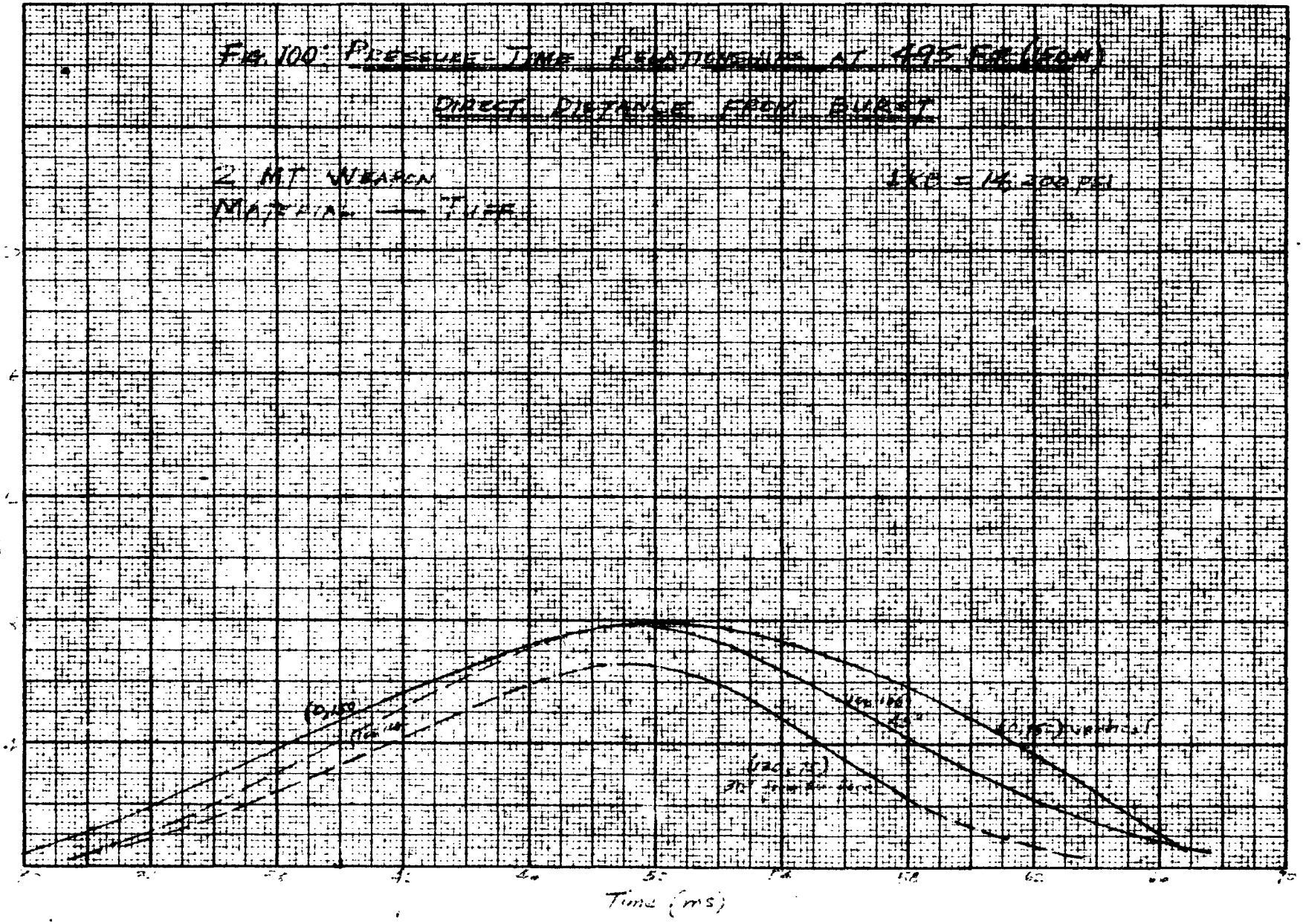

NO. 340R-20 DIETZGEN GRAPH PAPER
20 X 20 PER INCH

EUGENE DIETZGEN CO.
MADE IN U. S. A.

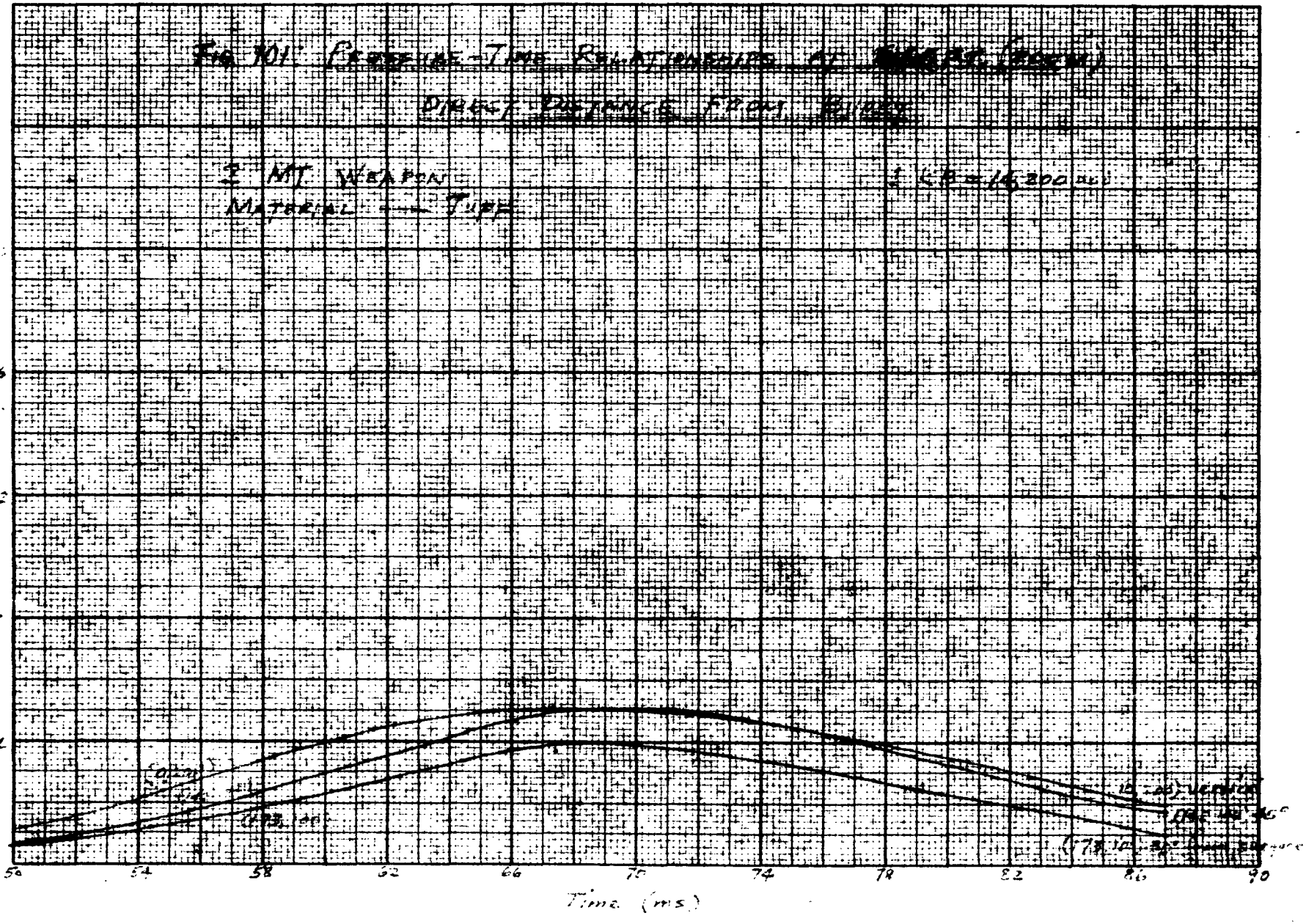

NO. 340-20 DIETZGEN GRAPH PAPER
20 X 20 PER INCH

EUGENE DIETZGEN CO.
MADE IN U. S. A.

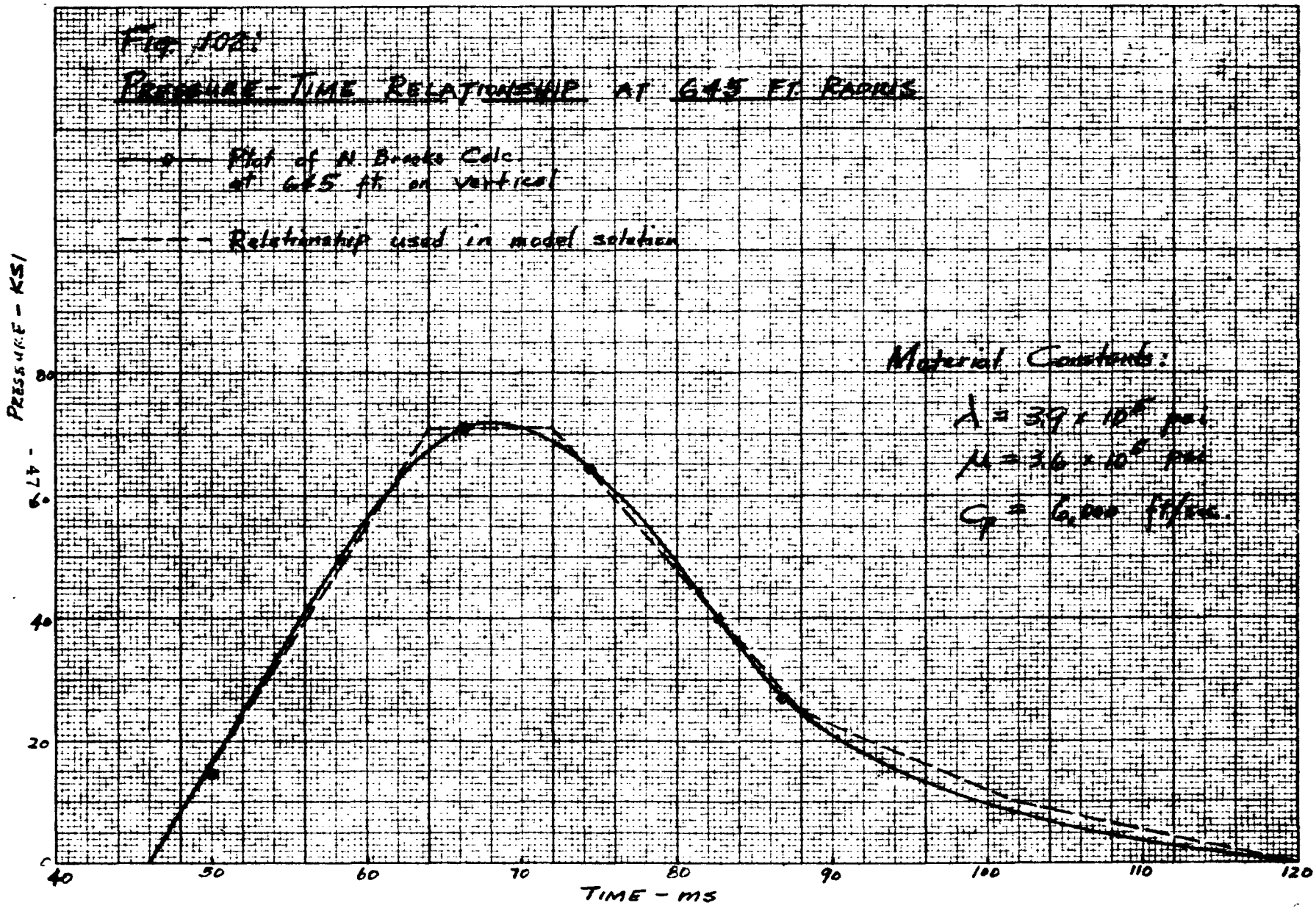

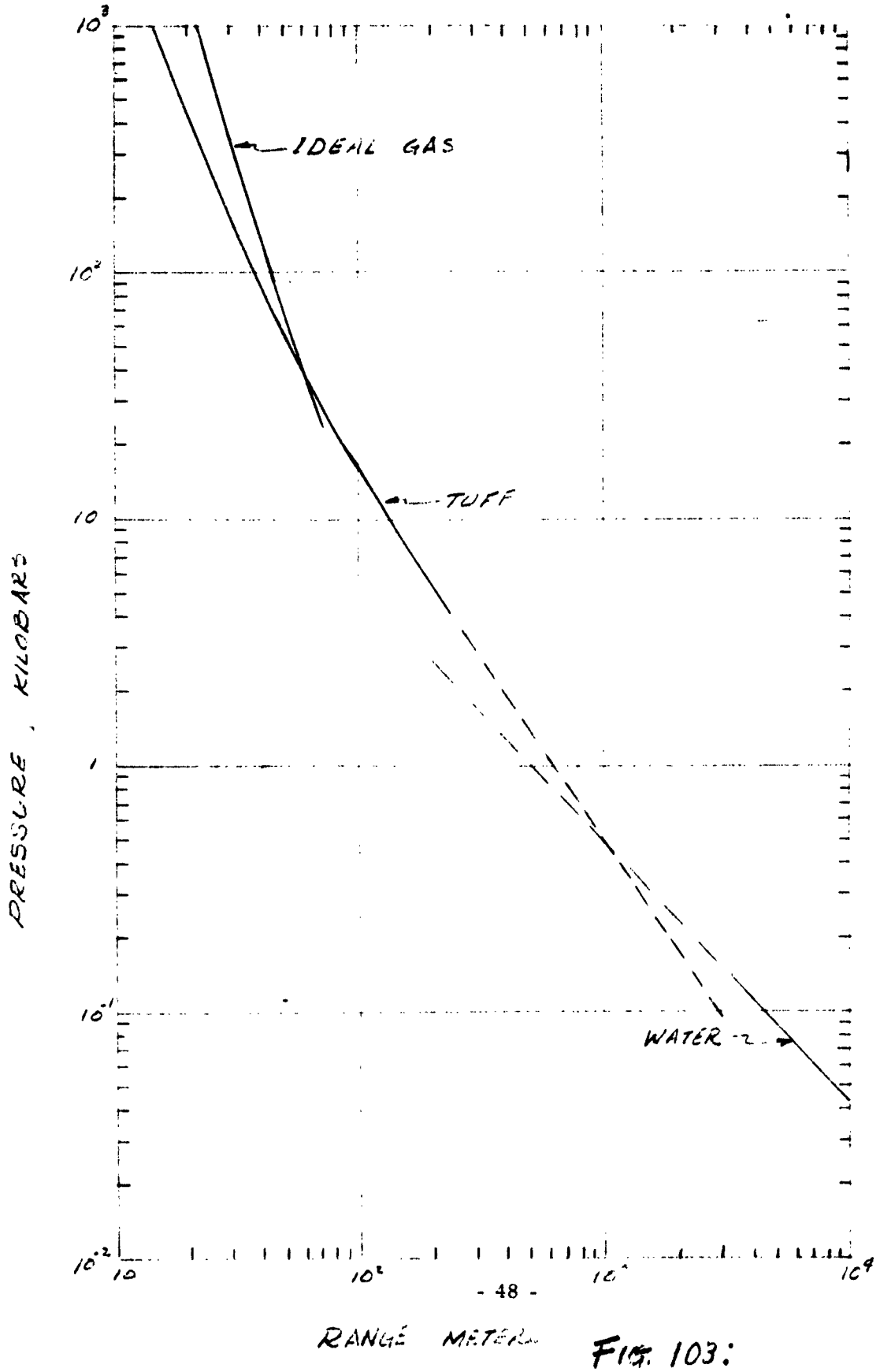
IDEAL GAS
TUFF
WATER
PRESSURE, KILOBARS
RANGE METERS
10^3
10^2
10
1
10^{-1}
10^{-2}
10
10^2
10^3
10^4

FIG. 103:

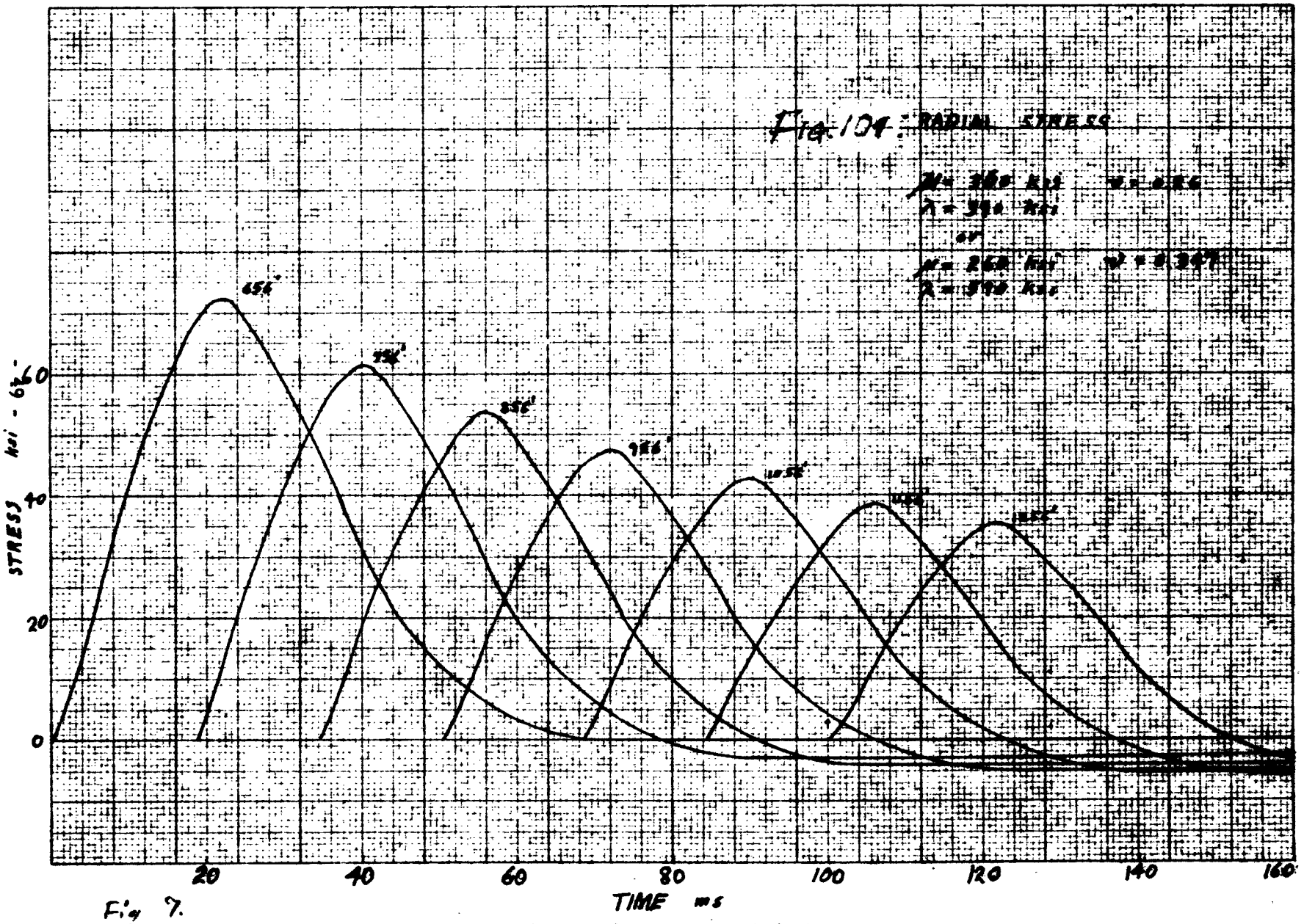
Fig. 10A: RADIAL STRESS
STRESS ksi - 60
0
20
40
60
20
40
60
80
100
120
140
160
TIME ms

Fig 7.

3405 DIET. GRA PER
20 X 20 PER INCH
EUGENE DIETZGEN CO.

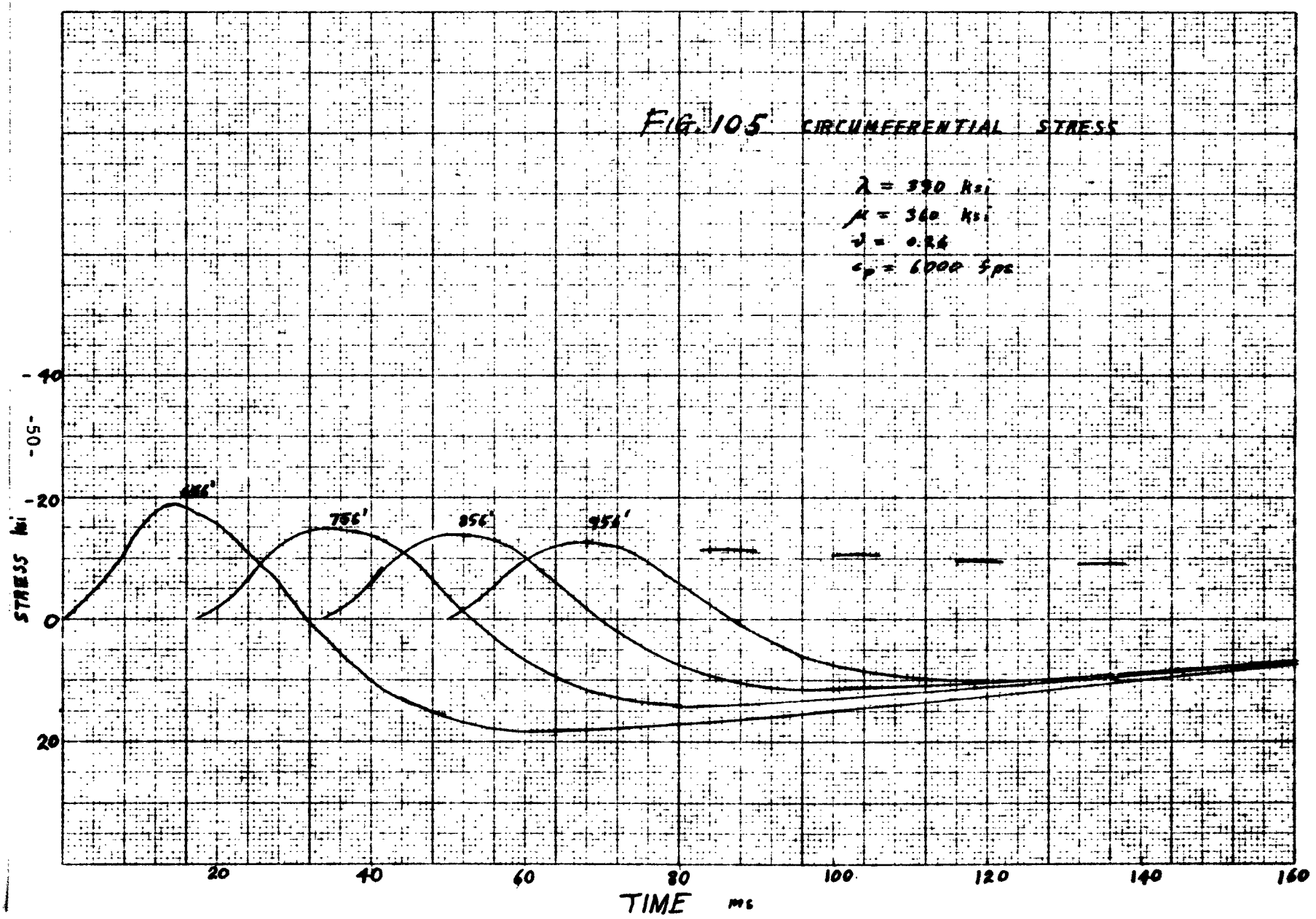

340 DIE GR PAPER
20 X 20 PER INCH
EUGENE DIETZGEN CO.
MADE IN U.S.A.

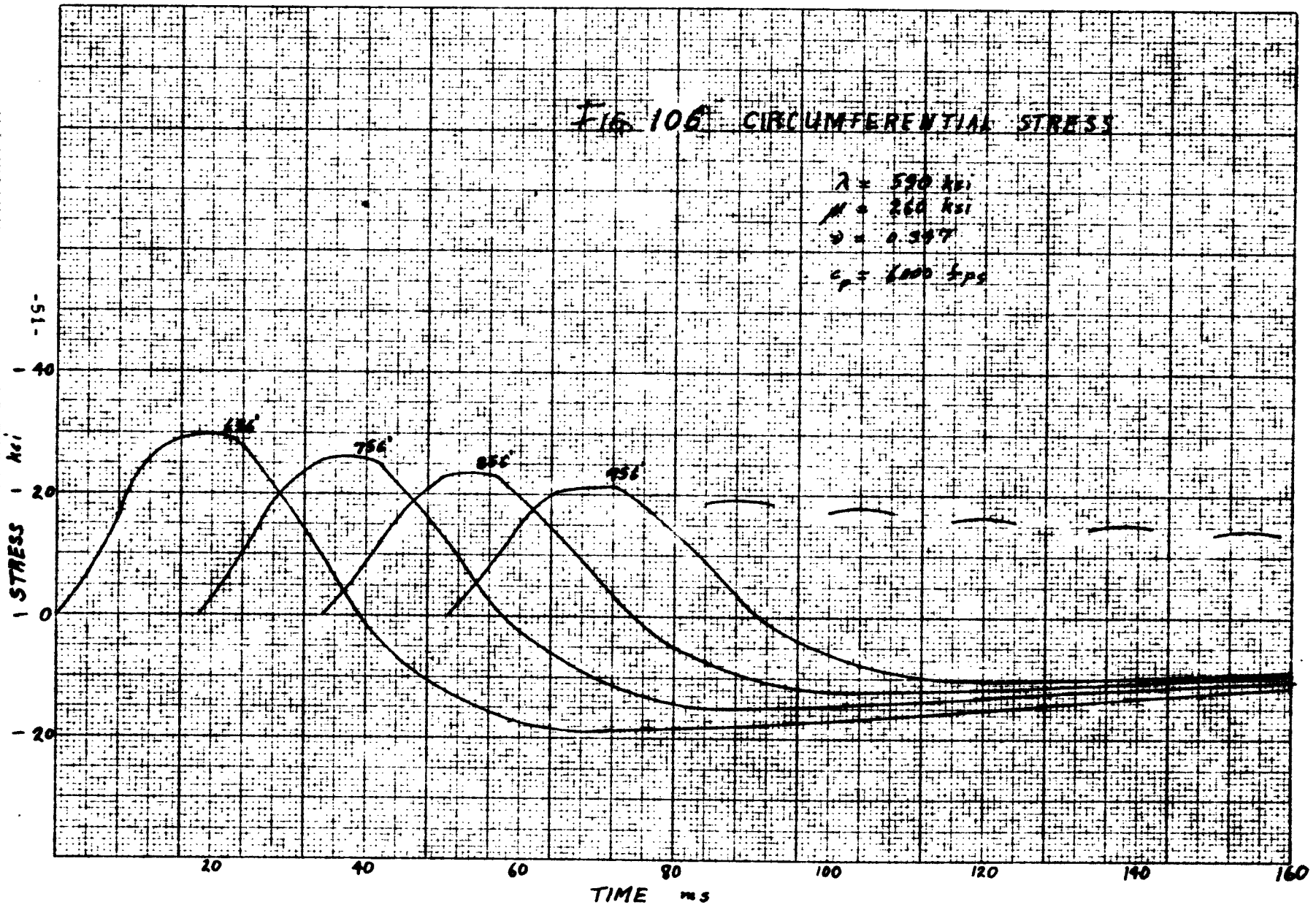

Fig 106 CIRCUMFERENTIAL STRESS

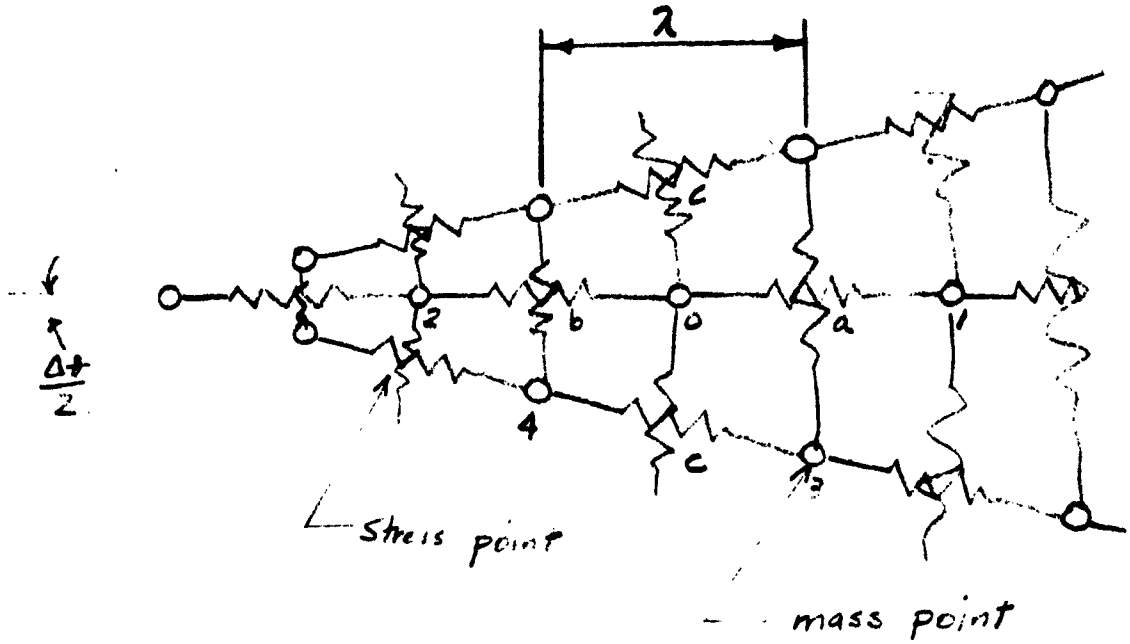

FIG. 107 - SPHERICAL DISCRETE MODEL

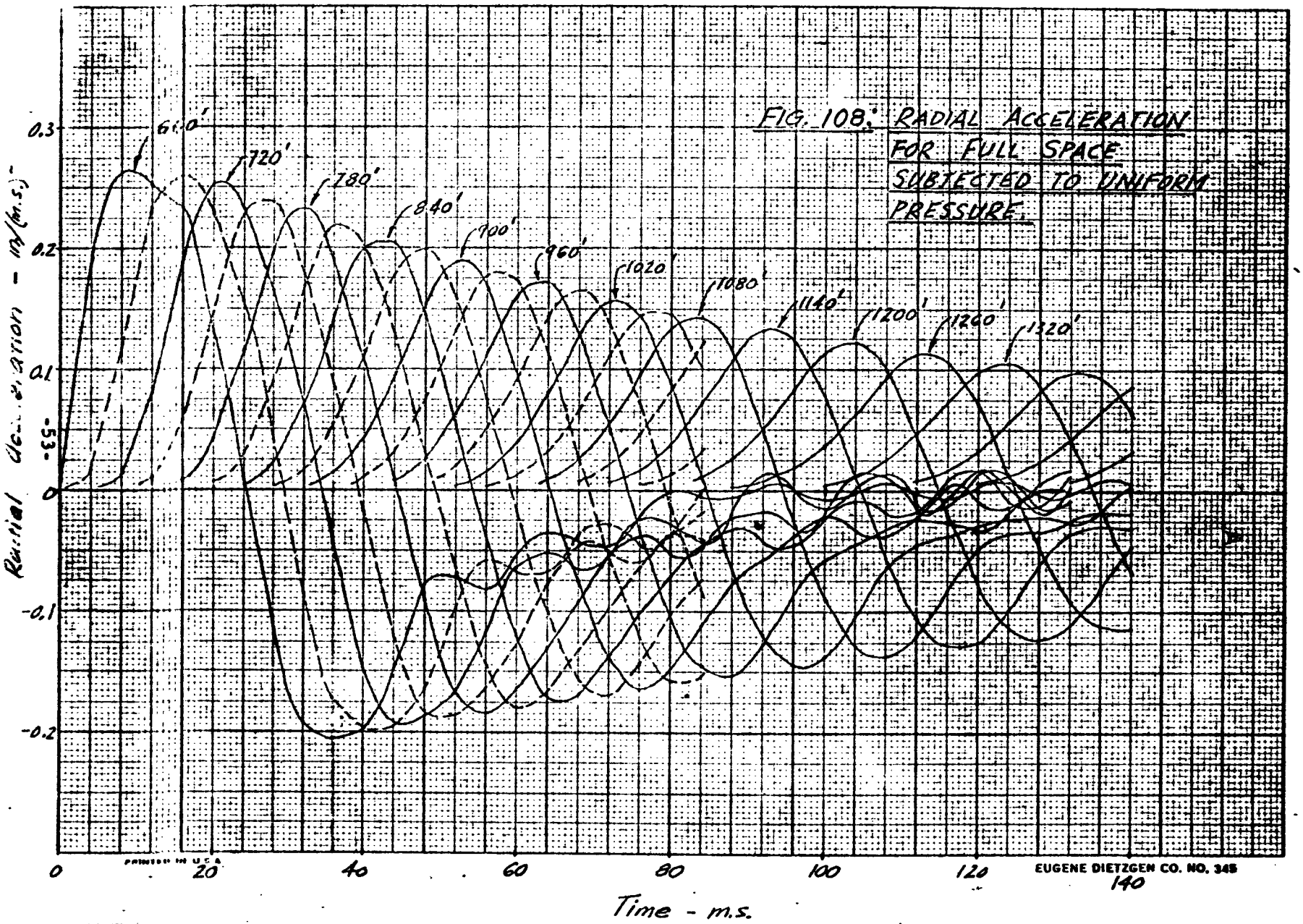

FIG. 108: RADIAL ACCELERATION FOR FULL SPACE SUBJECTED TO UNIFORM PRESSURE.

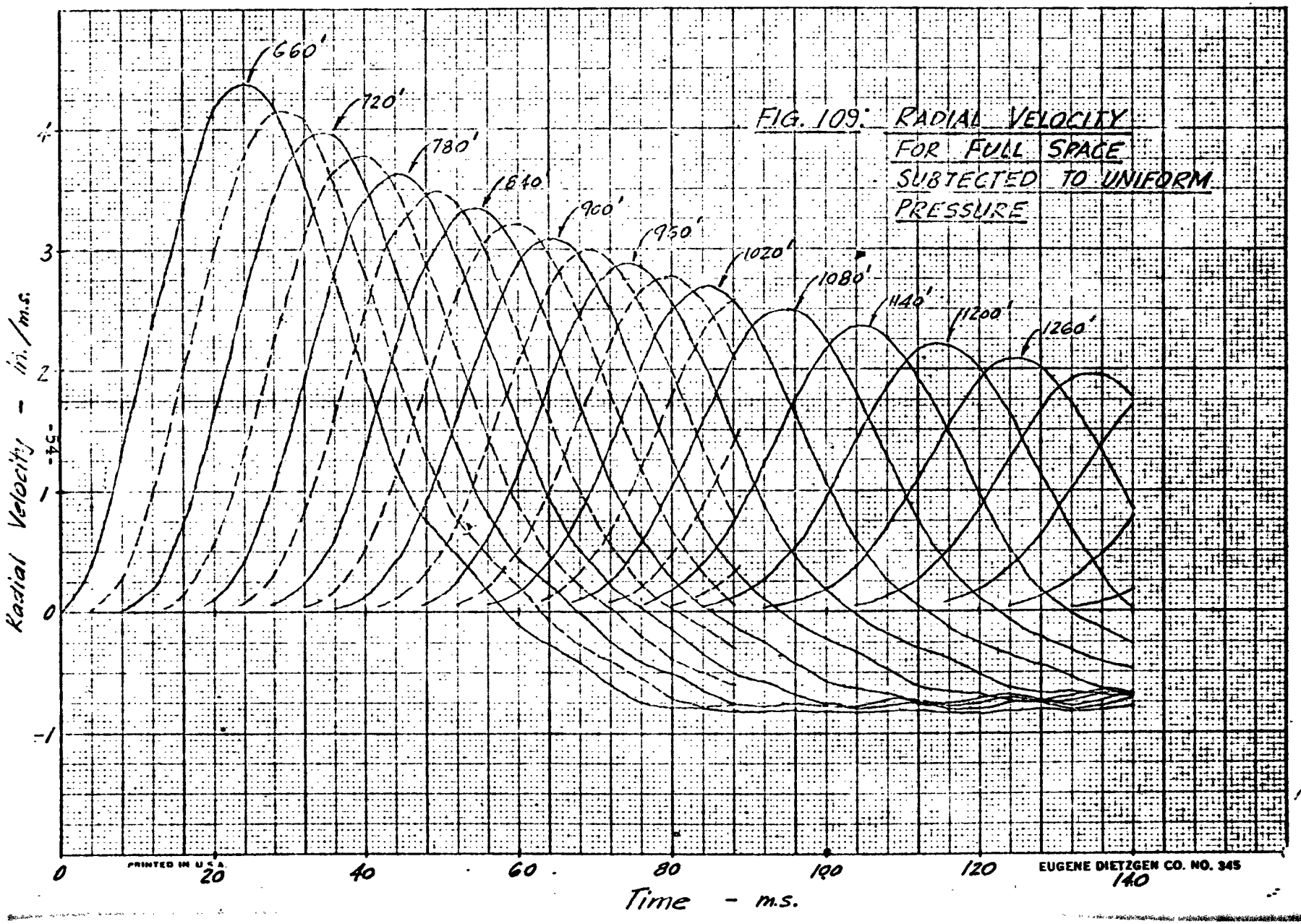

FIG. 109: RADIAL VELOCITY FOR FULL SPACE SUBJECTED TO UNIFORM PRESSURE

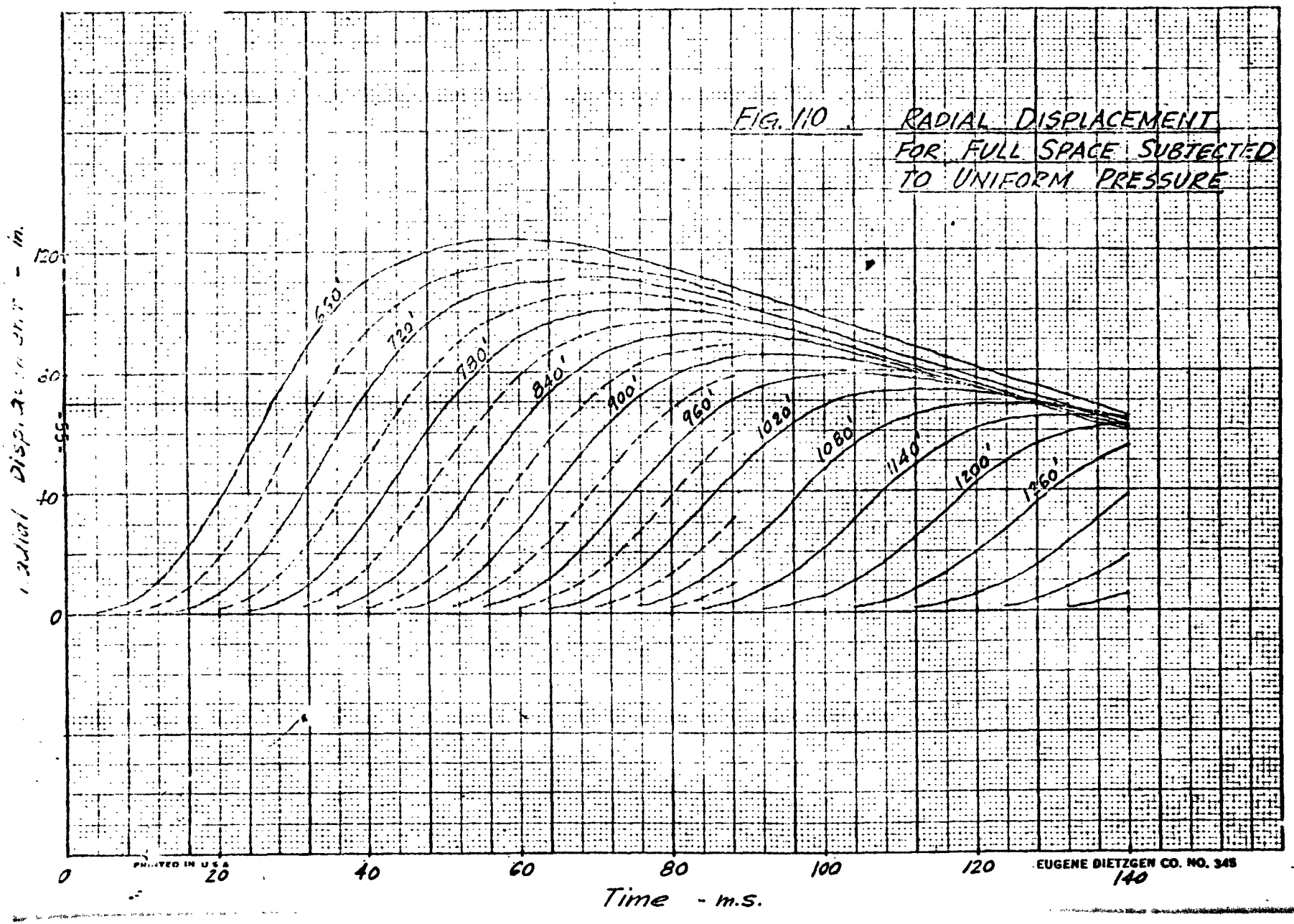
FIG. 110 RADIAL DISPLACEMENT FOR FULL SPACE SUBJECTED TO UNIFORM PRESSURE
Radial Displacement - in.
120
80
40
0
630'
720'
730'
840'
900'
960'
1020'
1080'
1140'
1200'
1260'
0
20
40
60
80
100
120
140
Time - m.s.
PRINTED IN U.S.A.
EUGENE DIETZGEN CO. NO. 348

NO. 341-20 DIETZGEN GRAPH PAPER
20 X 20 PER INCH
EUGENE DIETZGEN CO.
MADE IN U. S. A.

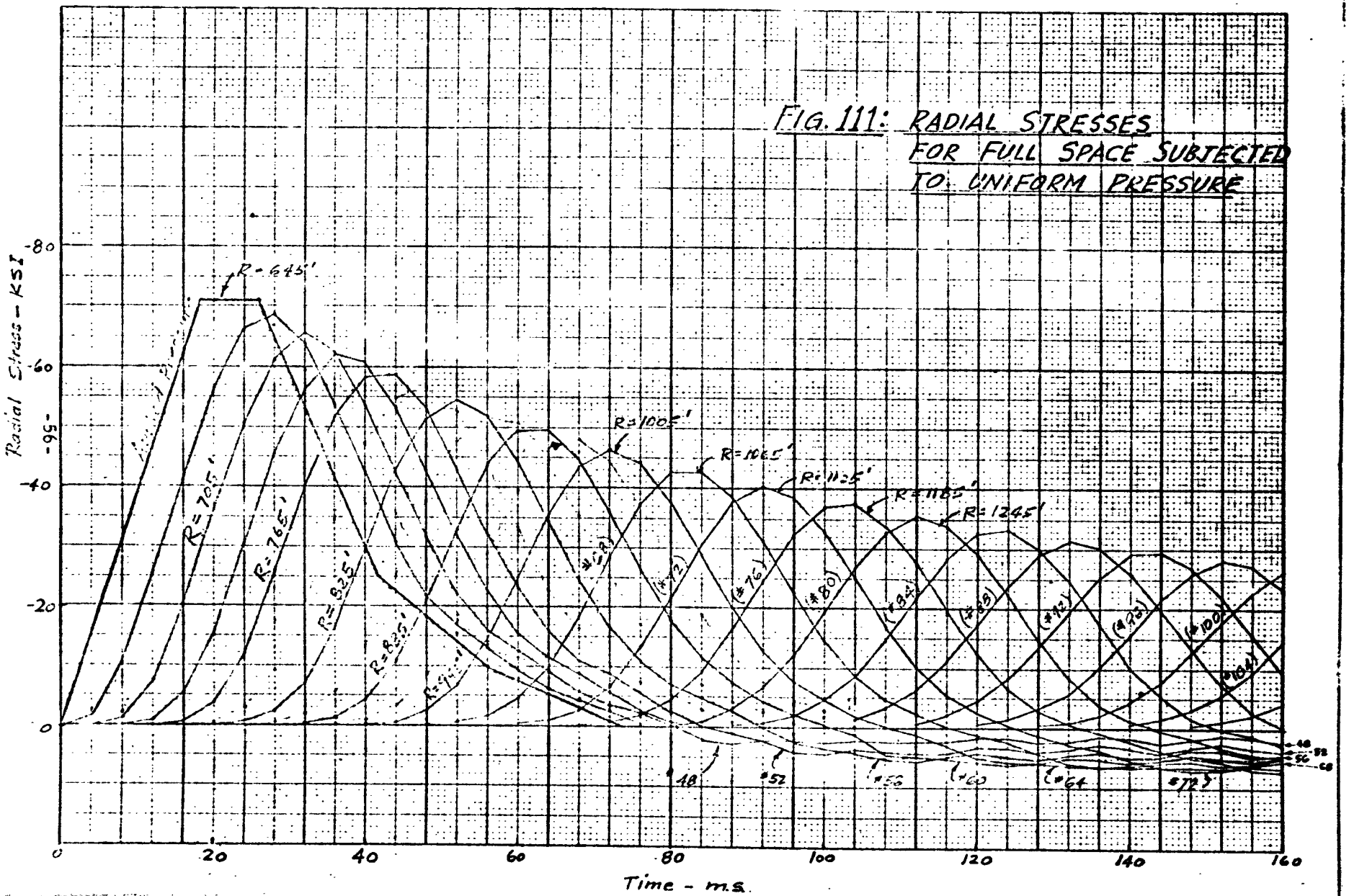

FIG. 111: RADIAL STRESSES FOR FULL SPACE SUBJECTED TO UNIFORM PRESSURE

NO. 341-20 DIETZGEN GRAPH PAPER
20 X 20 PER INCH
EUGENE DIETZGEN CO.
MADE IN U. S. A.

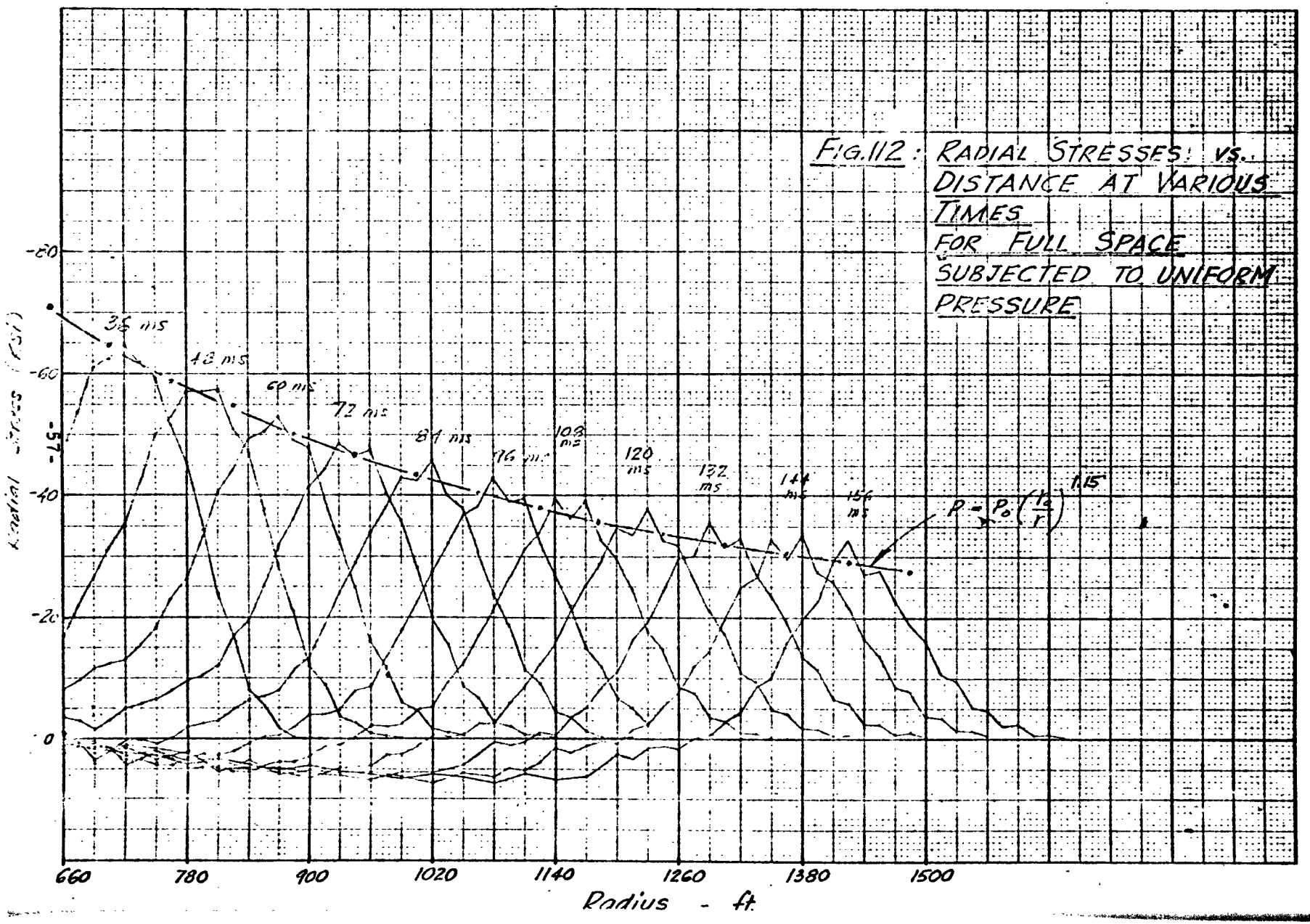

NO. 341-20 DIETZGEN GRAPH PAPER
20 X 20 PER INCH
EUGENE DIETZGEN CO.
MADE IN U. S. A.

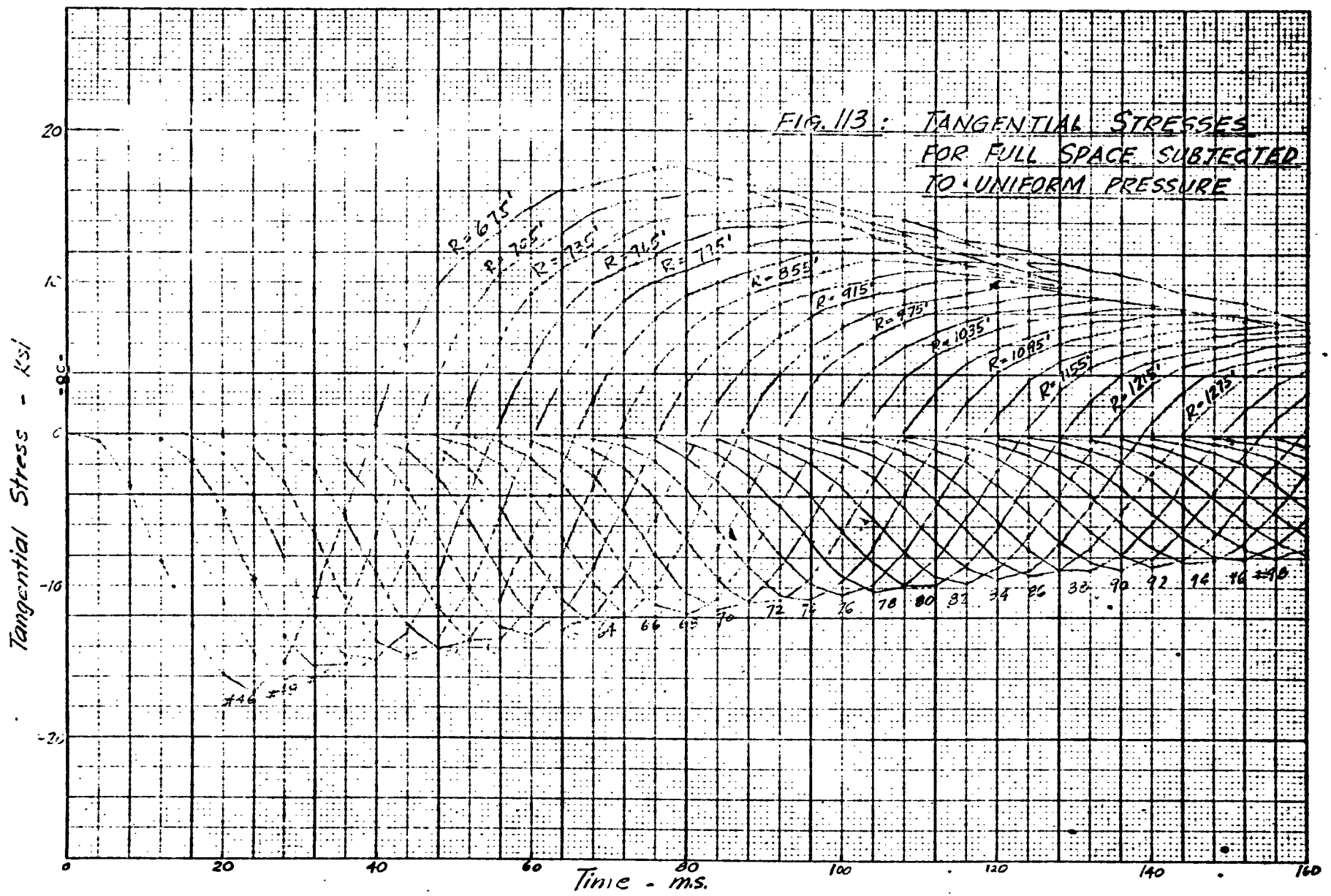

NO. 341-20 DIETZGEN GRAPH PAPER
20 X 20 PER INCH

EUGENE DIETZGEN CO.
MADE IN U. S. A.

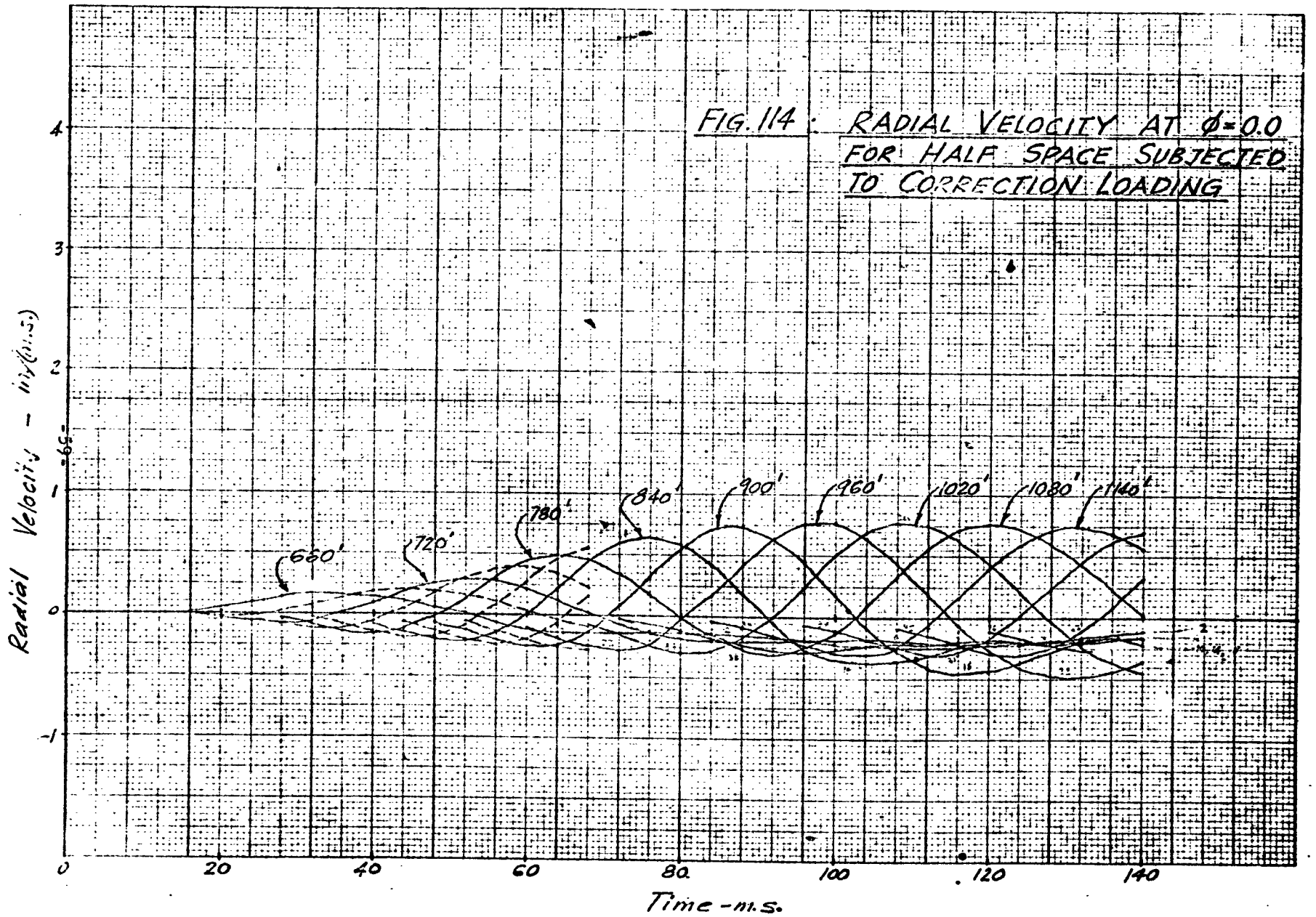

FIG. 114: RADIAL VELOCITY AT $\phi = 0.0$ FOR HALF SPACE SUBJECTED TO CORRECTION LOADING

NO. 341-20 DIETZGEN GRAPH PAPER
20 X 20 PER INCH

EUGENE DIETZGEN CO.
MADE IN U. S. A.

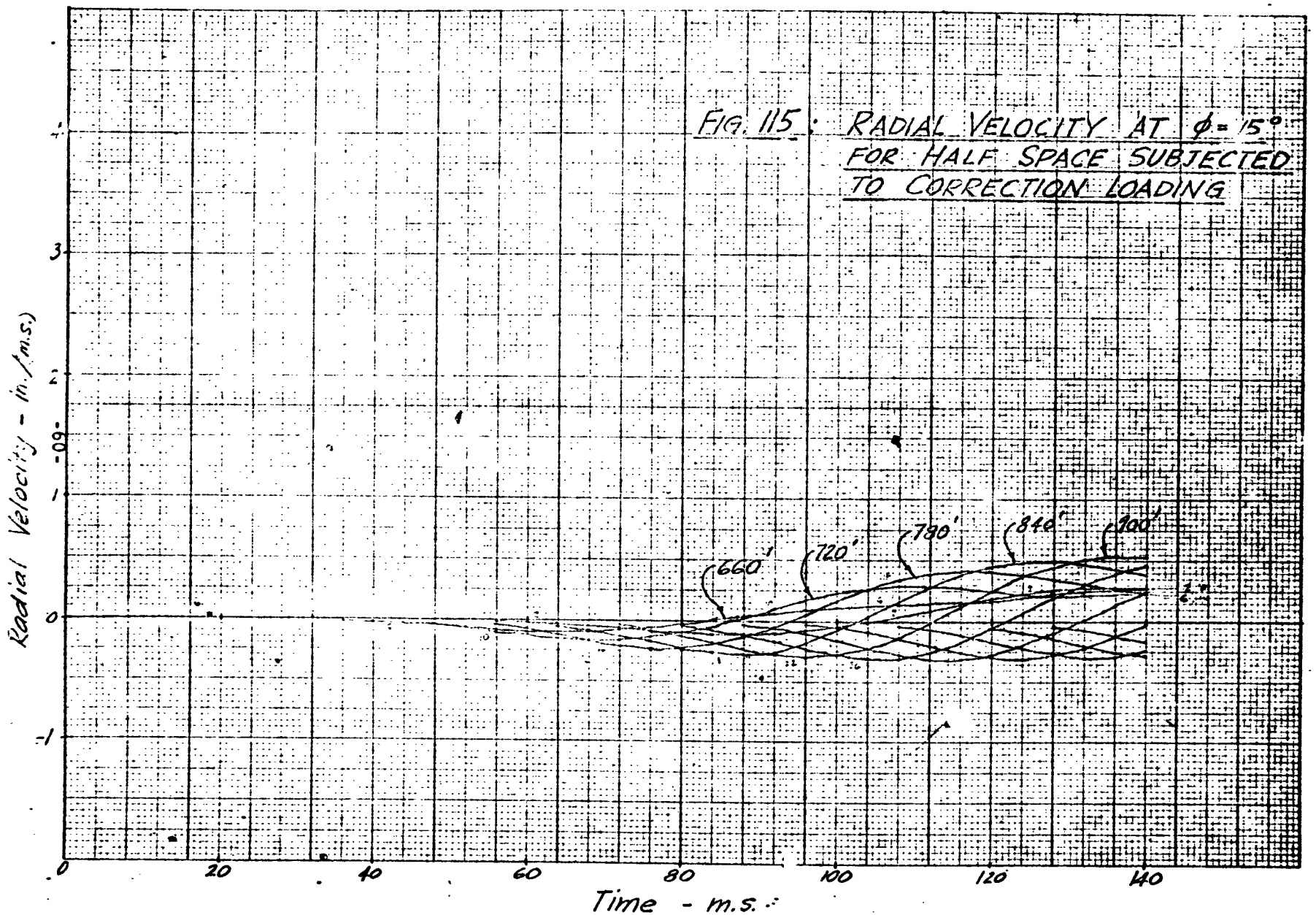

FIG. 115: RADIAL VELOCITY AT $\phi = 15°$ FOR HALF SPACE SUBJECTED TO CORRECTION LOADING

NO. 341-20 DIETZGEN GRAPH PAPER
20 X 20 PER INCH
EUGENE DIETZGEN CO.
MADE IN U. S. A.

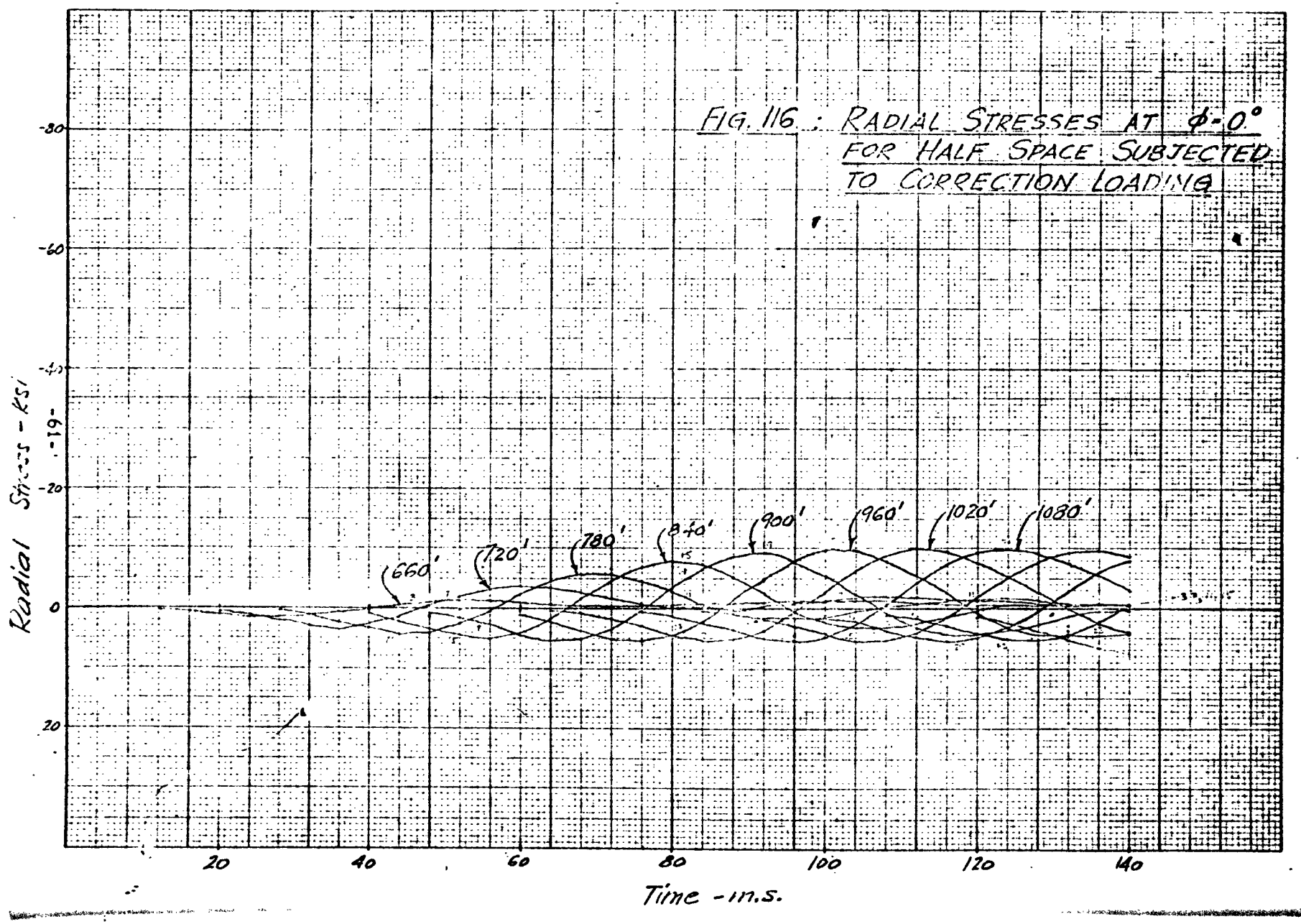

NO. 341-20 DIETZGEN GRAPH PAPER
20 X 20 PER INCH

EUGENE DIETZGEN CO.
MADE IN U. S. A.

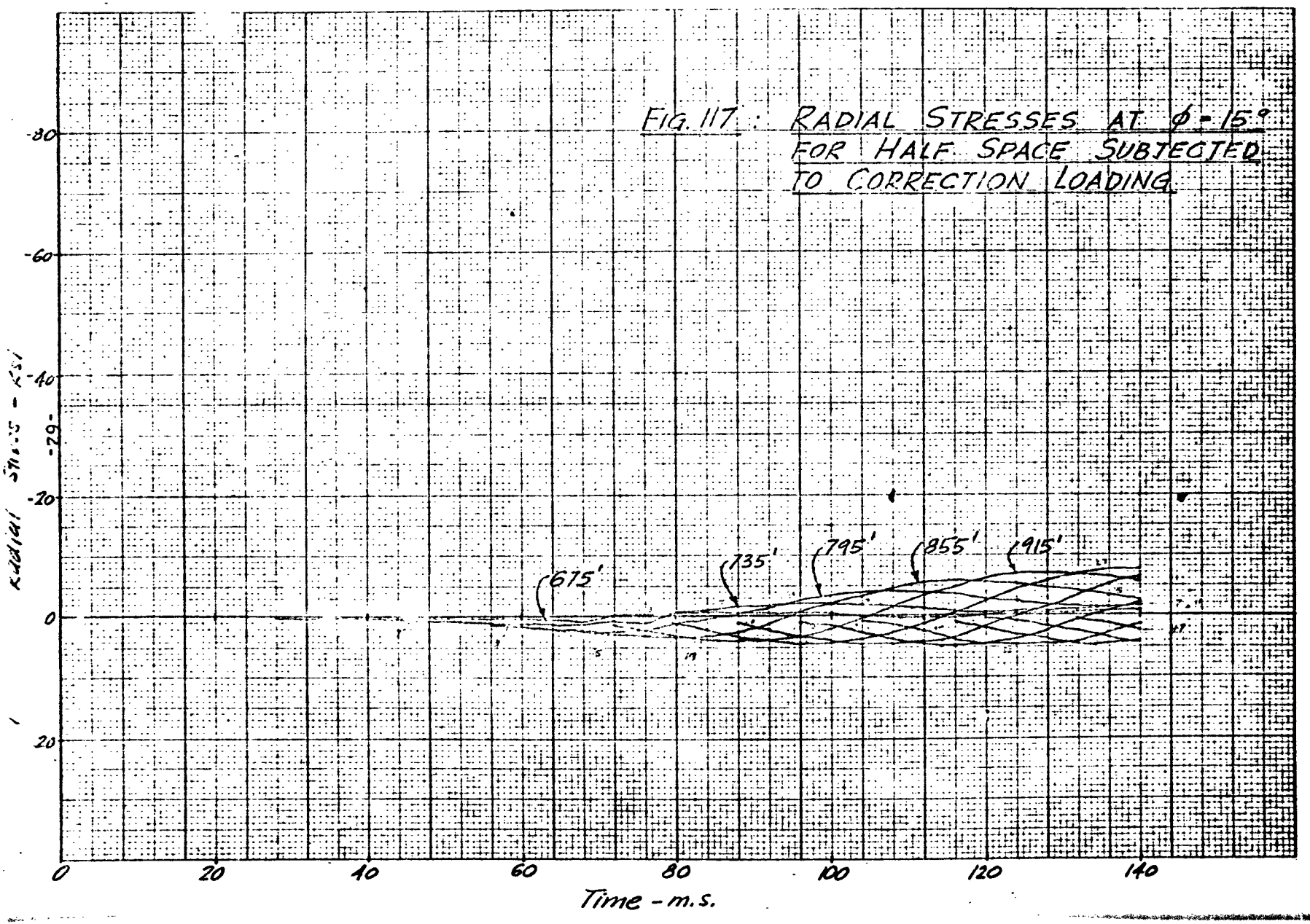

FIG. 117: RADIAL STRESSES AT $\phi = 15°$ FOR HALF SPACE SUBJECTED TO CORRECTION LOADING

NO. 341-20 DIETZGEN GRAPH PAPER
20 X 20 PER INCH

EUGENE DIETZGEN CO.
MADE IN U. S. A.

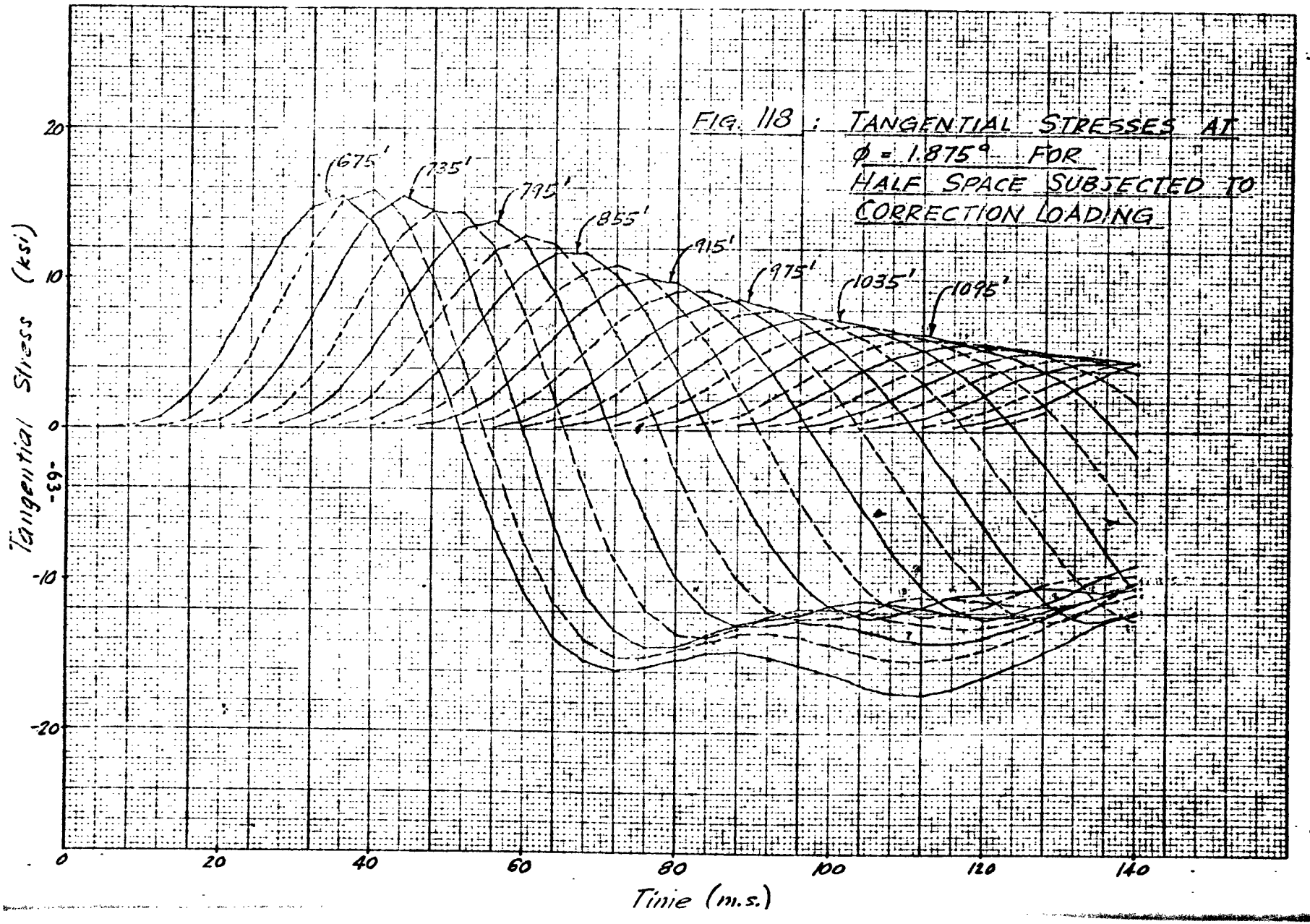

FIG. 118 : TANGENTIAL STRESSES AT $\phi = 1.875°$ FOR HALF SPACE SUBJECTED TO CORRECTION LOADING

NO. 341-20 DIETZGEN GRAPH PAPER
20 X 20 PER INCH

EUGENE DIETZGEN CO.
MADE IN U. S. A.

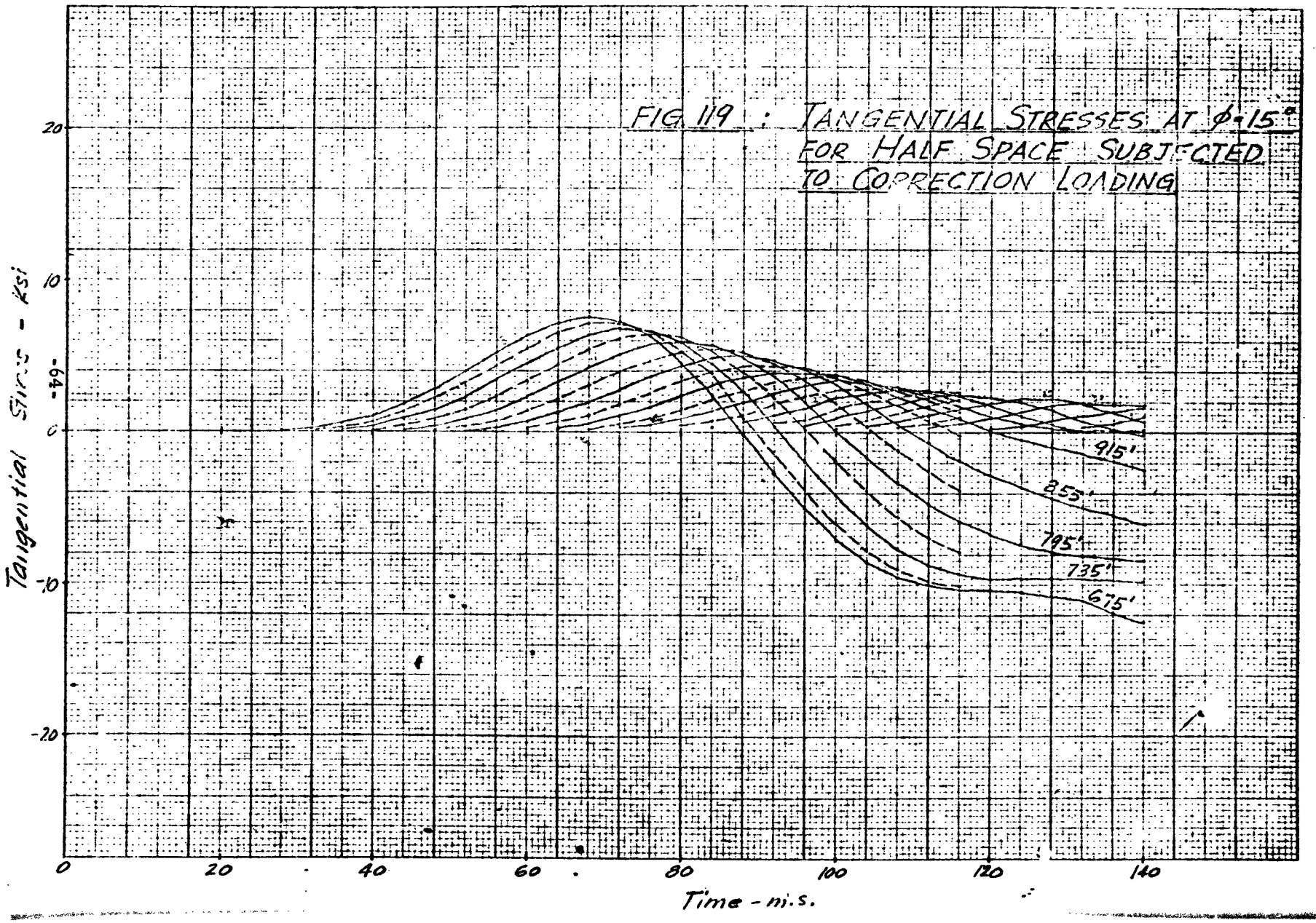

NO. 341-20 DIETZGEN GRAPH PAPER
20 X 20 PER INCH

EUGENE DIETZGEN CO.
MADE IN U. S. A.

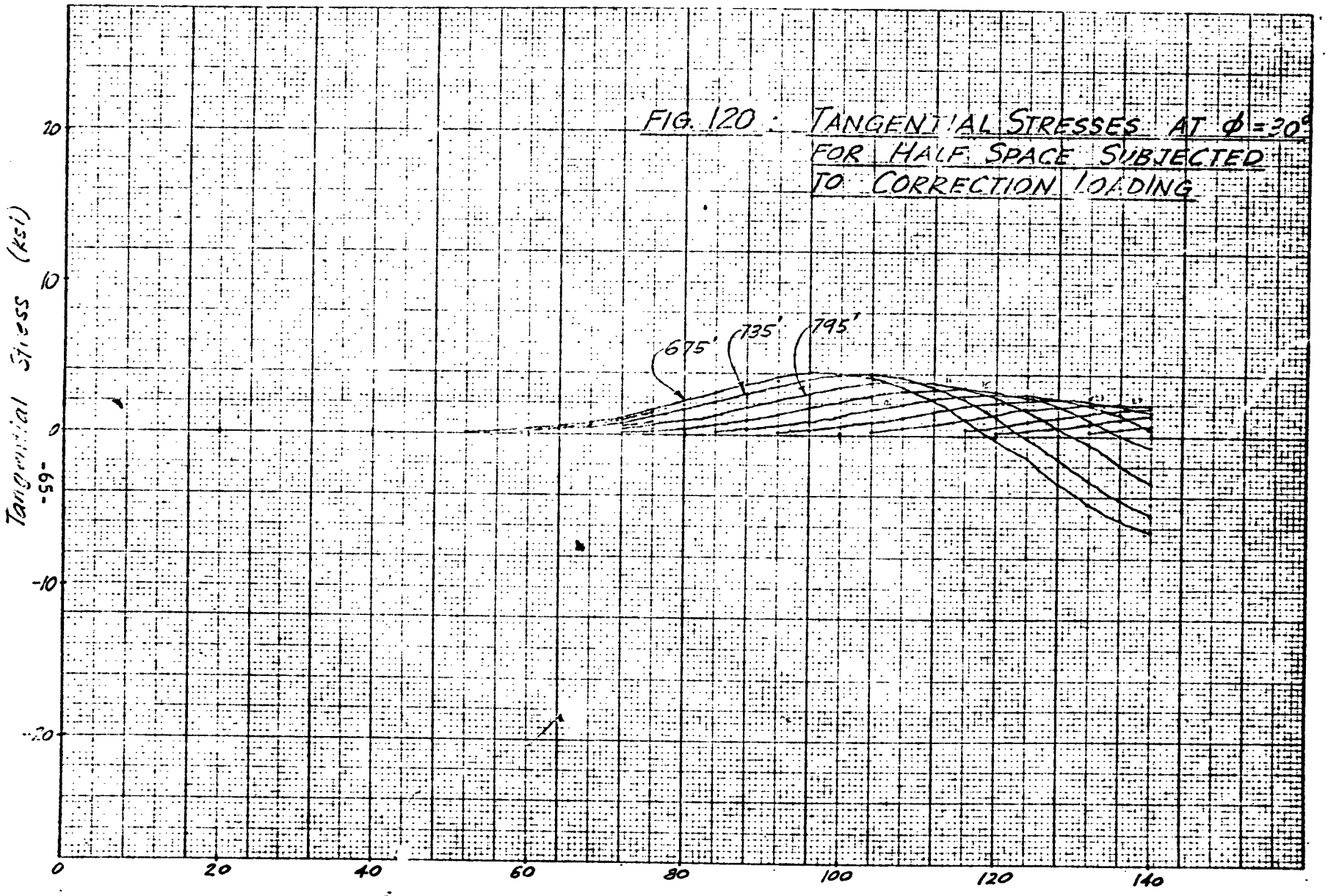

FIG. 120 : TANGENTIAL STRESSES AT $\phi = 30°$ FOR HALF SPACE SUBJECTED TO CORRECTION LOADING

NO. 341-20 DIETZGEN GRAPH PAPER
20 X 20 PER INCH
EUGENE DIETZGEN CO.
MADE IN U. S. A.

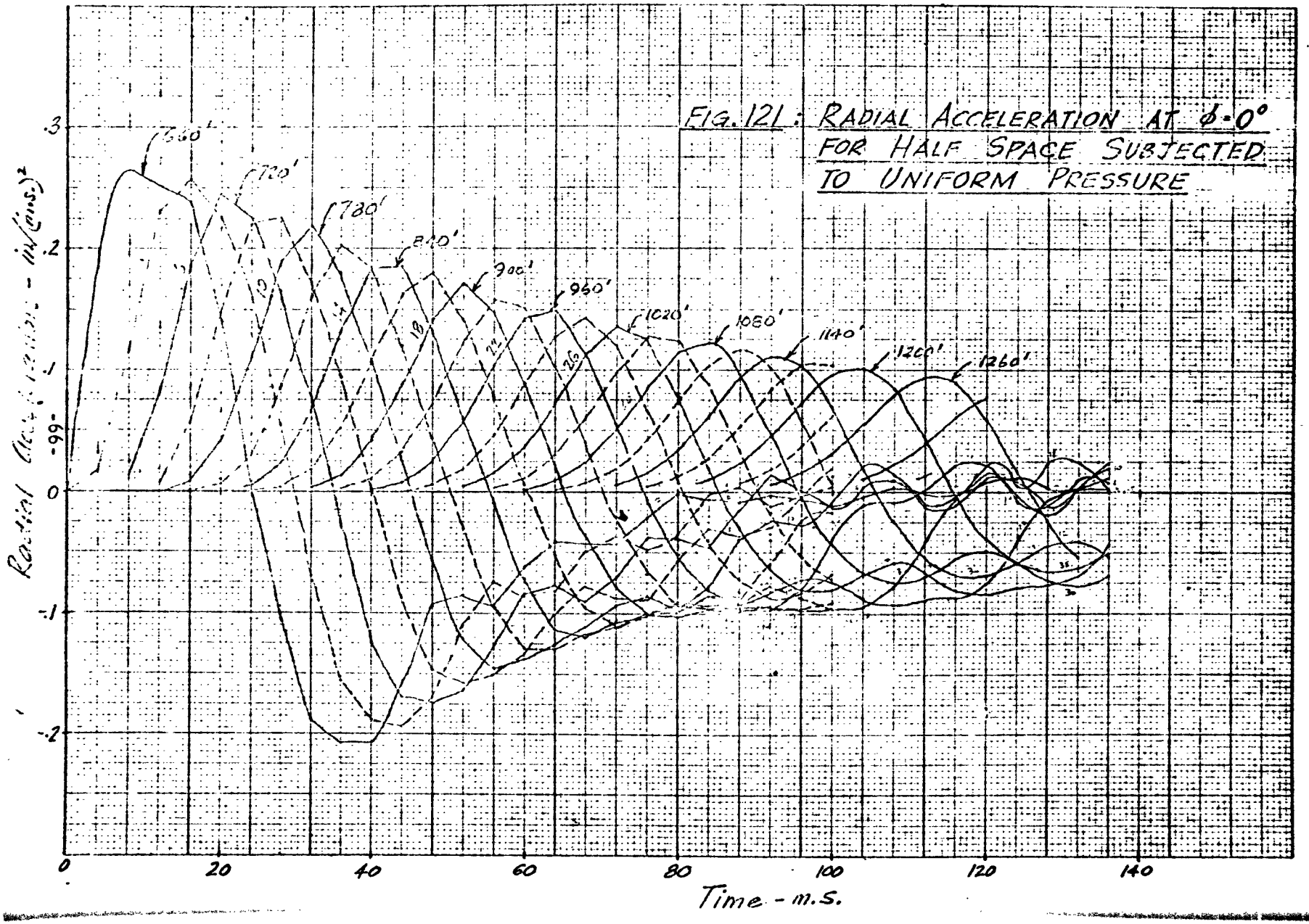

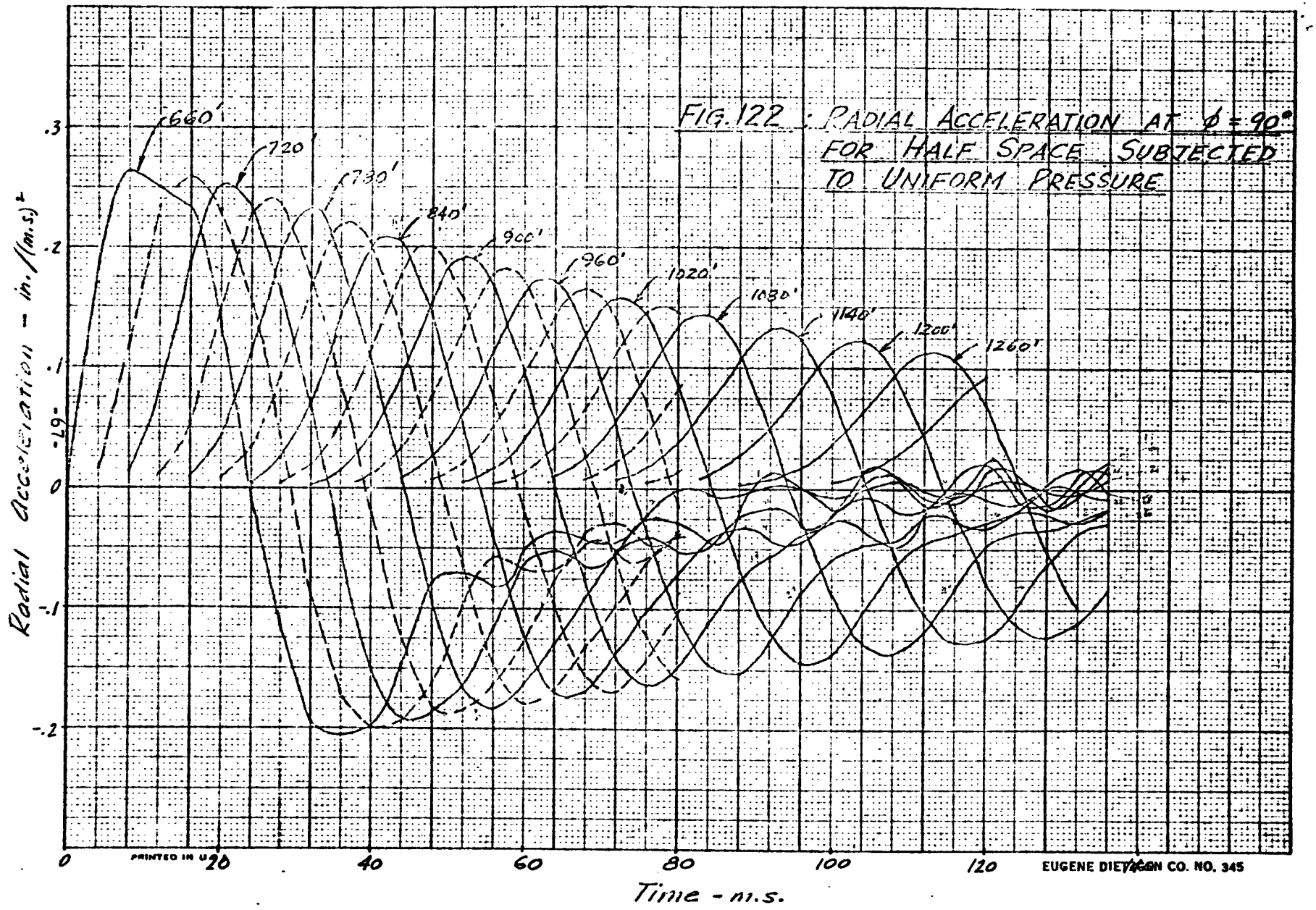

FIG. 122: RADIAL ACCELERATION AT $\phi = 90°$ FOR HALF SPACE SUBJECTED TO UNIFORM PRESSURE

NO. 341-20 DIETZGEN GRAPH PAPER
20 X 20 PER INCH

EUGENE DIETZGEN CO.
MADE IN U. S. A.

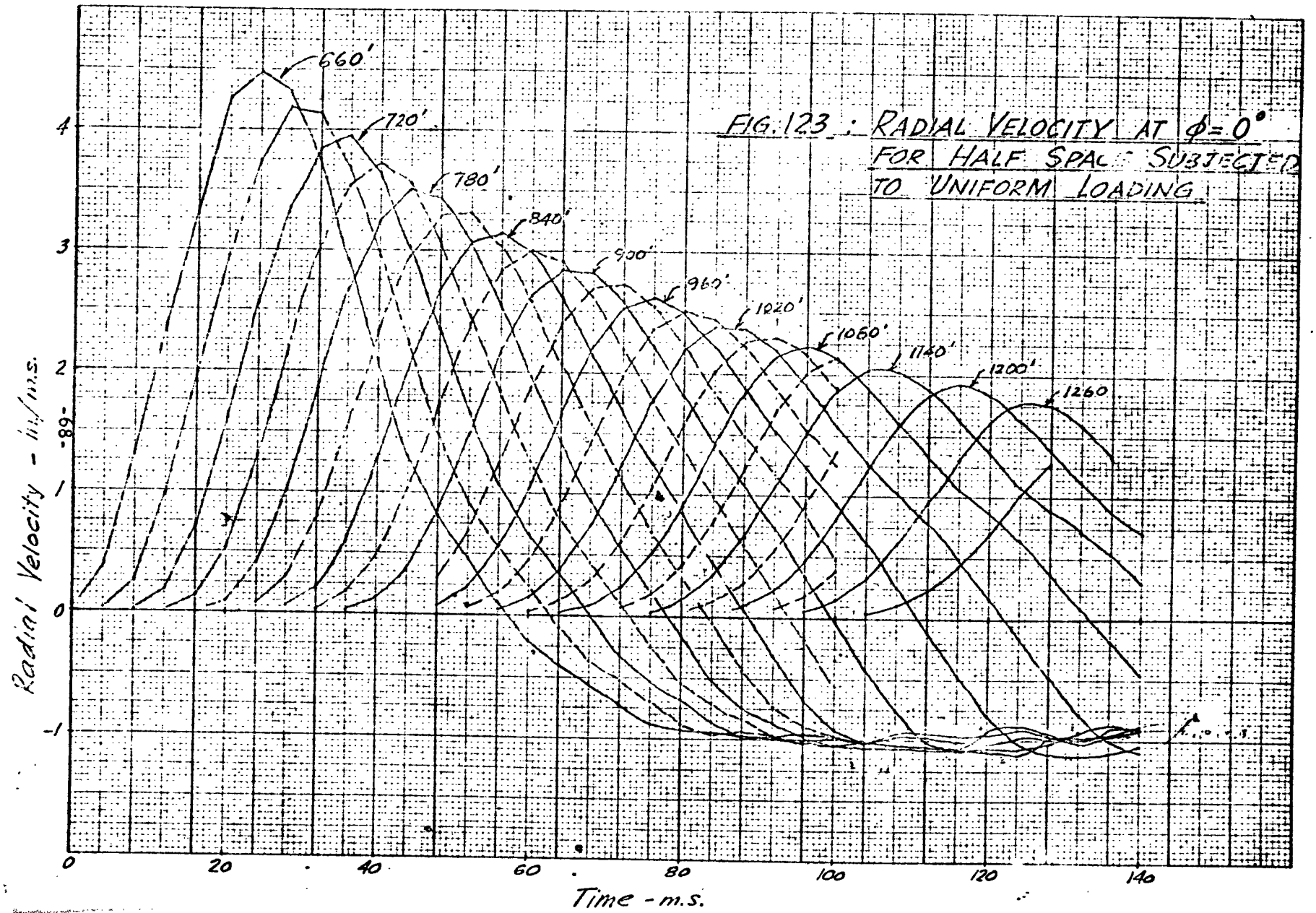

FIG. 123 : RADIAL VELOCITY AT $\phi = 0°$ FOR HALF SPACE SUBJECTED TO UNIFORM LOADING

NO. 341-20 DIETZGEN GRAPH PAPER
20 X 20 PER INCH

EUGENE DIETZGEN CO.
MADE IN U. S. A.

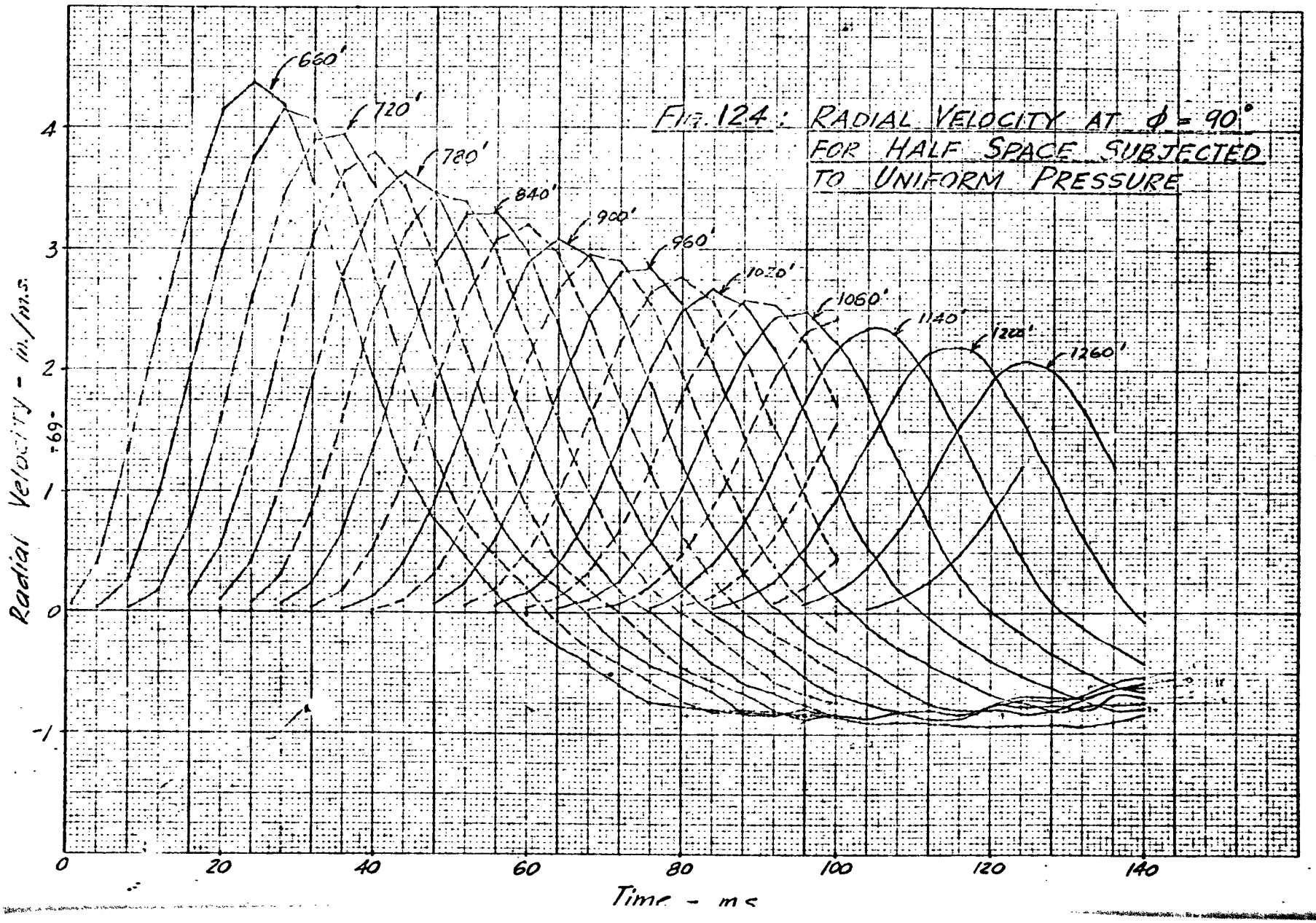

FIG. 124: RADIAL VELOCITY AT $\phi = 90°$ FOR HALF SPACE SUBJECTED TO UNIFORM PRESSURE

NO. 341-20 DIETZGEN GRAPH PAPER
20 X 20 PER INCH

EUGENE DIETZGEN CO.
MADE IN U. S. A.

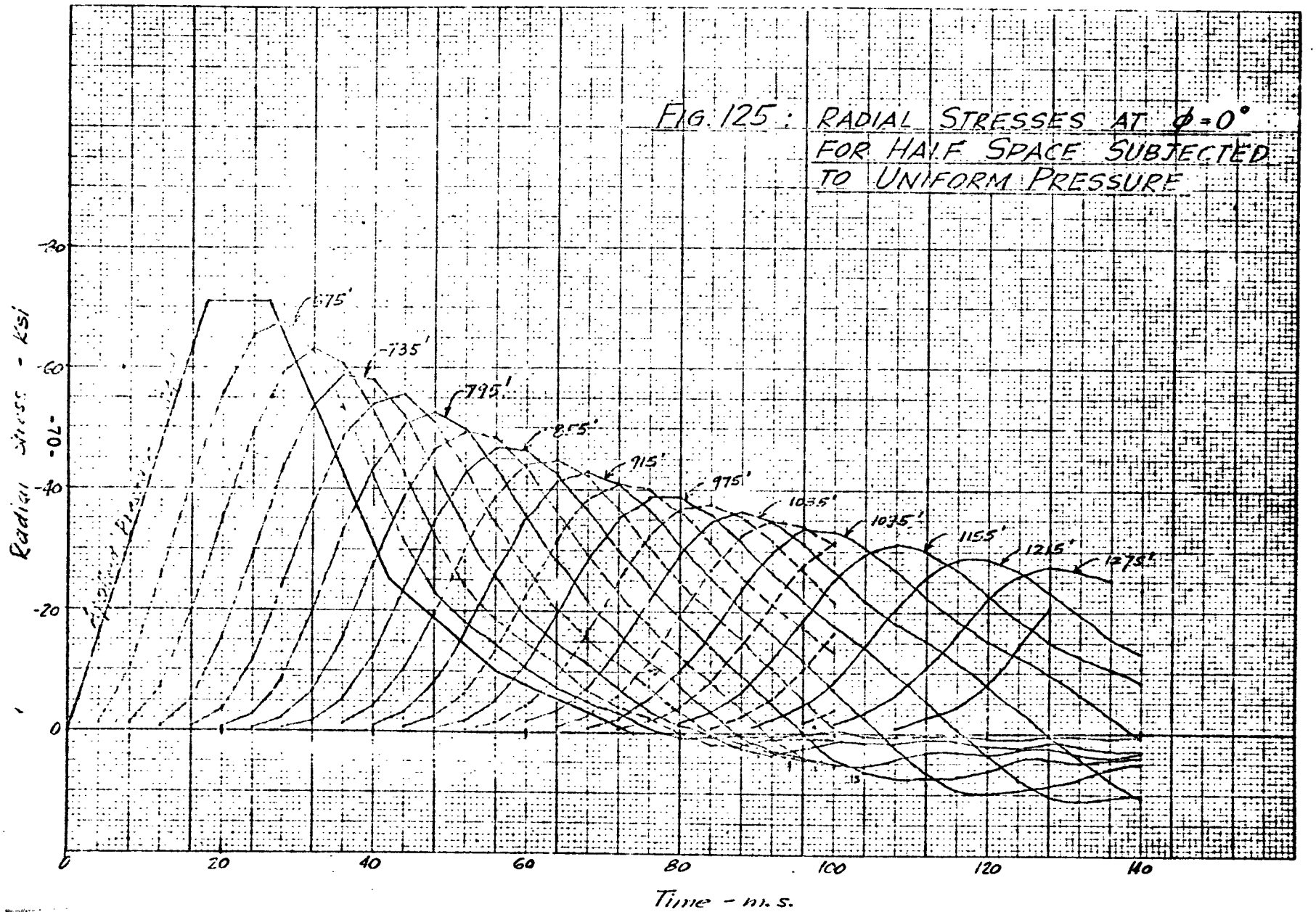

NO. 341-20 DIETZGEN GRAPH PAPER
20 X 20 PER INCH

EUGENE DIETZGEN CO.
MADE IN U. S. A.

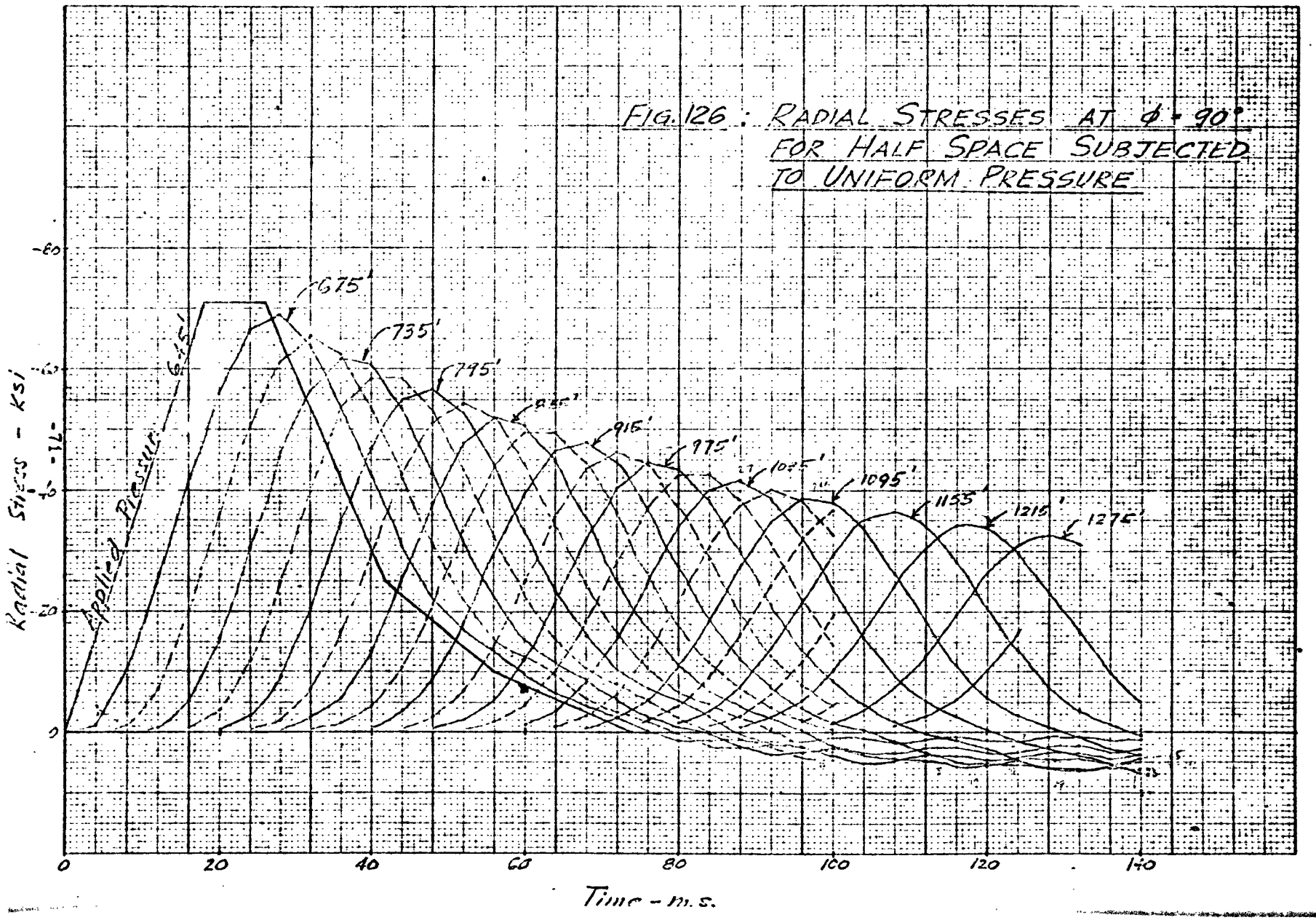

FIG. 126: RADIAL STRESSES AT $\phi = 90°$ FOR HALF SPACE SUBJECTED TO UNIFORM PRESSURE

NO. 341-20 DIETZGEN GRAPH PAPER
20 X 20 PER INCH

EUGENE DIETZGEN CO.
MADE IN U. S. A.

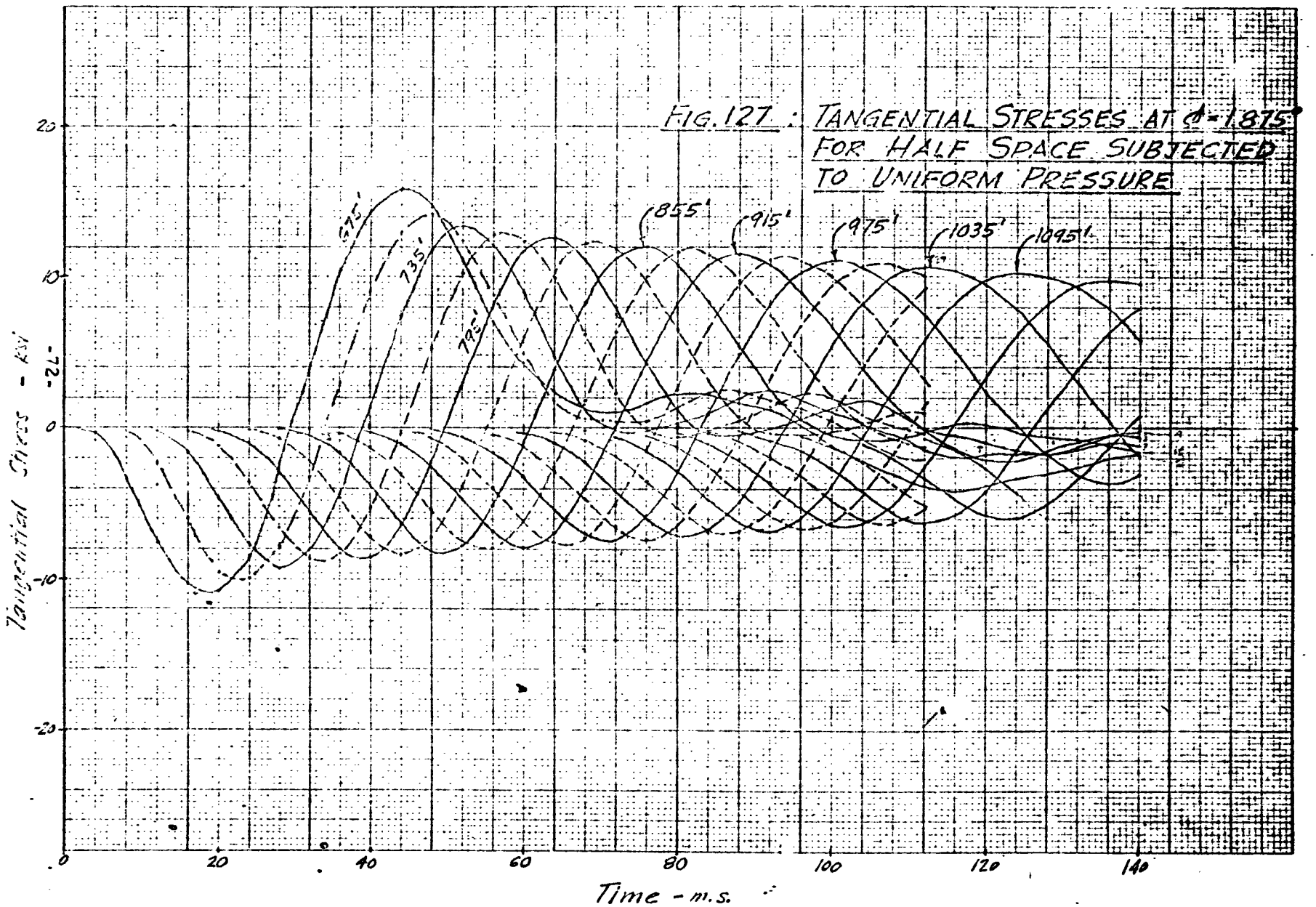

FIG. 127 : TANGENTIAL STRESSES AT $\phi = 1.875$ FOR HALF SPACE SUBJECTED TO UNIFORM PRESSURE

NO. 341-20 DIETZGEN GRAPH PAPER
20 X 20 PER INCH

EUGENE DIETZGEN CO.
MADE IN U. S. A.

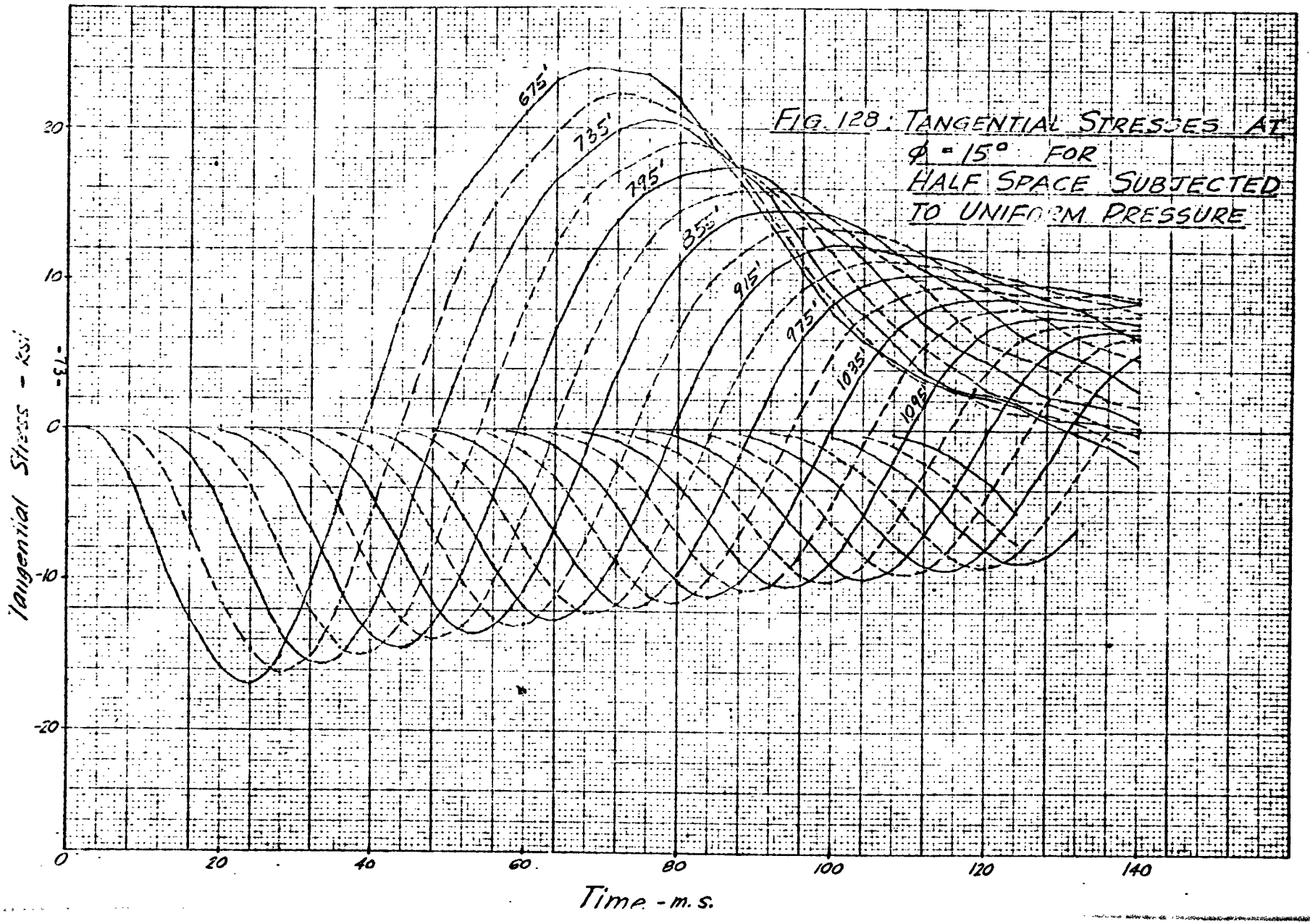

FIG. 128: TANGENTIAL STRESSES AT $\phi = 15°$ FOR HALF SPACE SUBJECTED TO UNIFORM PRESSURE

NO. 341-20 DIETZGEN GRAPH PAPER
20 X 20 PER INCH

EUGENE DIETZGEN CO.
MADE IN U. S. A.

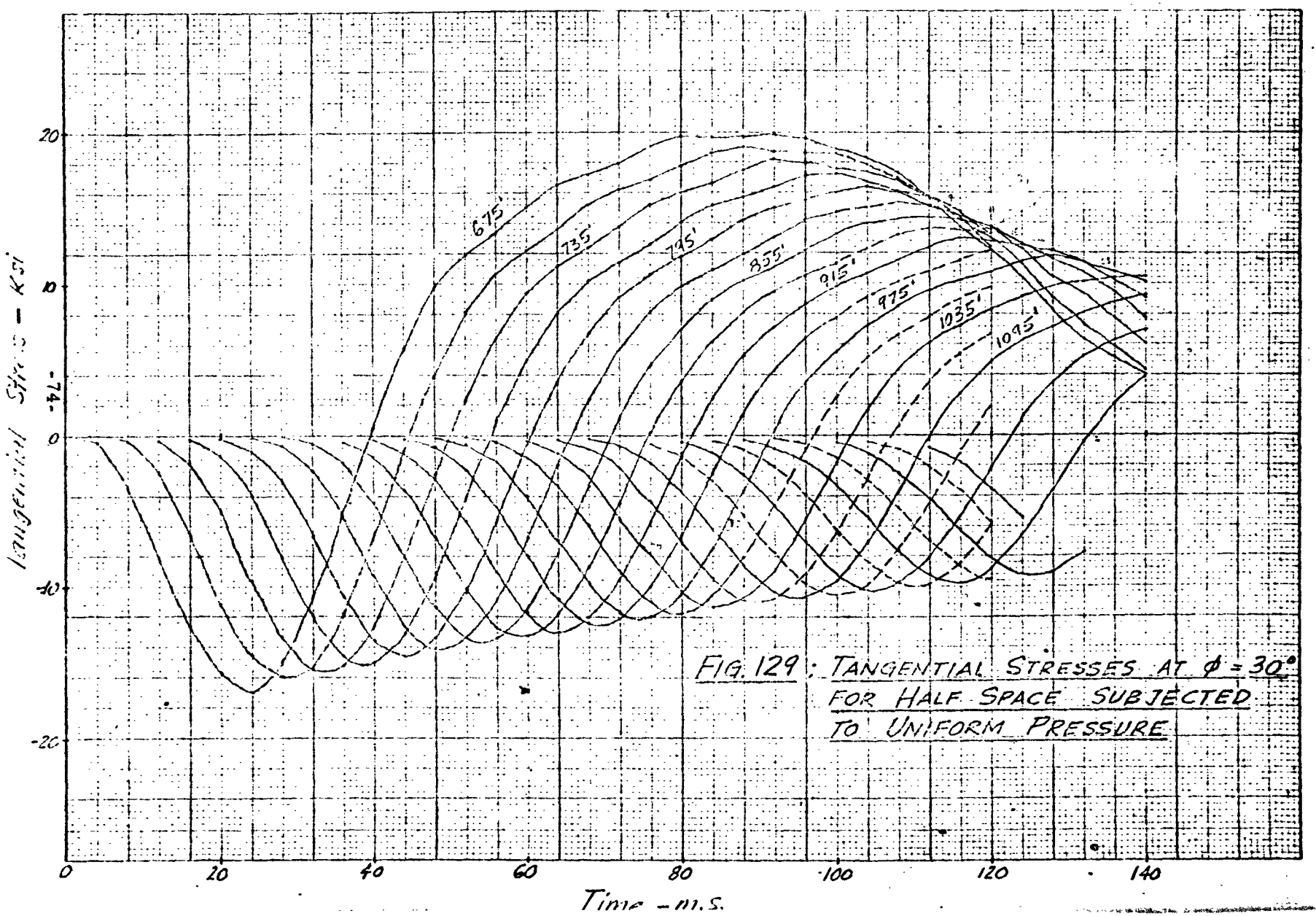

FIG. 129: TANGENTIAL STRESSES AT $\phi = 30°$ FOR HALF SPACE SUBJECTED TO UNIFORM PRESSURE

NO. 341-20 DIETZGEN GRAPH PAPER
20 X 20 PER INCH
EUGENE DIETZGEN CO.
MADE IN U. S. A.

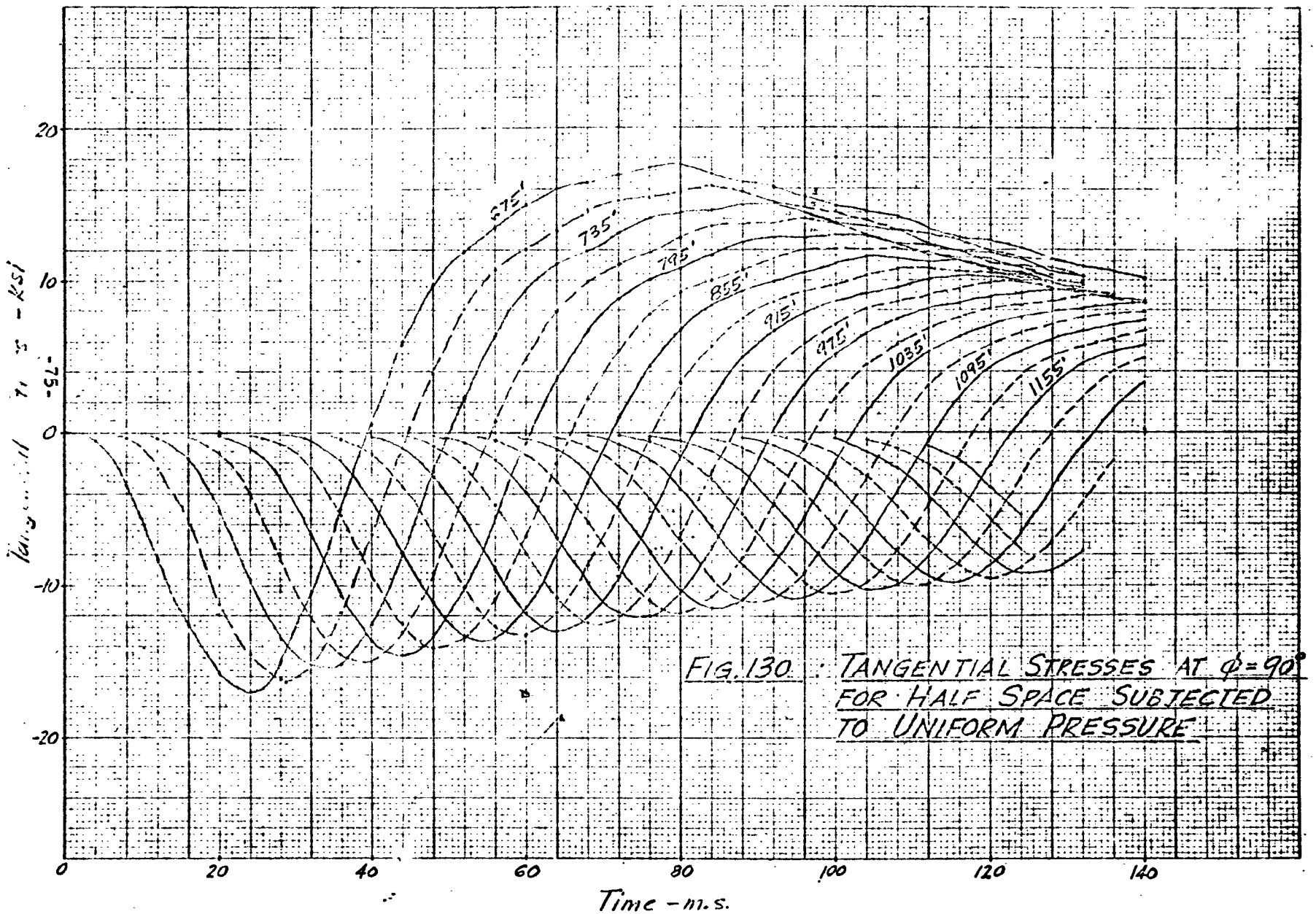

FIG. 130 : TANGENTIAL STRESSES AT $\phi = 90°$ FOR HALF SPACE SUBJECTED TO UNIFORM PRESSURE

NO. 340-L21 DIETZGEN GRAPH PAPER
LOGARITHMIC 2 X 1-5 INCH CYCLES
EUGENE DIETZGEN CO.
MADE IN U. S. A.

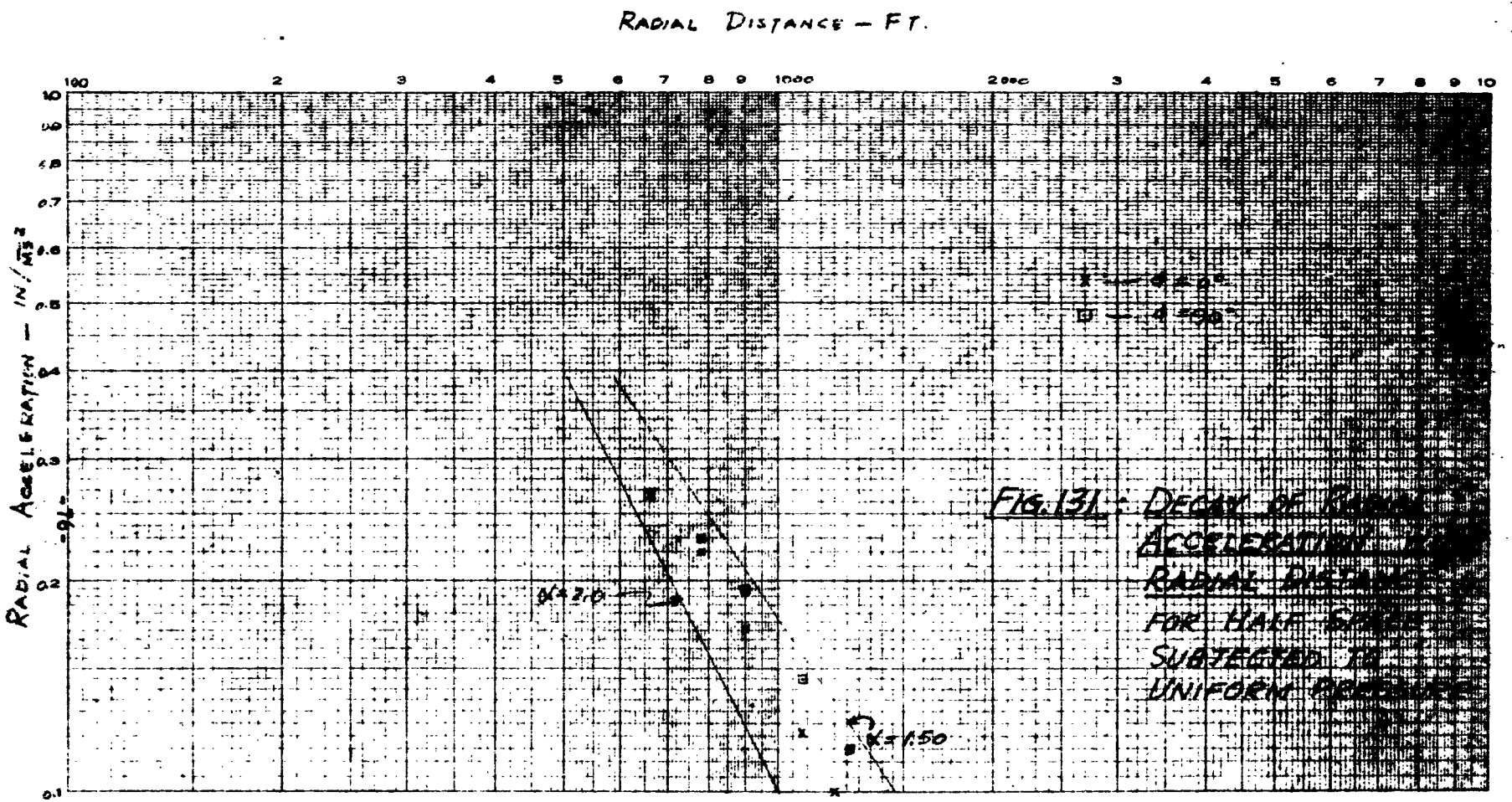

FIG. 131 - DECAY OF RADIAL ACCELERATION WITH RADIAL DISTANCE FOR HALF SPACE SUBJECTED TO UNIFORM PRESSURE

No. 34 DIETZGEN GRAPH PAPER
LOGARITHMIC 2 X 1-5 INCH CYCLES
EUGENE DIETZGEN CO.
MADE IN U.S.A.

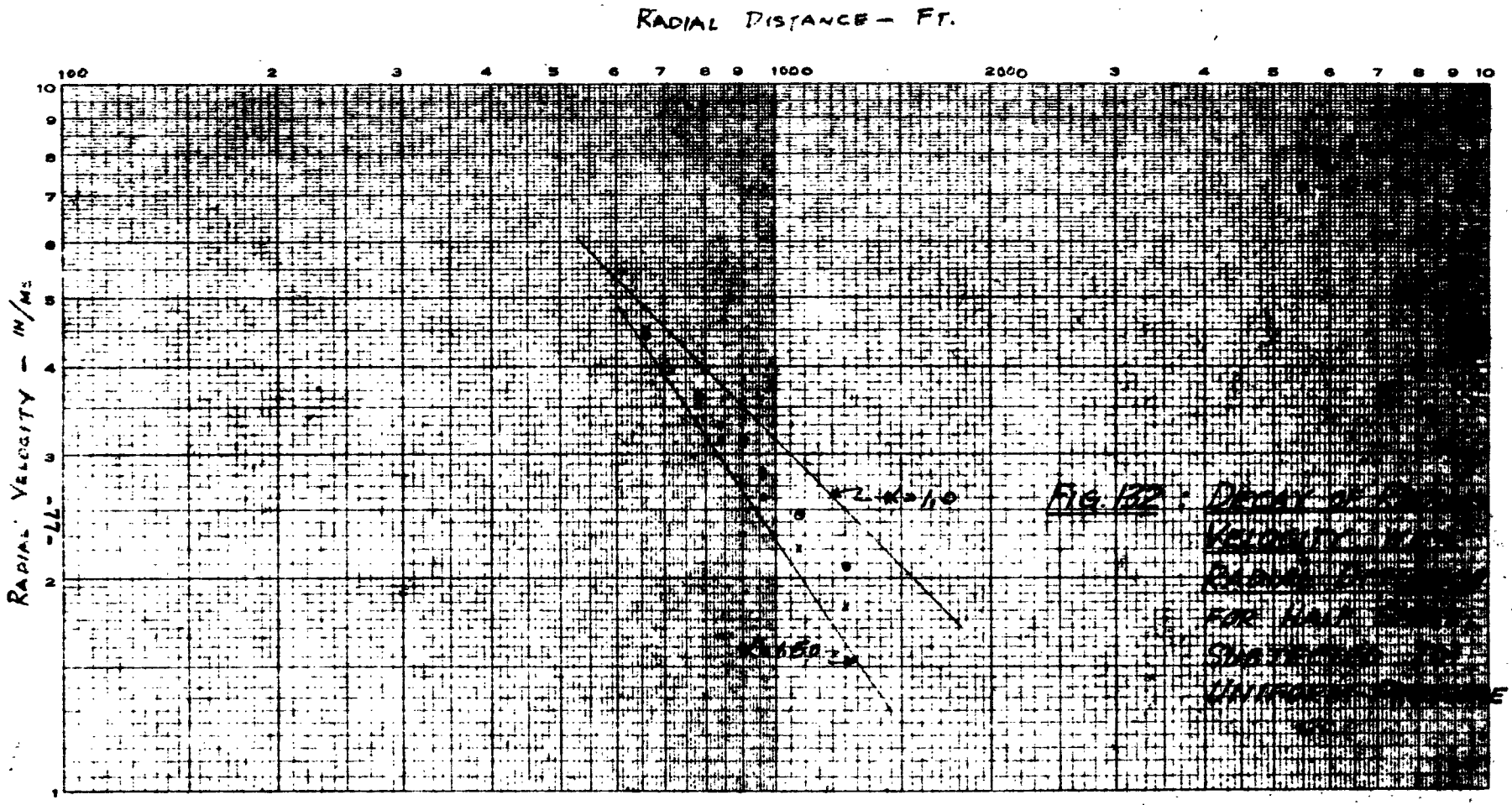

FIG. 132: [illegible]

NO. 340 C21 DIE KUEN GR. PAPER
LOGARITHMIC 2 X 1-5 INCH CYCLES
EUGENE DIETZGEN CO.
MADE IN U.S.A.

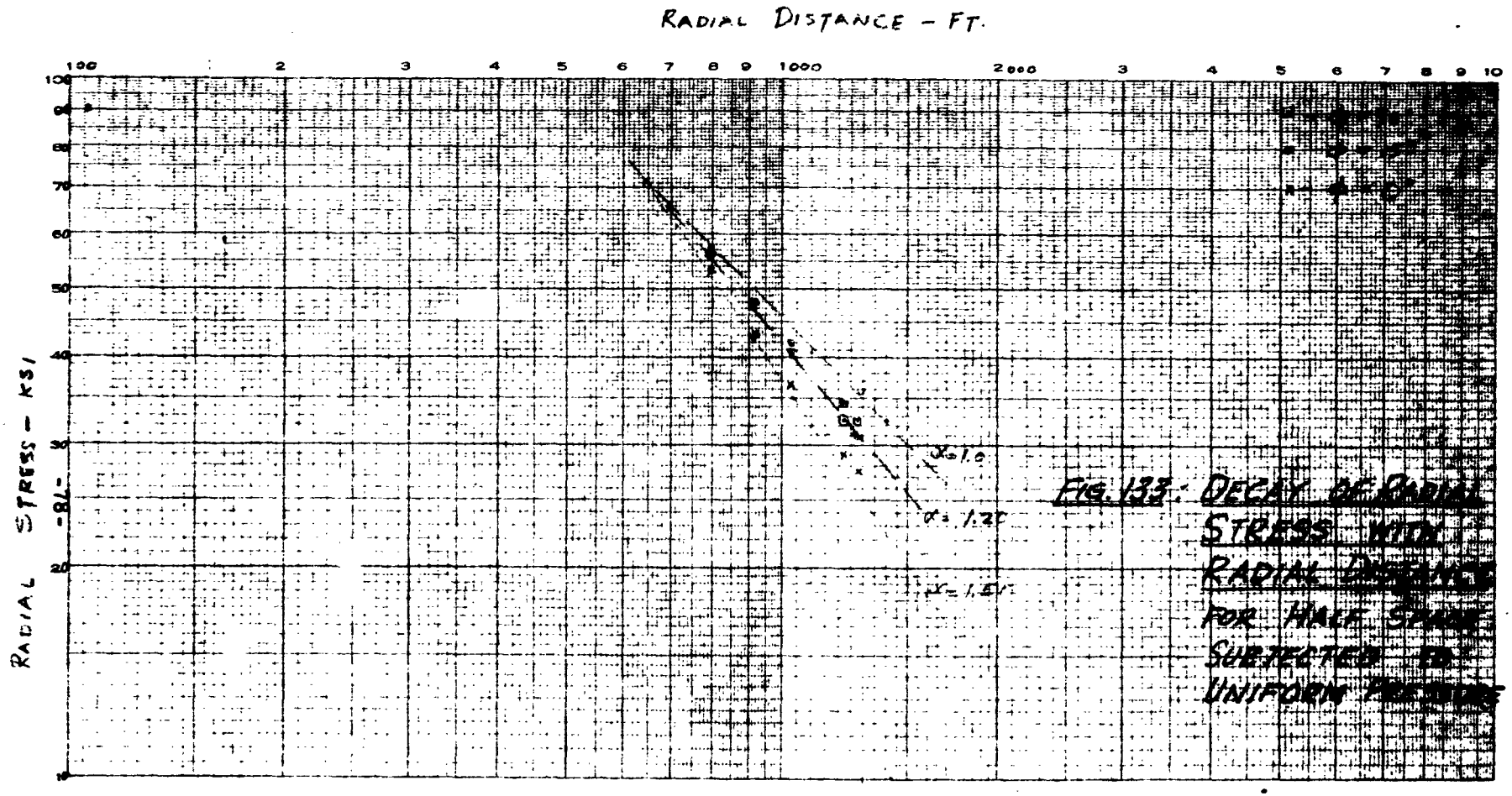

FIG. 133: DECAY OF RADIAL STRESS WITH RADIAL DISTANCE FOR HALF SPACE SUBJECTED TO UNIFORM PRESSURE

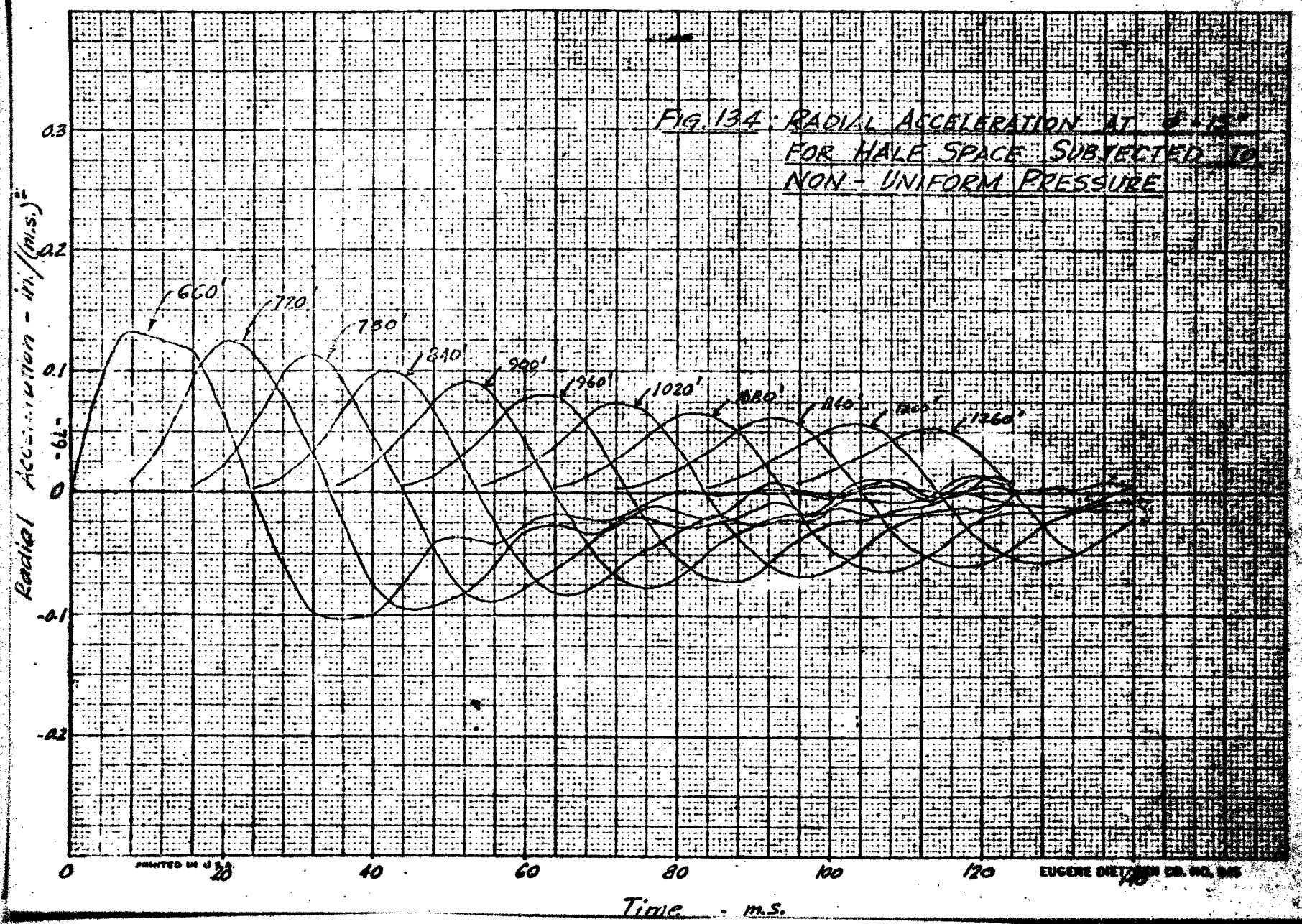

FIG. 134 · RADIAL ACCELERATION AT [illegible] FOR HALF SPACE SUBJECTED TO NON-UNIFORM PRESSURE

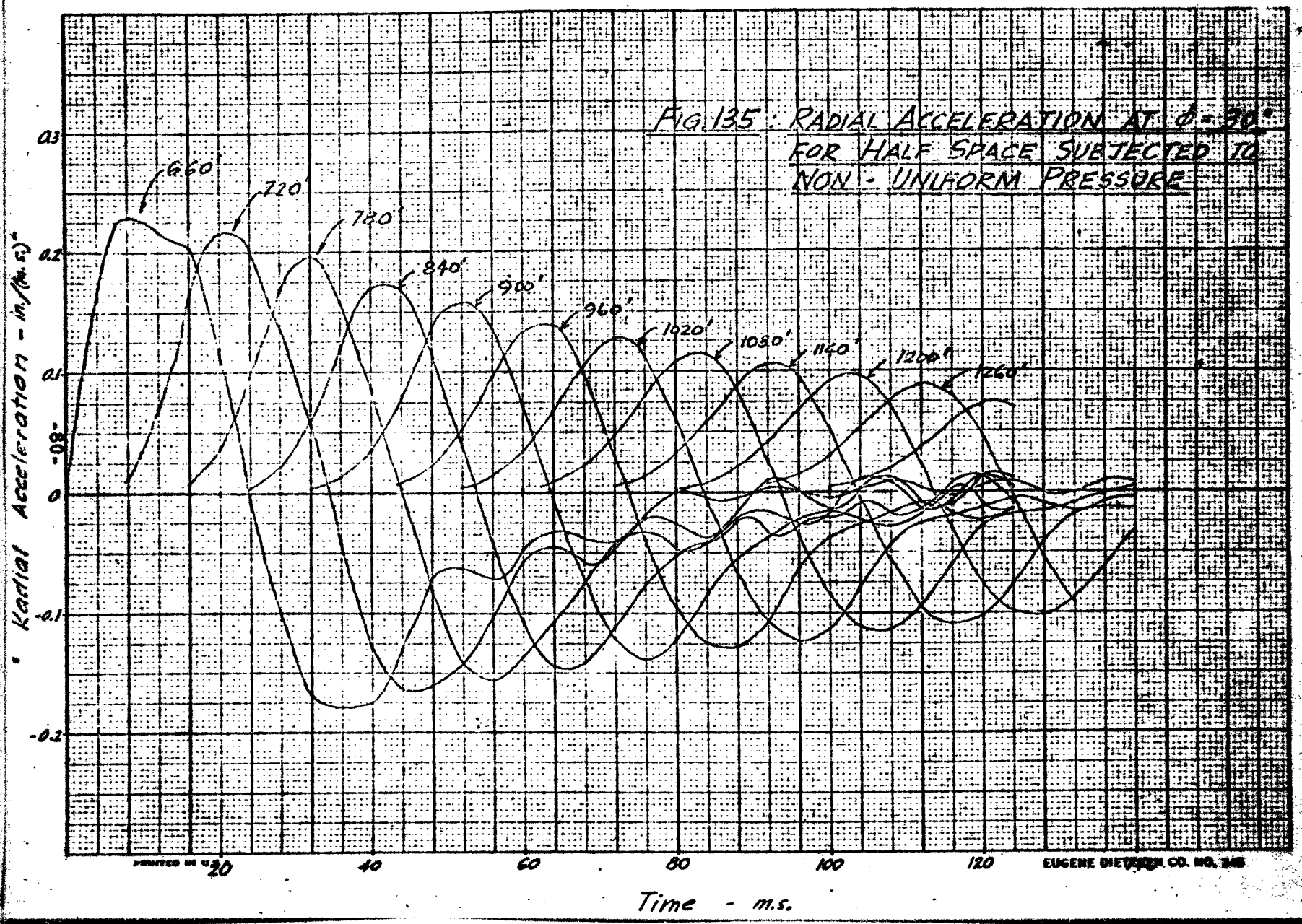

FIG. 135: RADIAL ACCELERATION AT $\phi = 30°$ FOR HALF SPACE SUBJECTED TO NON-UNIFORM PRESSURE

NO. 341-20 DIETZGEN GRAPH PAPER
20 X 20 PER INCH

EUGENE DIETZGEN CO.
MADE IN U. S. A.

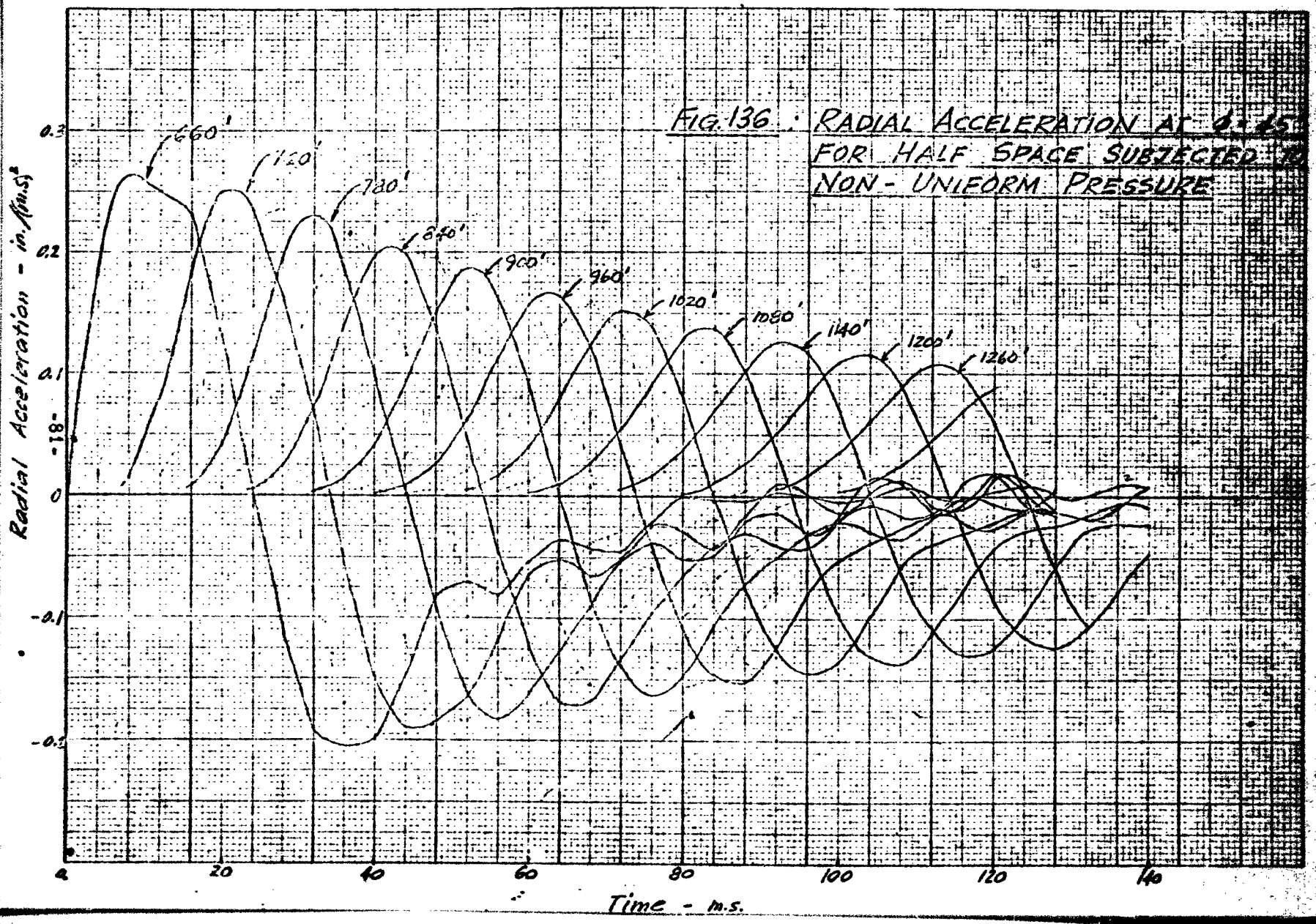

FIG. 136 : RADIAL ACCELERATION AT θ = 45°
FOR HALF SPACE SUBJECTED TO
NON-UNIFORM PRESSURE

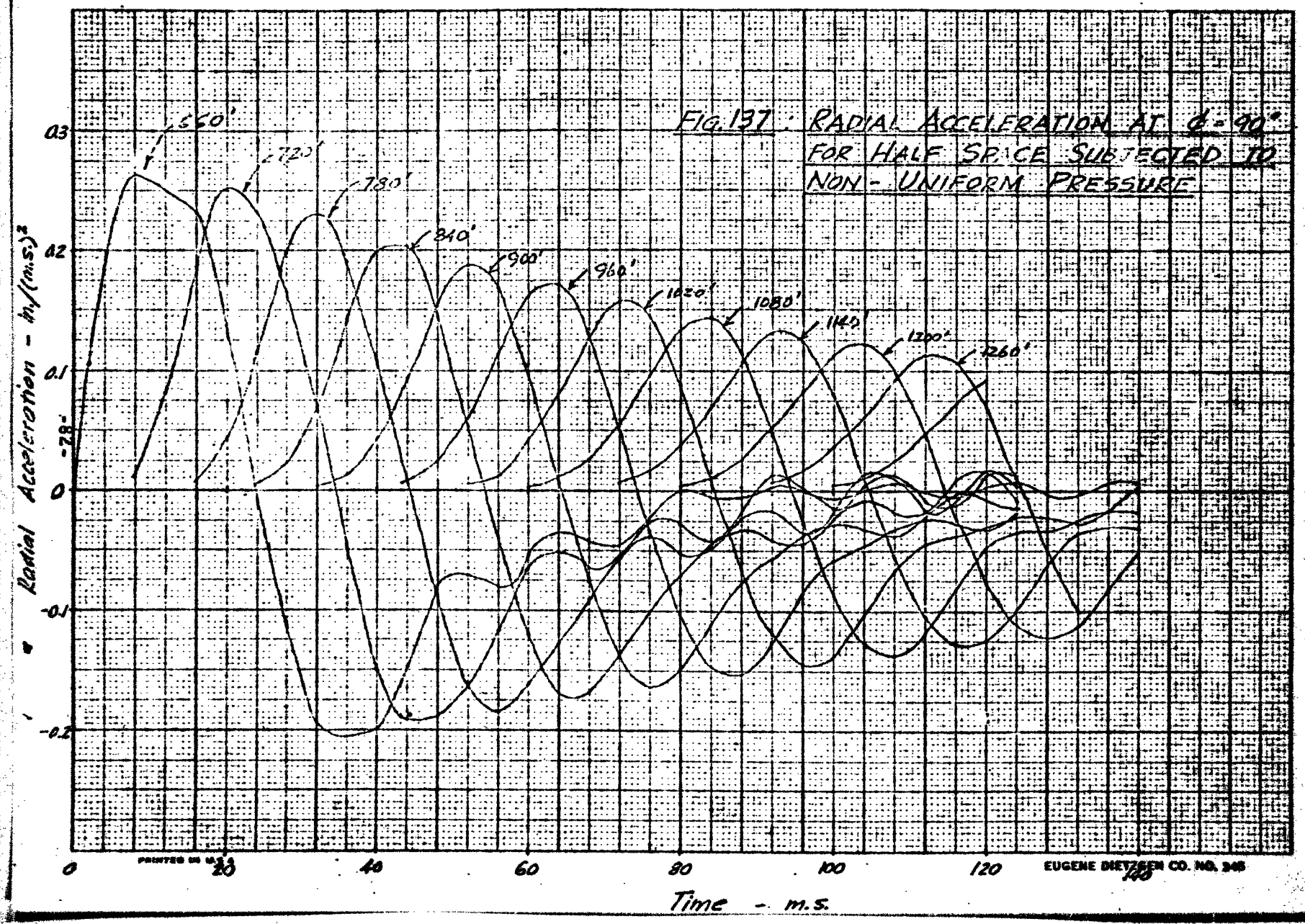

Fig. 137: RADIAL ACCELERATION AT $\phi = 90°$ FOR HALF SPACE SUBJECTED TO NON-UNIFORM PRESSURE

NO. 341-20 DIETZGEN GRAPH PAPER
20 X 20 PER INCH

EUGENE DIETZGEN CO.
MADE IN U. S. A.

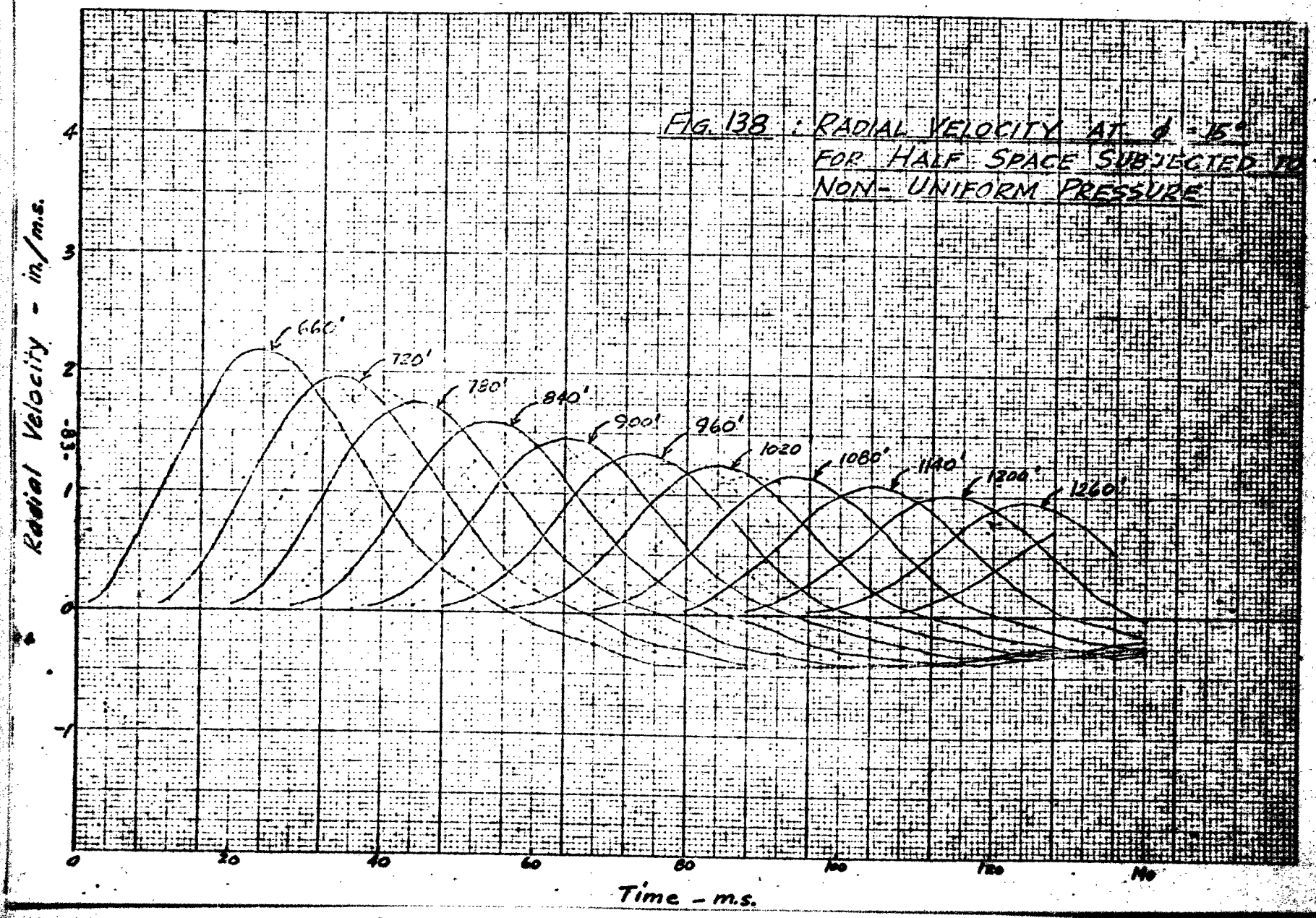

FIG. 138 : RADIAL VELOCITY AT $\phi = 15°$ FOR HALF SPACE SUBJECTED TO NON-UNIFORM PRESSURE

NO. 341-20 DIETZGEN GRAPH PAPER
20 X 20 PER INCH

EUGENE DIETZGEN CO.
MADE IN U. S. A.

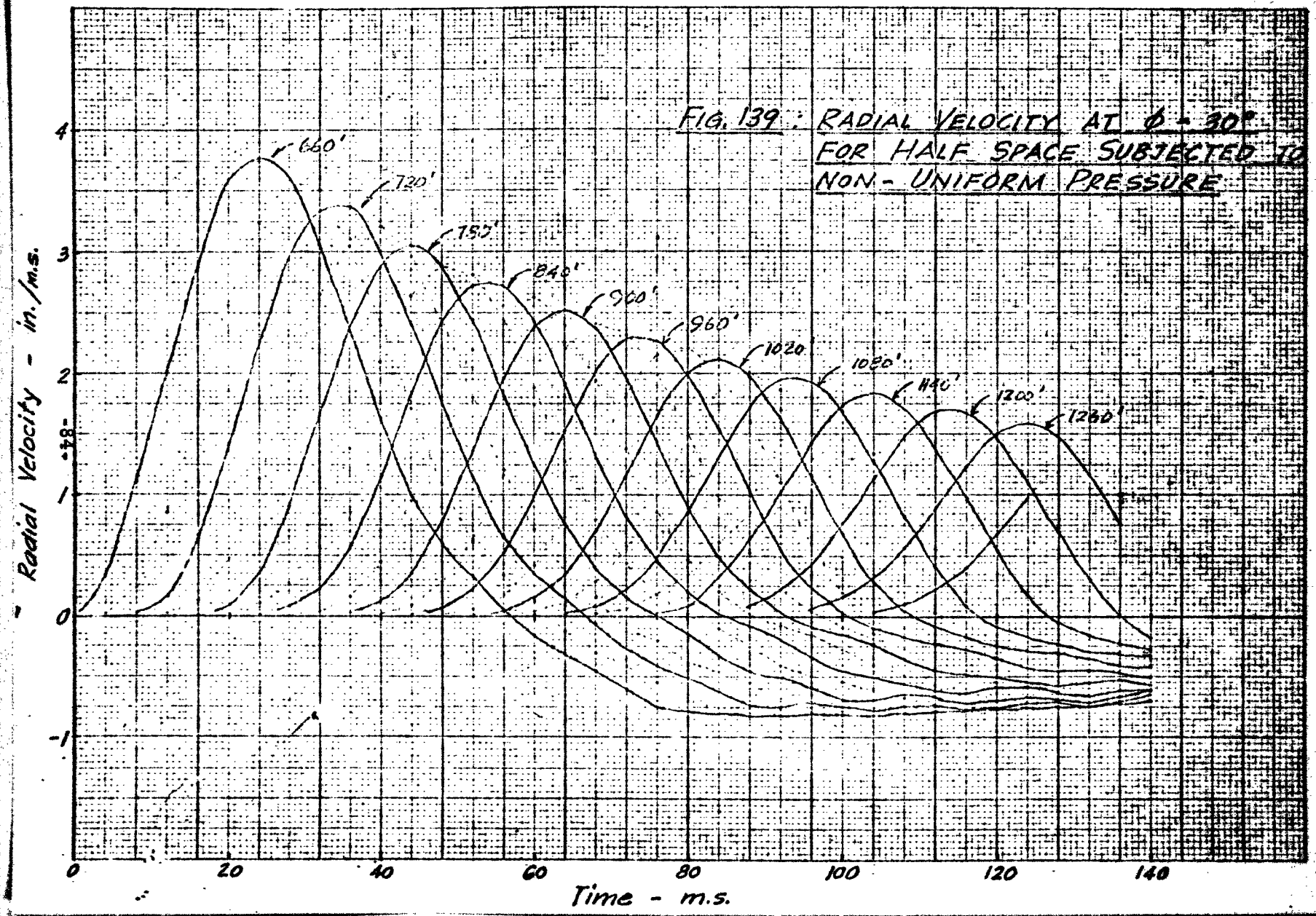

FIG. 139: RADIAL VELOCITY AT $\phi = 30°$ FOR HALF SPACE SUBJECTED TO NON-UNIFORM PRESSURE

NO. 341-20 DIETZGEN GRAPH PAPER
20 X 20 PER INCH

EUGENE DIETZGEN CO.
MADE IN U. S. A.

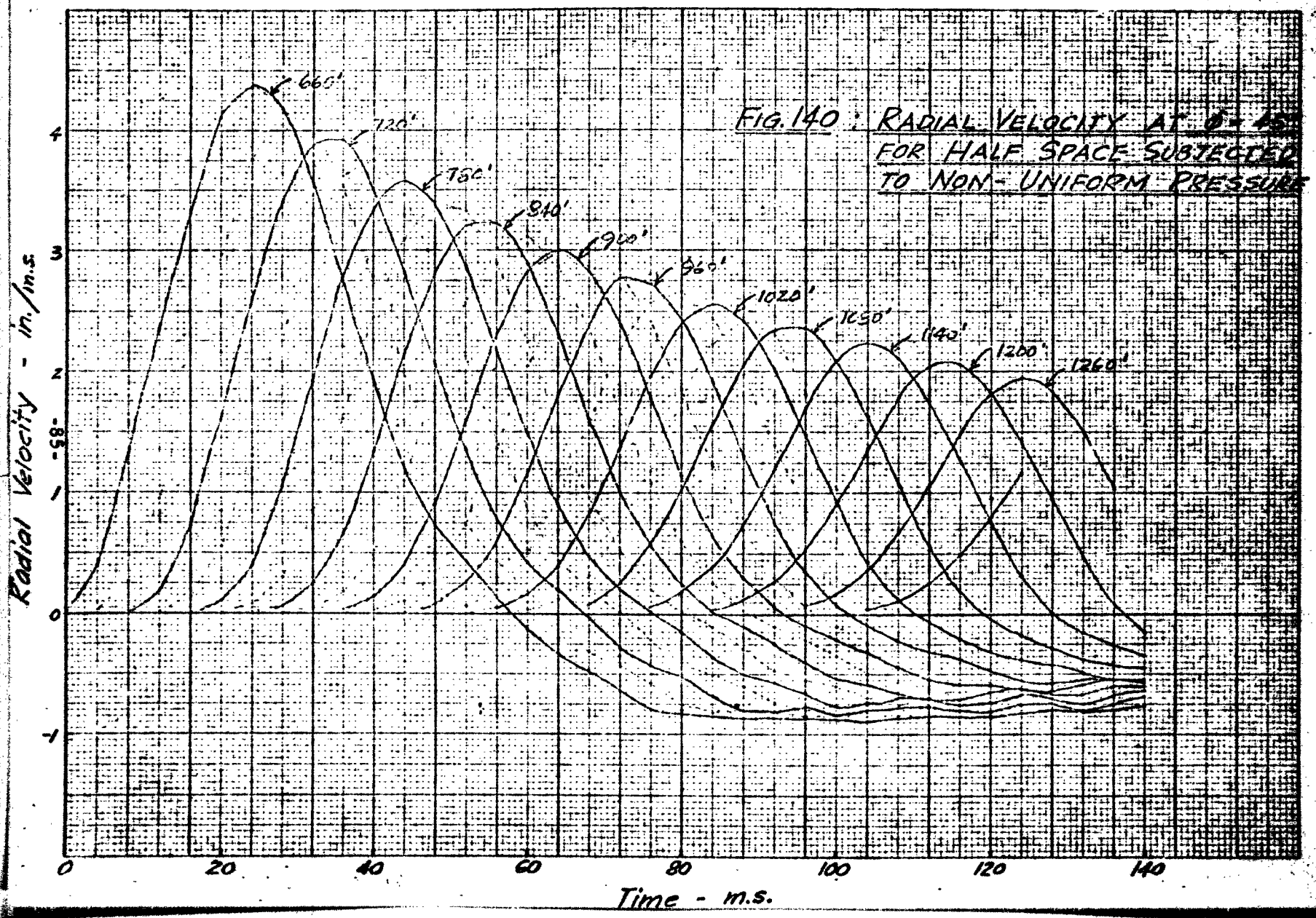

FIG. 140 : RADIAL VELOCITY AT $\phi = 45°$ FOR HALF SPACE SUBJECTED TO NON-UNIFORM PRESSURE

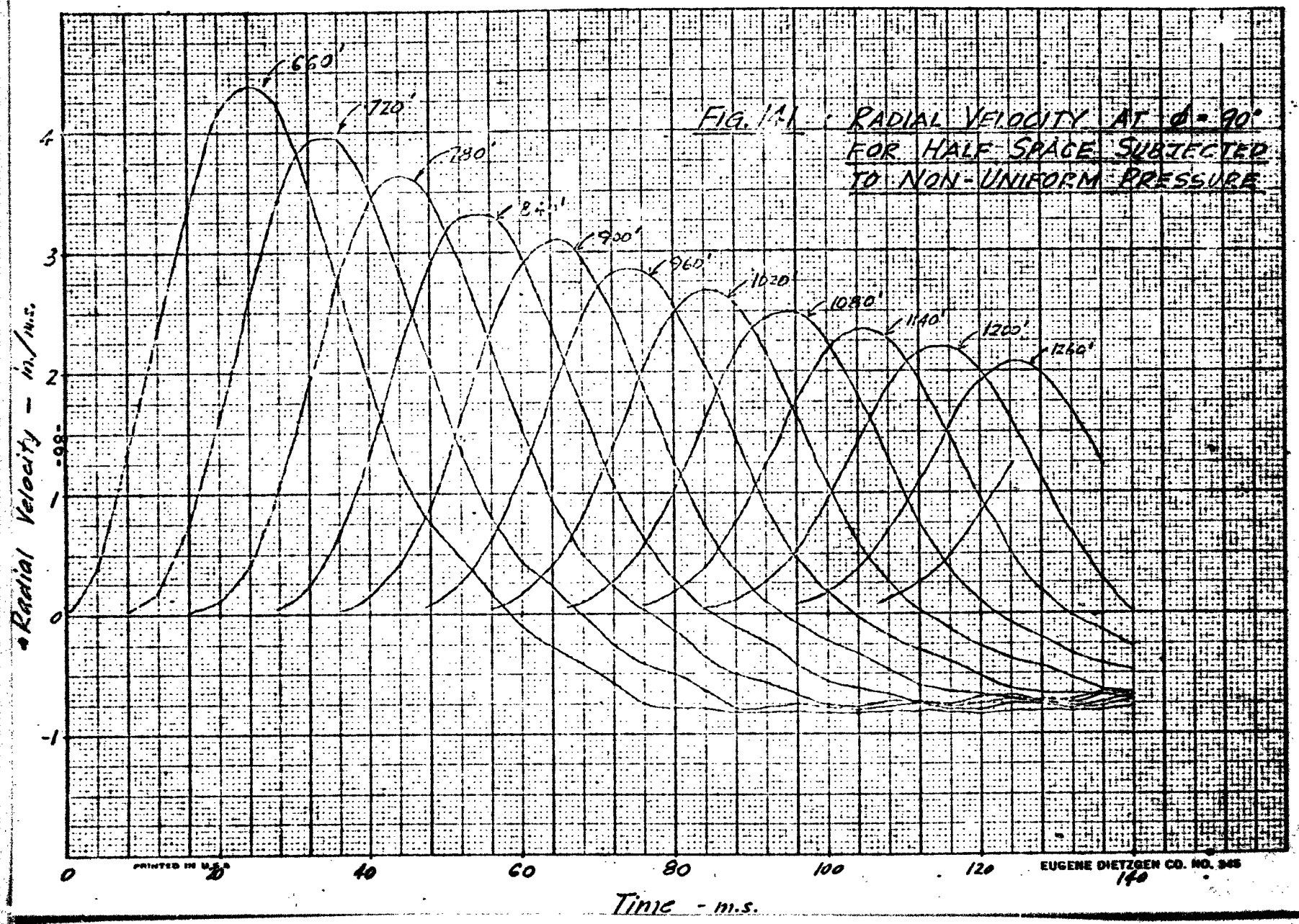

FIG. 14.1 : RADIAL VELOCITY AT $\phi = 90°$ FOR HALF SPACE SUBJECTED TO NON-UNIFORM PRESSURE

NO. 341-20 DIETZGEN GRAPH PAPER
20 X 20 PER INCH
EUGENE DIETZGEN CO.
MADE IN U. S. A.

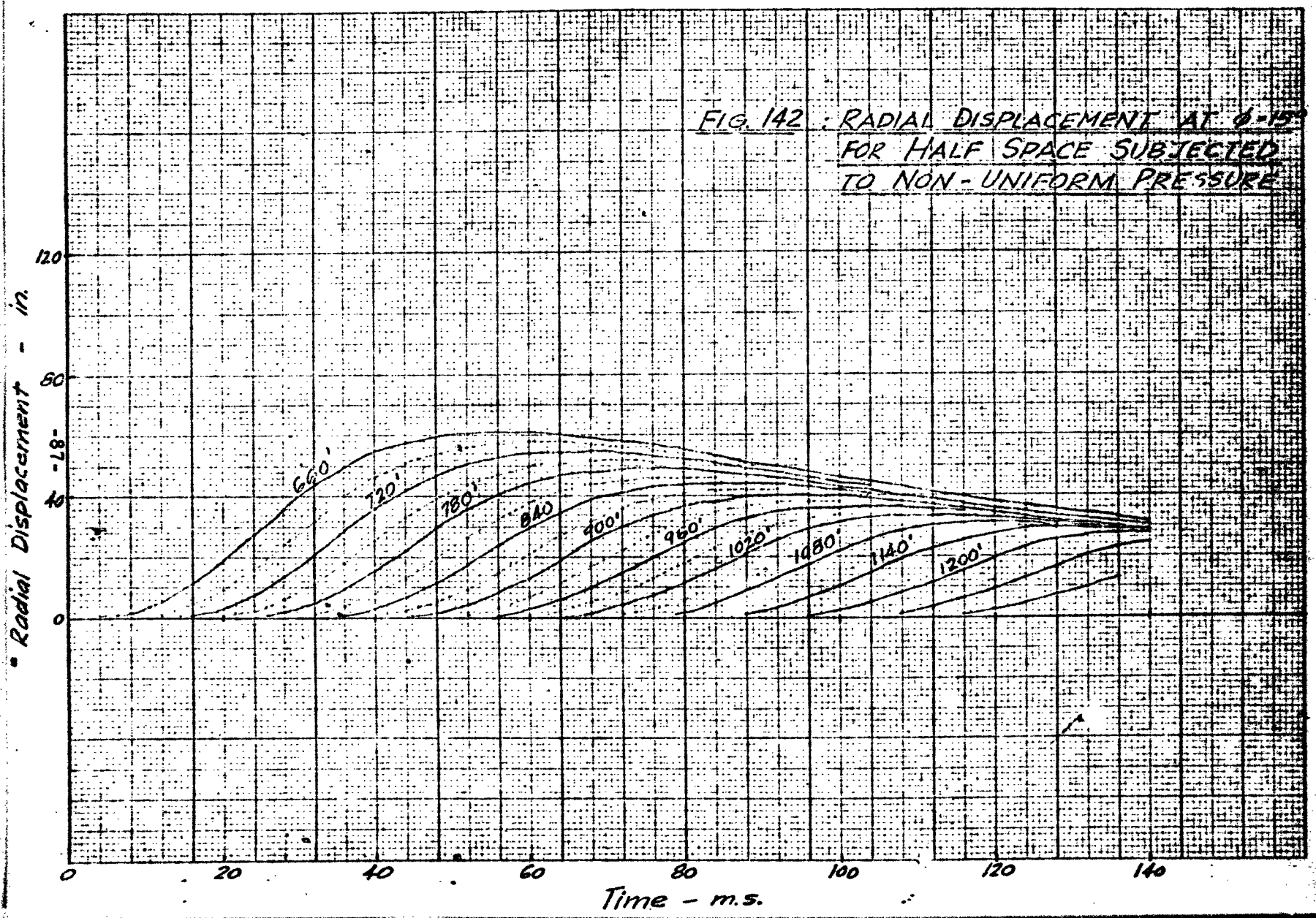

FIG. 142 : RADIAL DISPLACEMENT AT $\phi = 15°$ FOR HALF SPACE SUBJECTED TO NON-UNIFORM PRESSURE

NO. 341-20 DIETZGEN GRAPH PAPER
20 X 20 PER INCH

EUGENE DIETZGEN CO.
MADE IN U. S. A.

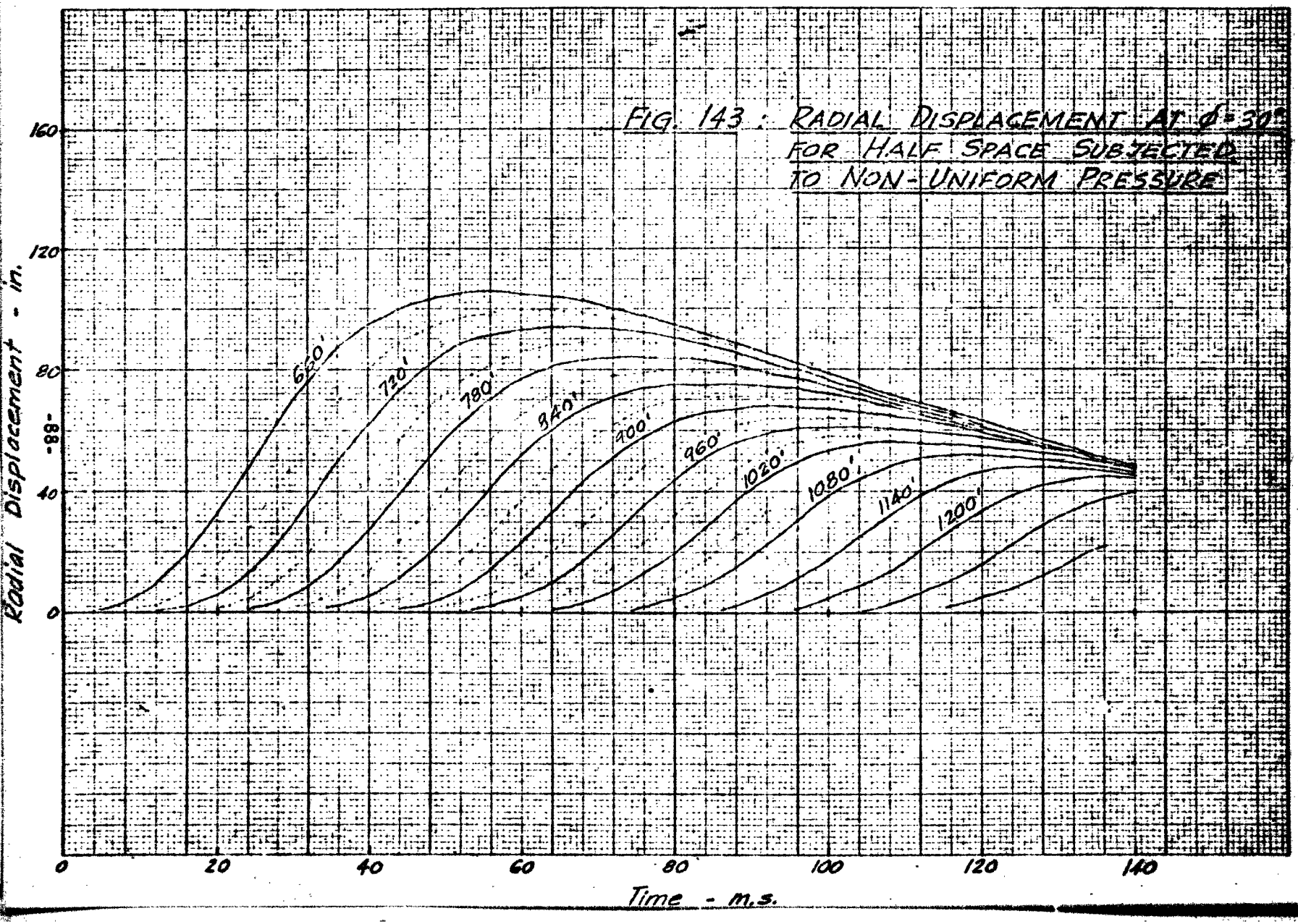

FIG. 143 : RADIAL DISPLACEMENT AT $\phi = 30°$ FOR HALF SPACE SUBJECTED TO NON-UNIFORM PRESSURE

NO. 341-20 DIETZGEN GRAPH PAPER
20 X 20 PER INCH
EUGENE DIETZGEN CO.
MADE IN U. S. A.

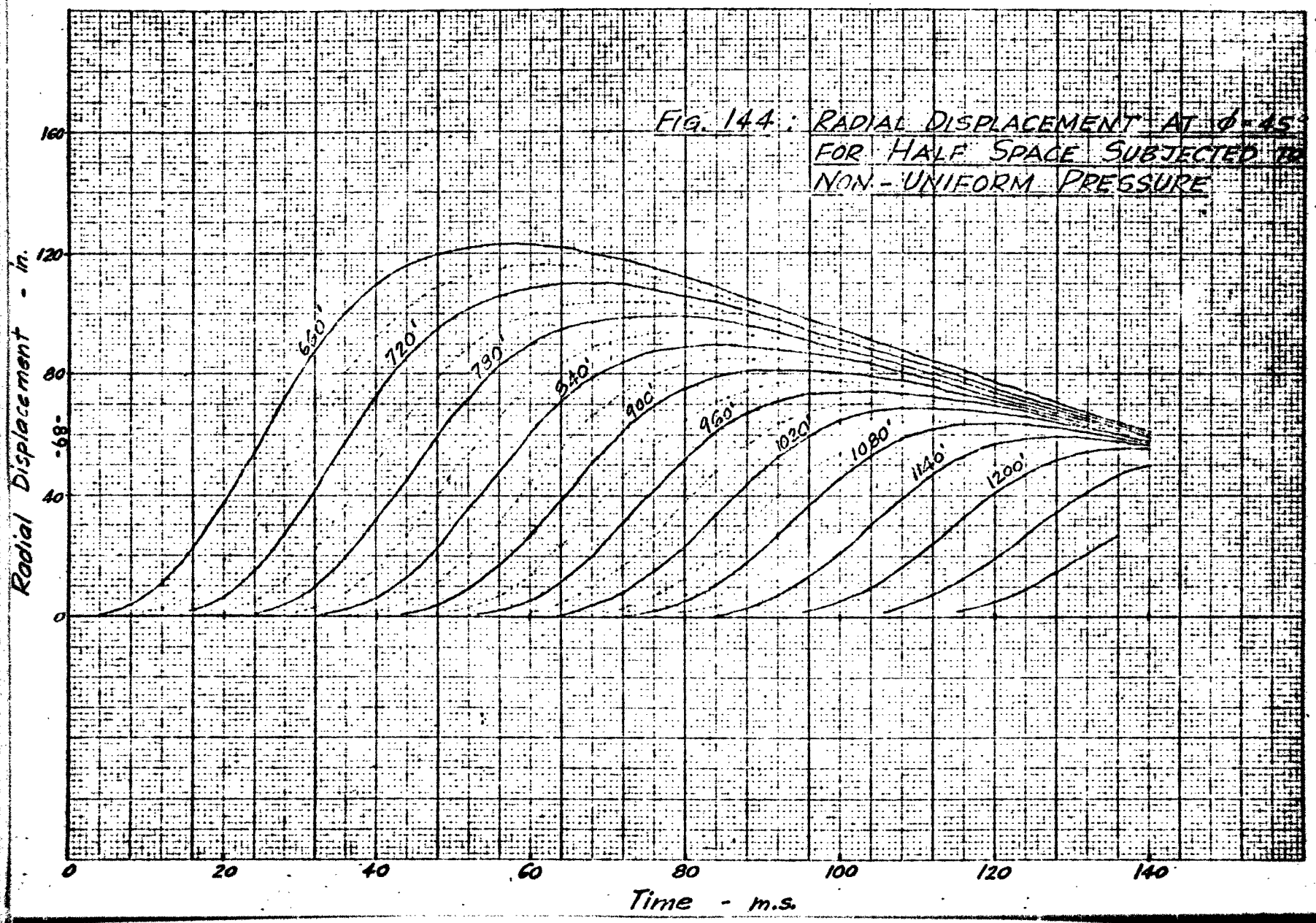

Fig. 144: RADIAL DISPLACEMENT AT $\phi = 45°$ FOR HALF SPACE SUBJECTED TO NON-UNIFORM PRESSURE

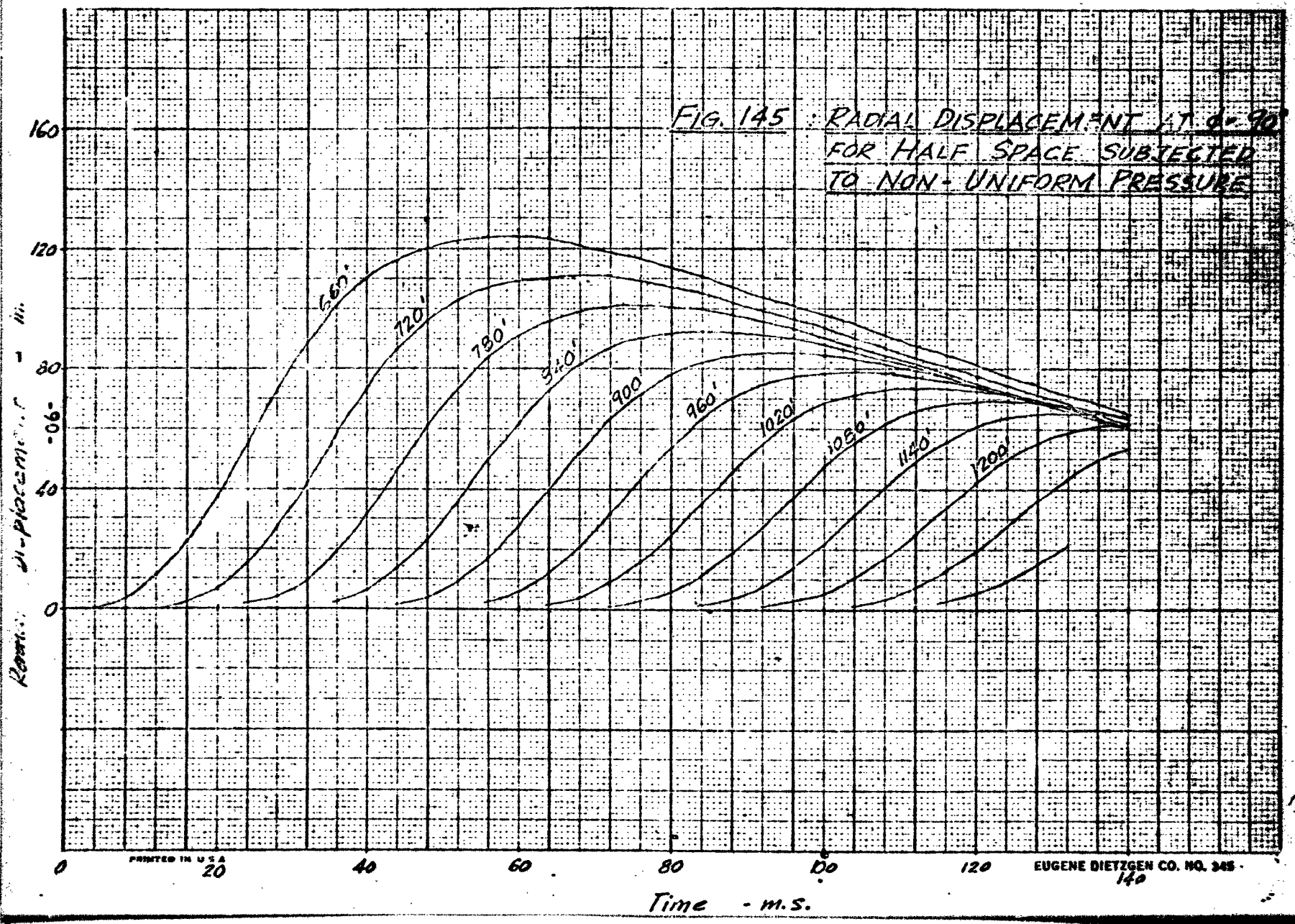
FIG. 145 : RADIAL DISPLACEMENT AT d = 90'
FOR HALF SPACE SUBJECTED
TO NON-UNIFORM PRESSURE
660'
720'
780'
840'
900'
960'
1020'
1080'
1140'
1200'
160
120
80
40
0
0
20
40
60
80
100
120
140
Time - m.s.
PRINTED IN U.S.A.
EUGENE DIETZGEN CO. NO. 345

NO. 341-20 DIETZGEN GRAPH PAPER
20 X 20 PER INCH
EUGENE DIETZGEN CO.
MADE IN U. S. A.

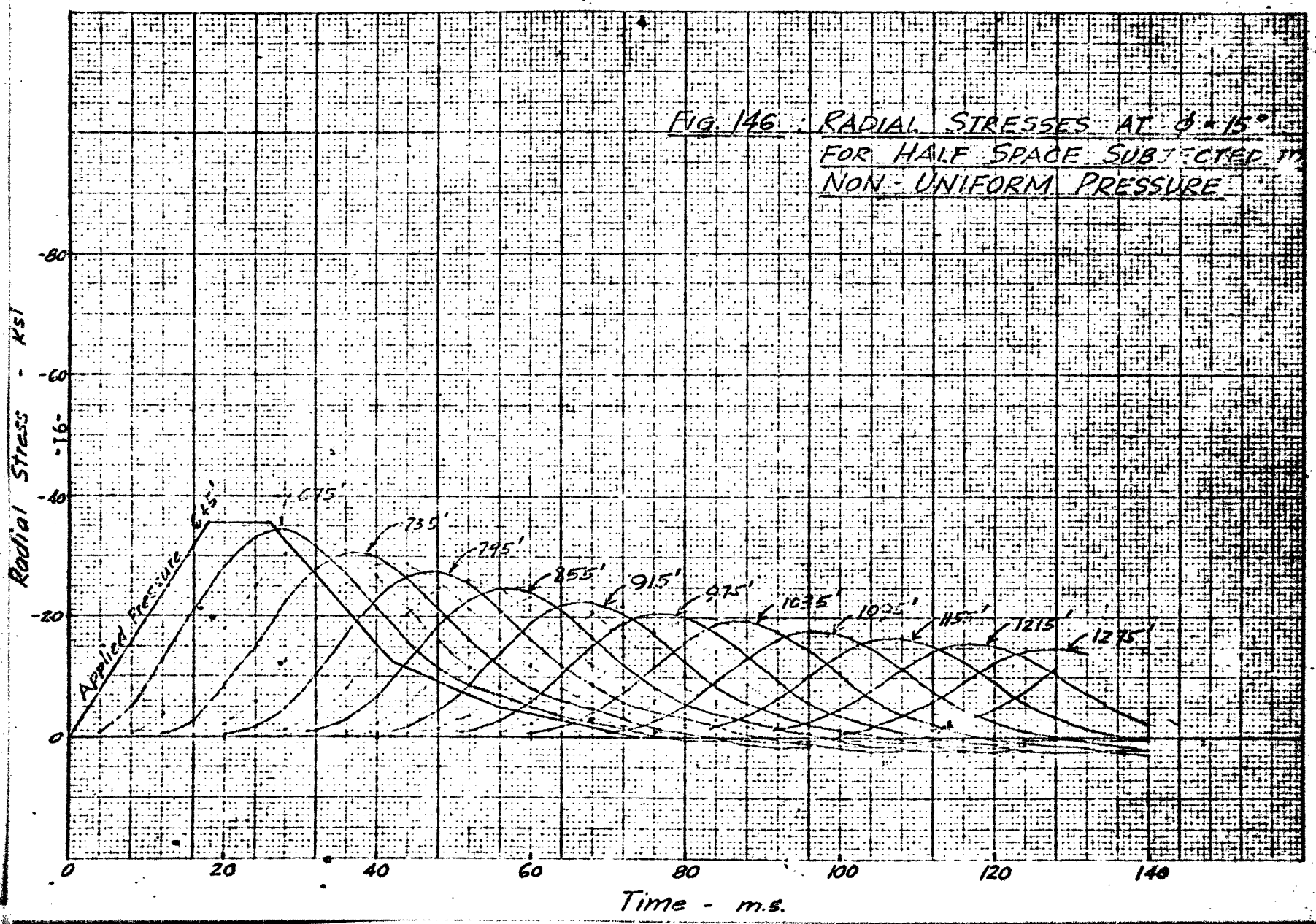

FIG. 146 : RADIAL STRESSES AT $\phi = 15°$ FOR HALF SPACE SUBJECTED TO NON-UNIFORM PRESSURE

NO. 341-20 DIETZGEN GRAPH PAPER
20 X 20 PER INCH
EUGENE DIETZGEN CO.
MADE IN U. S. A.

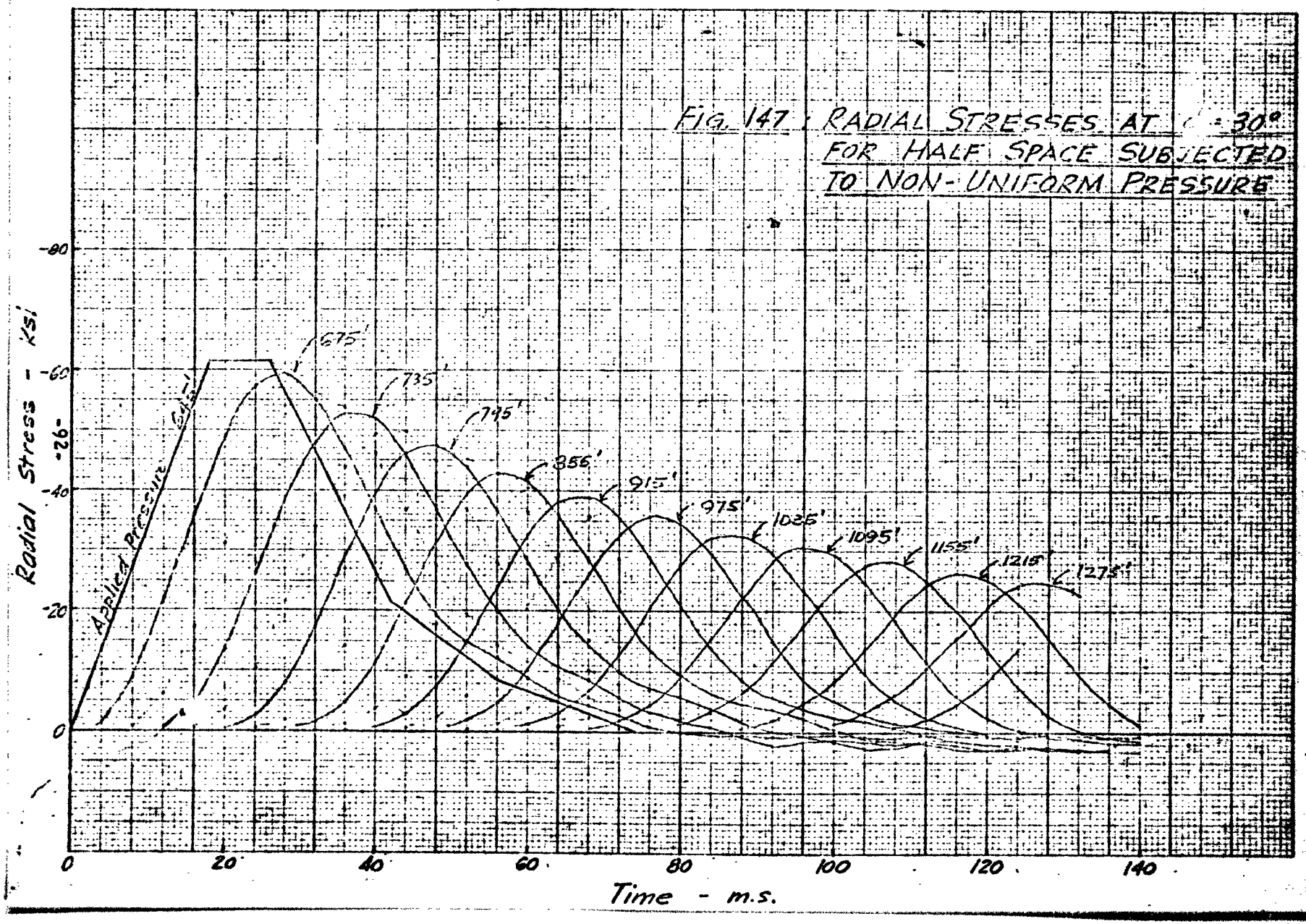

FIG. 147 : RADIAL STRESSES AT = 30°
FOR HALF SPACE SUBJECTED
TO NON-UNIFORM PRESSURE

NO. 341-20 DIETZGEN GRAPH PAPER
20 X 20 PER INCH
EUGENE DIETZGEN CO.
MADE IN U. S. A.

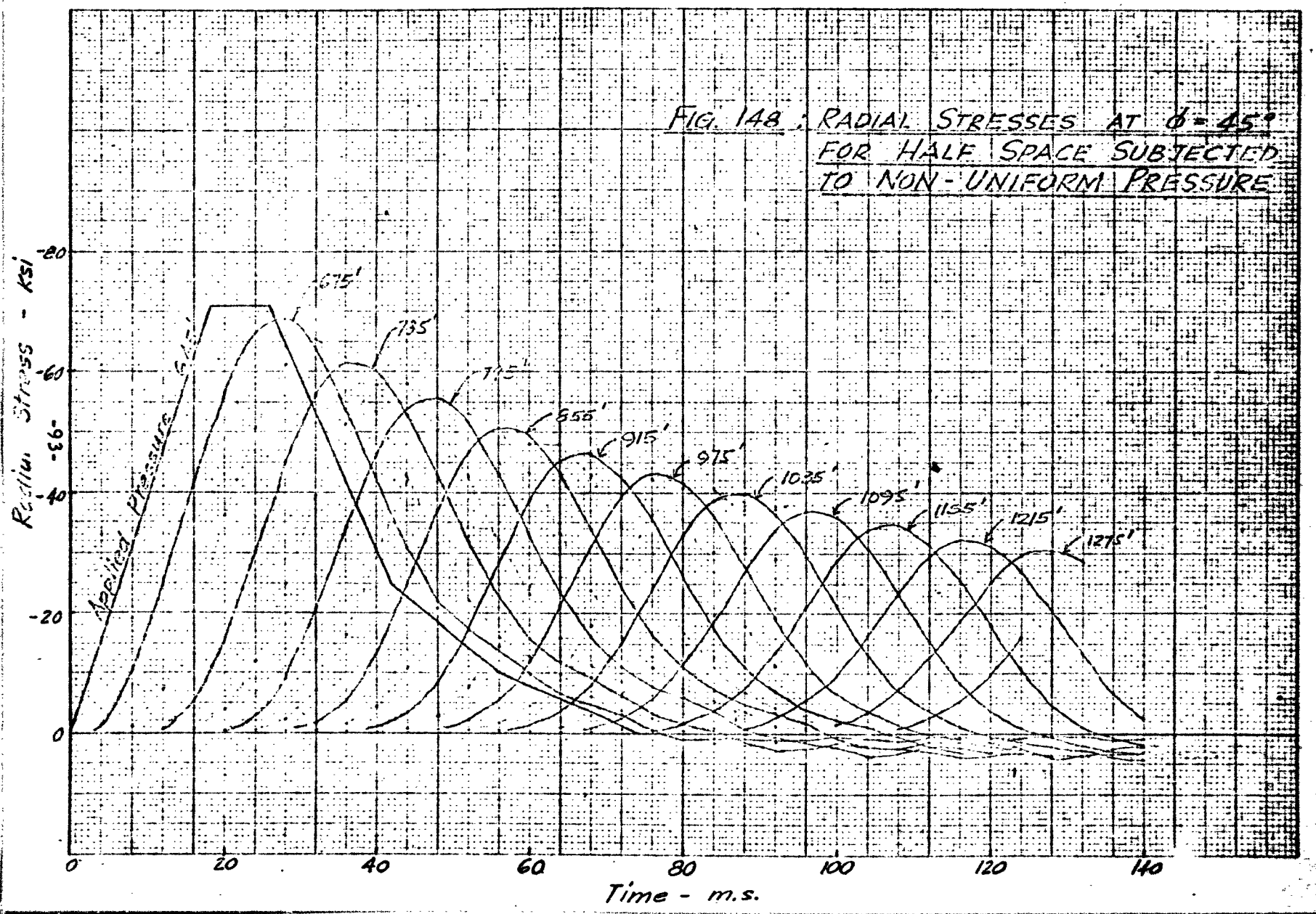

FIG. 148 : RADIAL STRESSES AT $\phi = 45°$ FOR HALF SPACE SUBJECTED TO NON-UNIFORM PRESSURE

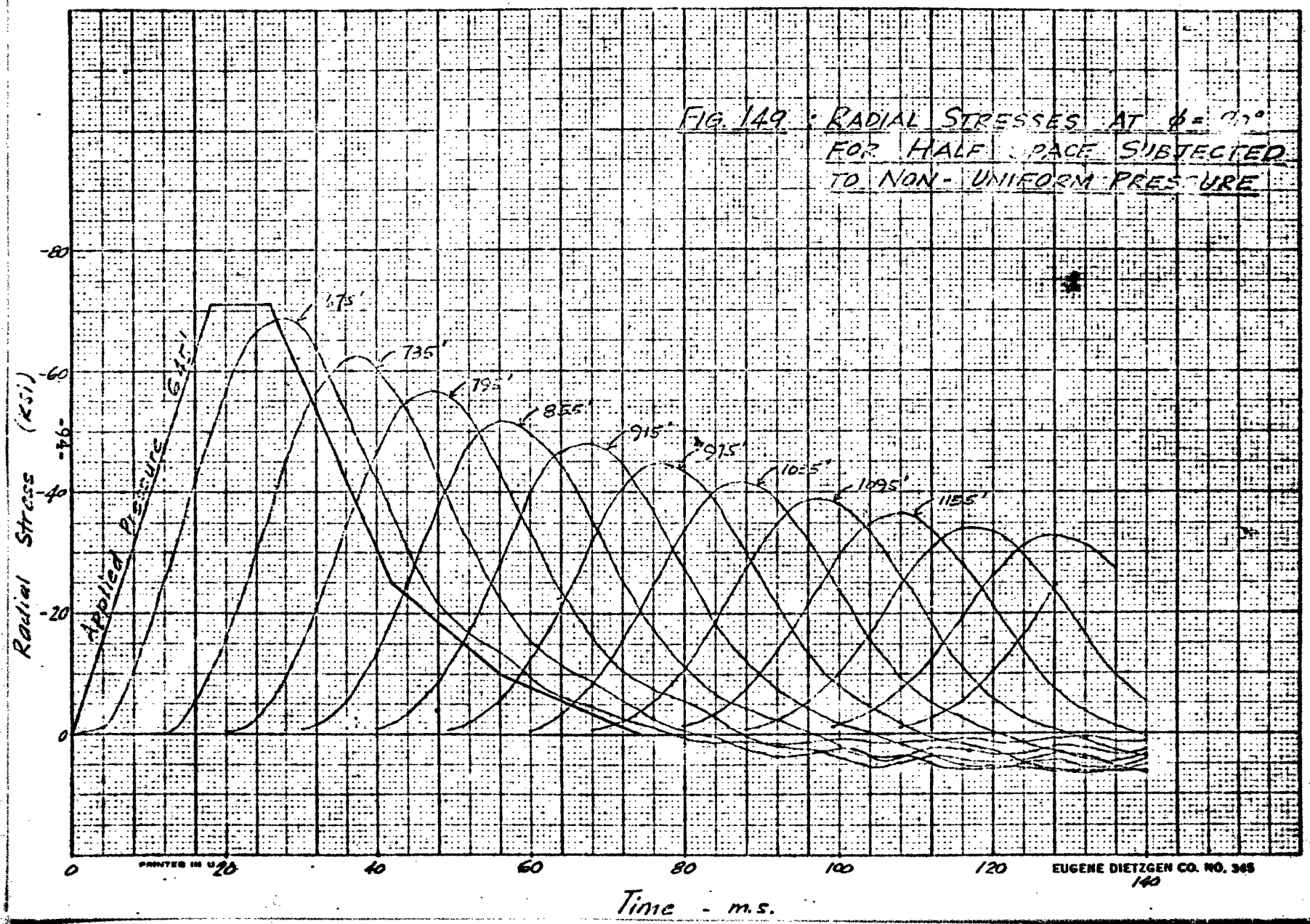

FIG. 149 : RADIAL STRESSES AT $\phi = 0°$ FOR HALF SPACE SUBJECTED TO NON-UNIFORM PRESSURE

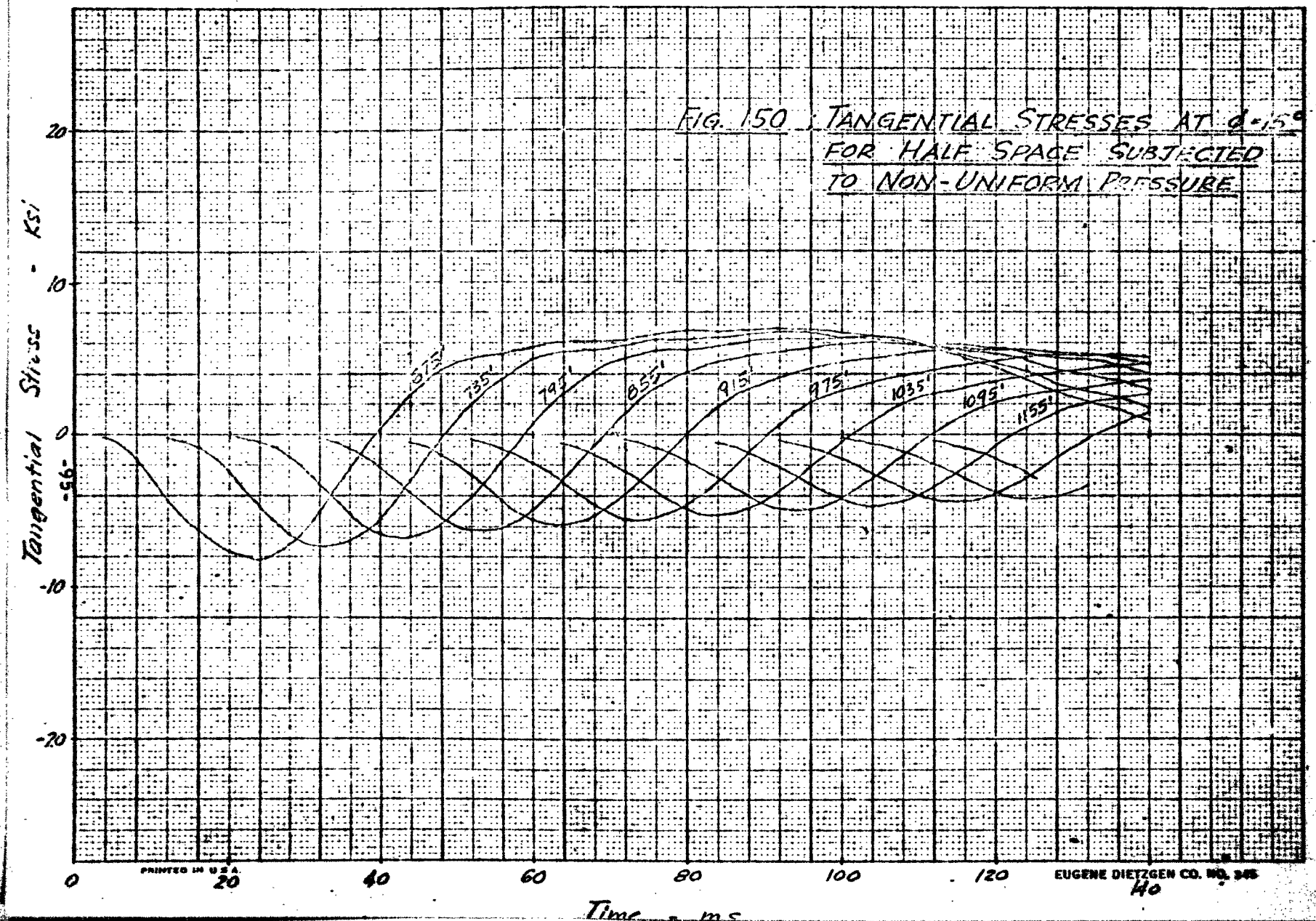
FIG. 150 : TANGENTIAL STRESSES AT d = 15°
FOR HALF SPACE SUBJECTED
TO NON-UNIFORM PRESSURE
Tangential Stress - Ksi
20
10
0
-5.6
-10
-20
0
20
40
60
80
100
120
140
Time - ms
675'
735'
795'
855'
915'
975'
1035'
1095'
1155'
PRINTED IN U.S.A.
EUGENE DIETZGEN CO. NO. 345

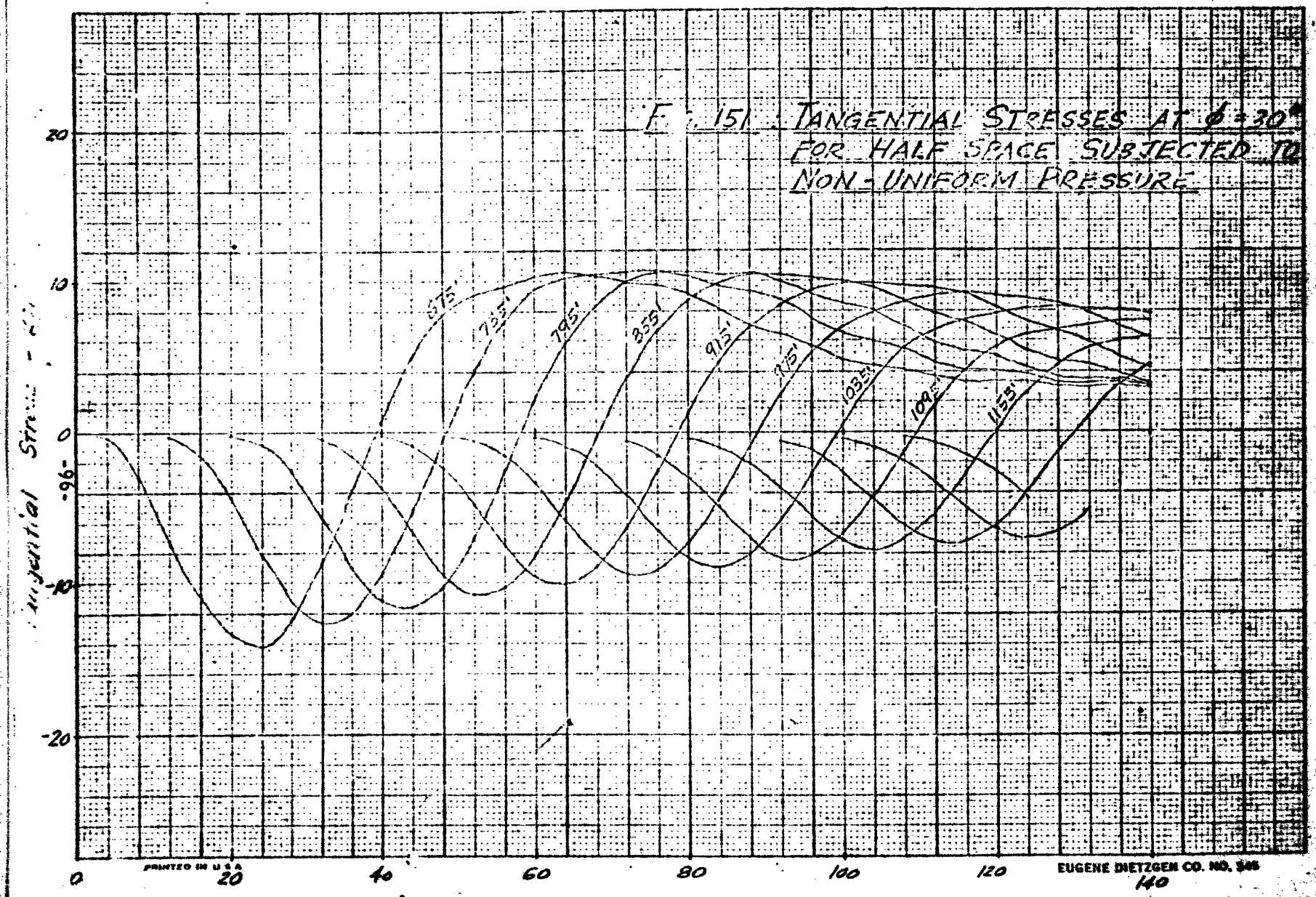

FIG. 15 TANGENTIAL STRESSES AT $\phi = 30°$ FOR HALF SPACE SUBJECTED TO NON-UNIFORM PRESSURE

NO. 341-20 DIETZGEN GRAPH PAPER
20 X 20 PER INCH
EUGENE DIETZGEN CO.
MADE IN U. S. A.

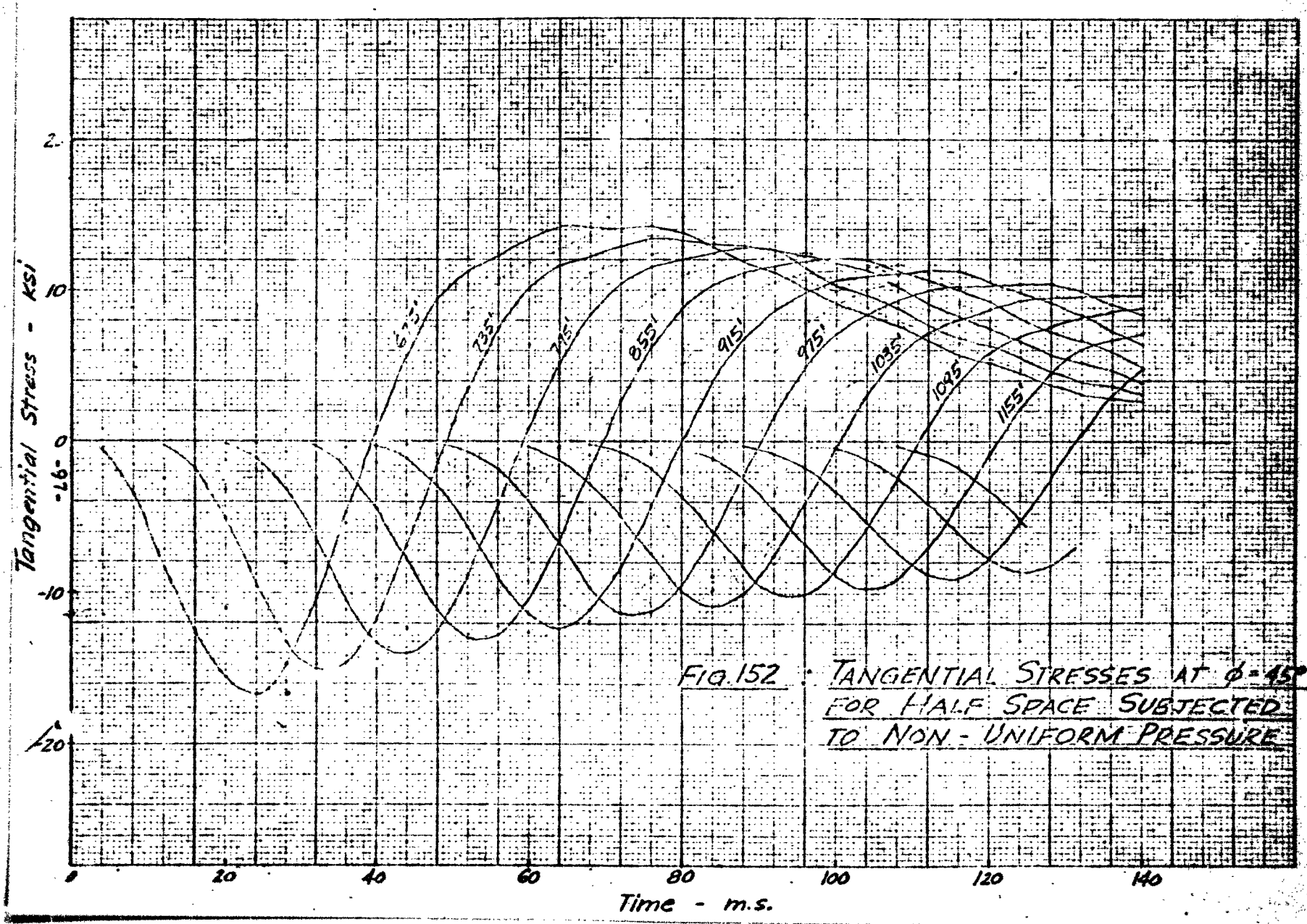

FIG. 152 : TANGENTIAL STRESSES AT $\phi = 45°$ FOR HALF SPACE SUBJECTED TO NON-UNIFORM PRESSURE

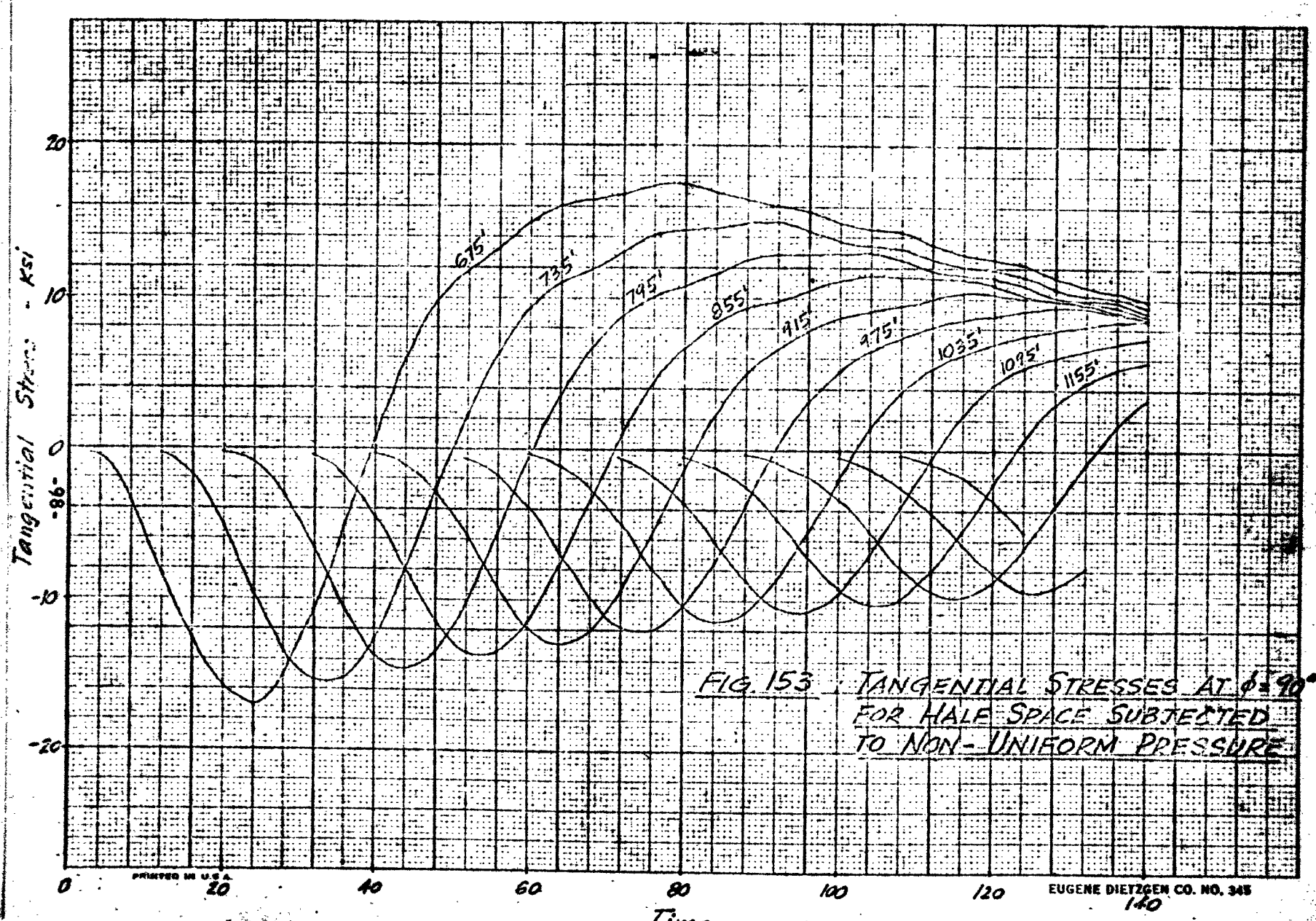

FIG. 153 : TANGENTIAL STRESSES AT $\phi = 90°$ FOR HALF SPACE SUBJECTED TO NON-UNIFORM PRESSURE

NO. 340-L21 DIETZGEN GRAPH PAPER
LOGARITHMIC 2 X 1-5 INCH CYCLES

EUGENE DIETZGEN CO.
MADE IN U. S. A.

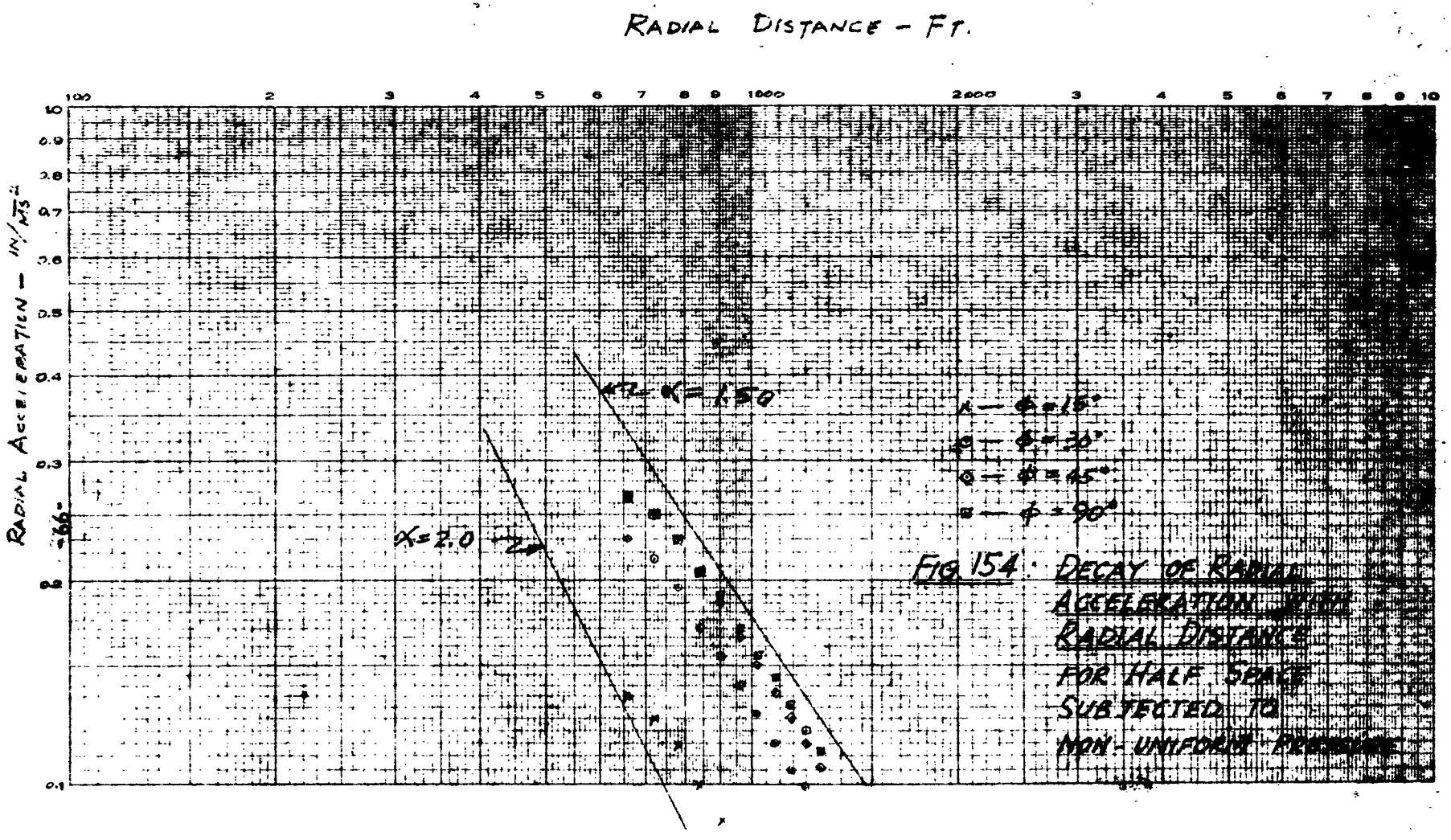

FIG 154 · DECAY OF RADIAL ACCELERATION WITH RADIAL DISTANCE FOR HALF SPACE SUBJECTED TO NON-UNIFORM PRESSURE

NO. 340 L2 DIETZGEN GRAPH PAPER
LOGARITHMIC 2 X 1-5 INCH CYCLES
EUGENE DIETZGEN CO.
MADE IN U.S.A.

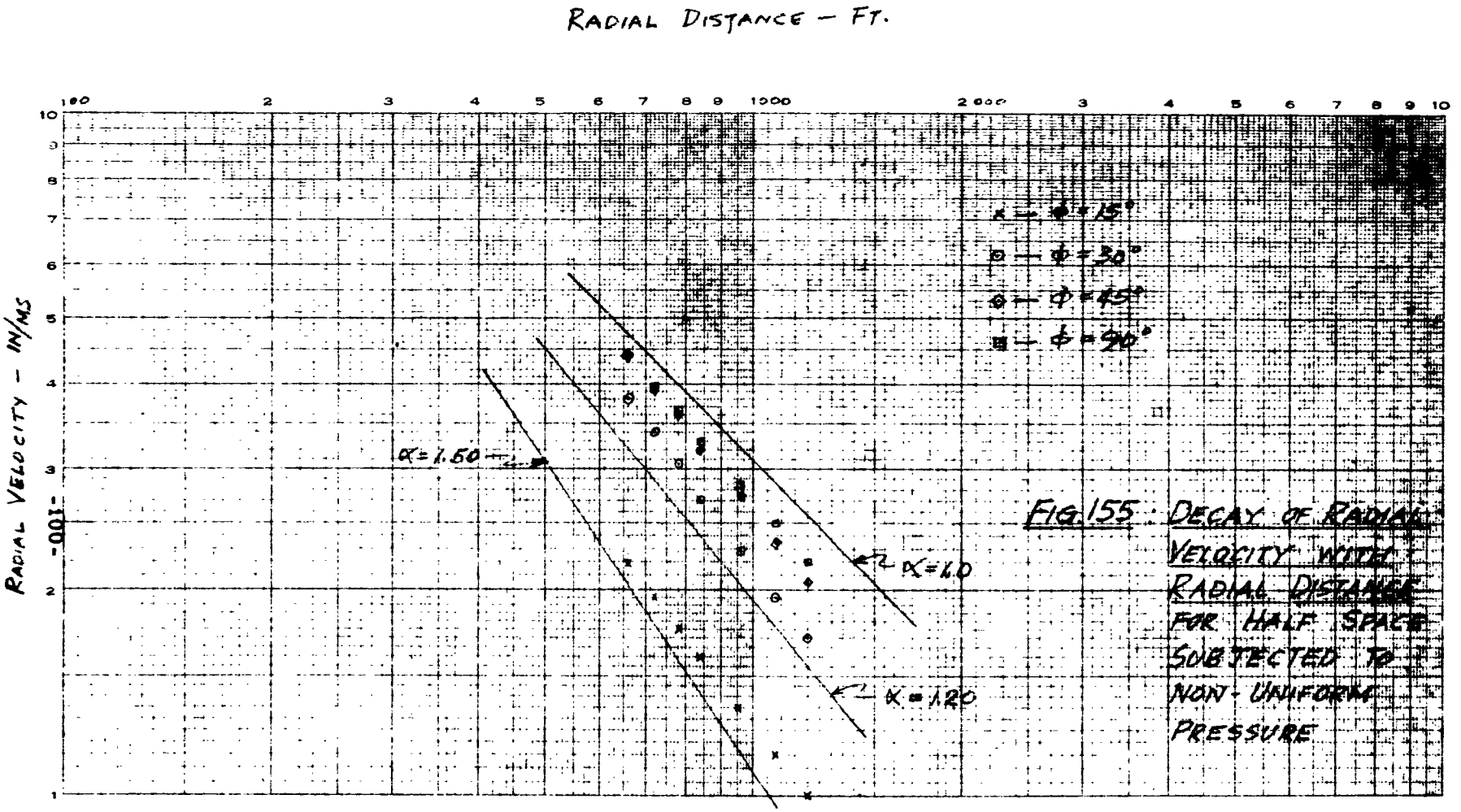

FIG. 155: DECAY OF RADIAL VELOCITY WITH RADIAL DISTANCE FOR HALF SPACE SUBJECTED TO NON-UNIFORM PRESSURE

NO. 34 ... DIE ... GR ... PAPER
LOGARITHMIC 2 X 1-.5 INCH CYCLES
EUGENE DIETZGEN CO.
MADE IN U.S.A.

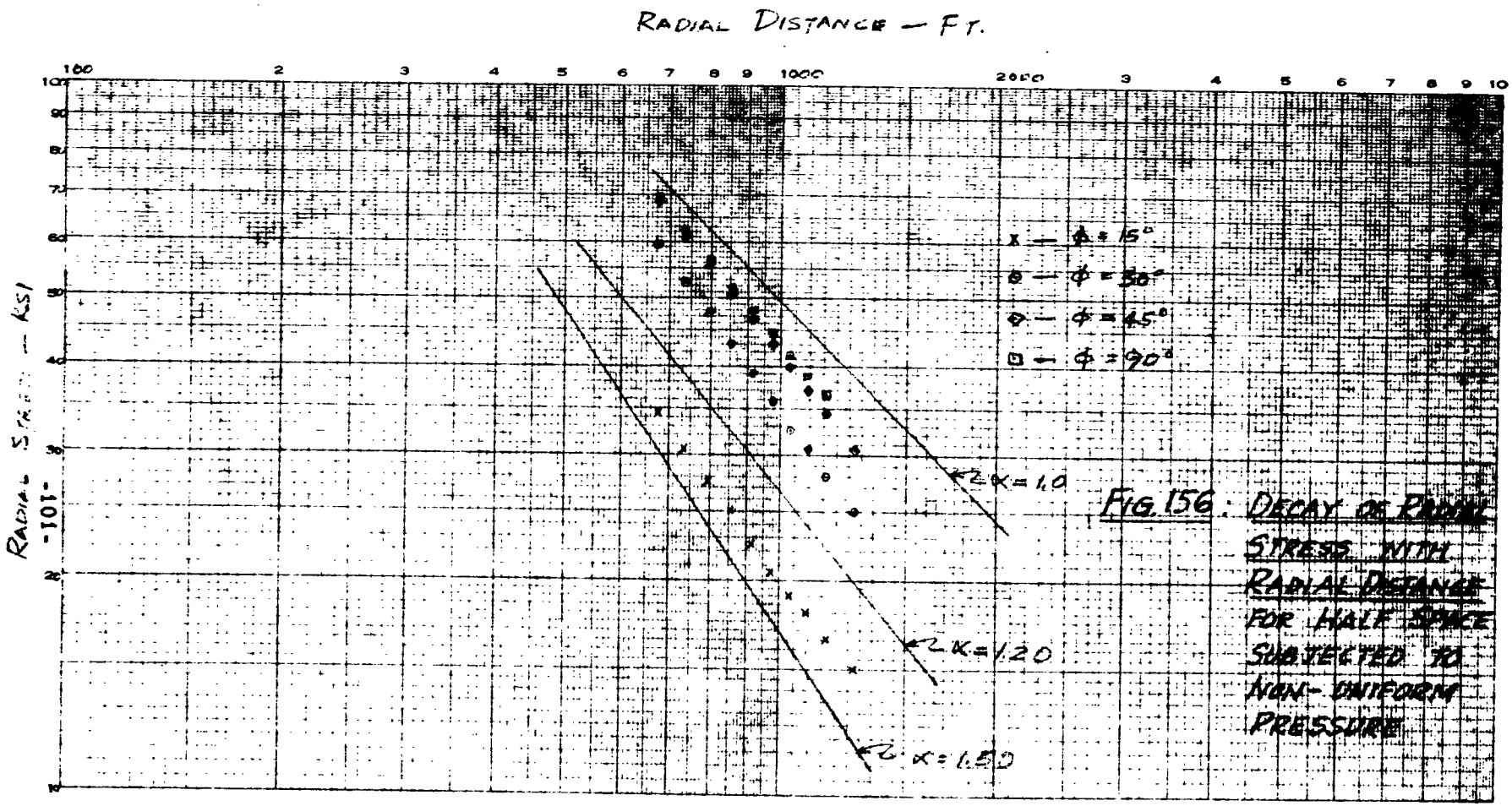

FIG. 156: DECAY OF RADIAL STRESS WITH RADIAL DISTANCE FOR HALF SPACE SUBJECTED TO NON-UNIFORM PRESSURE

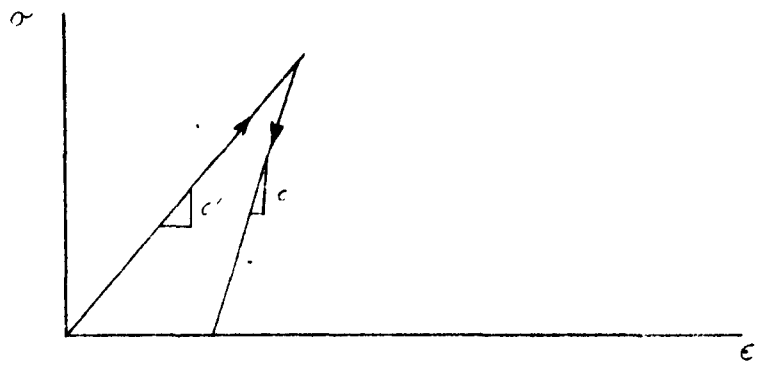

Figure 157a tress- train Relation

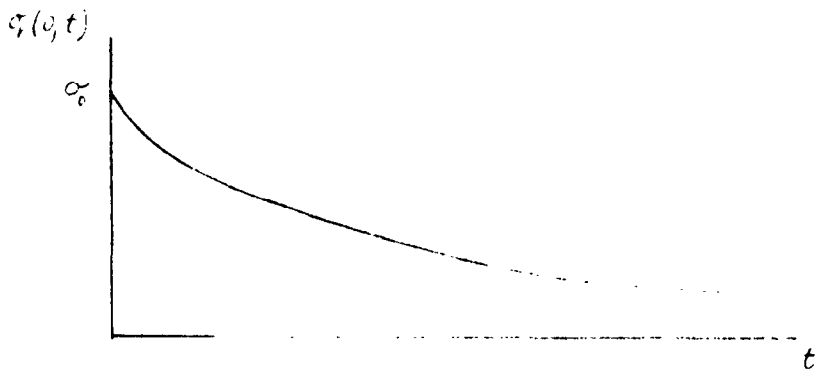

Figure 157b stress Input

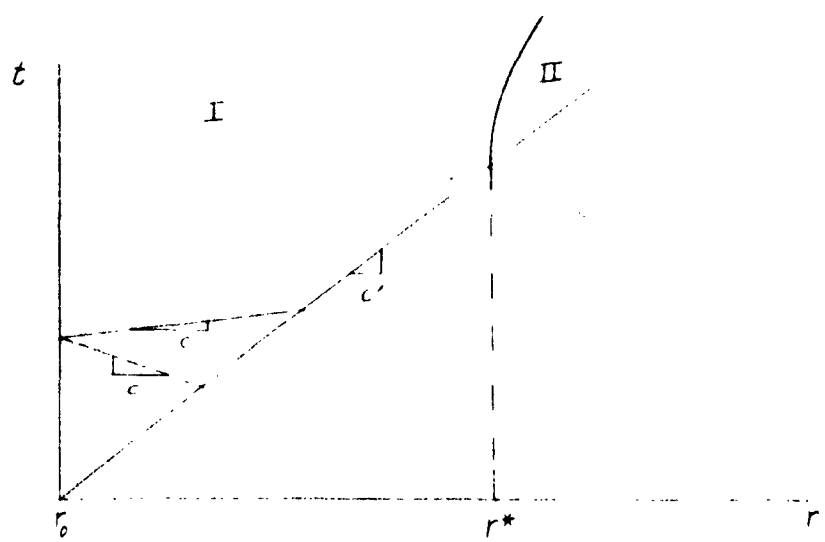

Figure 157c r - t l lane

CHAPTER V

DIRECTLY-TRANSMITTED GROUND PHENOMENA

ELASTO-PLASTIC ANALYSIS

A. INTRODUCTION

This study was originated in order to derive motion and stress values for directly-transmitted ground shock in the near-crater region, or so-called plastic zone, where neither hydrodynamic nor elastic theories is specifically applicable to obtain useful estimates of these values. The region of interest extends about the crater, from the ground surface to the vertical axis below. Very close-in, within the crater, shearing stresses are negligible in comparison with the extremely high pressures. Somewhat farther out, in the so-called plastic zone, shearing stresses become important. Still farther out, strains become small enough for elastic or visco-elastic theory to be used.

Of greater importance than determining the distribution of stress and motion throughout the plastic zone are the computations of stress and energy attenuation as a result of wave propagation through the plastic zone. This information is required because its availability, as inputs for the elastic models, immediately gives greater realism to the estimate of motions and stresses in the elastic zone.

In order to satisfy these requirements for energy attenuation and motion solutions, it is, of course, essential to formulate the problem as an elasto-plastic, two-dimensional model. The problem is a taxing technical operation involving the solution of non-linear, two-dimensional, partial differential equations and requiring the use of complex and advanced computational techniques.

A first step toward these objectives has been made in this study. A formulation of the physical model has been expressed in terms which permit a tractable computational procedure. This procedure has been tested and debugged after the usual amount of false starts and try-outs. At this stage only a pilot problem has been completed albeit with a smaller number of degrees-of-freedom than the formulation is capable of. The results demonstrate the adequacy of the computational approach and coding details in handling a realistic physical situation. They also indicate a very rapid attenuation with distance of both energy and stress. Modification of the computational procedure has been studied and planned to the end of handling a larger number of degrees-of-freedom and of speeding the routine. This is needed in order to obtain better details in the stress and deformation pattern.

In addition, the simplified method used in the pilot problem prevents the computation of the residual strains which determine the precise boundary between the plastic and the elastic zones. Modifications of the procedure again is necessary to get a measure of these strains.

The study has been performed by Dr. J. A. Brooks, who has been assisted by W. L. Frank, Director, Systems Analysis, Informatics, Inc., in the computational aspects of the work.

B. STATEMENT OF PROBLEM

The specific objective of this study is to compute the response to directly-transmitted ground shock of an elasto-plastic, semi-infinite half-space subjected to a surface explosion of a multi-megaton weapon. Close to the burst, pressures in the medium are extremely high and the shearing stresses which the medium can sustain are insignificant compared with the normal stresses and can be neglected. Somewhat farther out, shearing stresses become important and the full stress tensor must be considered. The material is strained well beyond its elastic limit and elastic theory can be used only as a first approximation. Still farther out, elastic theory or visco-elastic theory is quite appropriate.

The region of interest, as shown in the following sketch, is bounded by an inner hemispherical surface of radius r_o, the ground surface $\theta = \pi/2$, and the outer spherical surface, r_1.

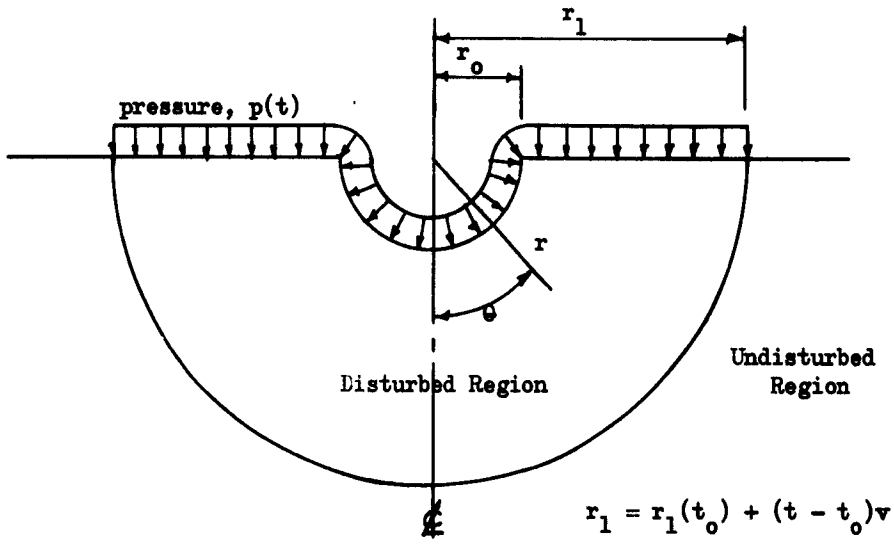

The outer radius, r_1, advances with time at a velocity, v, such that it separates the disturbed and undisturbed regions.

Solution objectives are to define the extent of the plastic zone to determine the attenuation of energy through the plastic zone, and to describe stresses, strains, displacements and velocities within the plastic zone.

C. FORMULATION

The problem is non-linear and two dimensional and therefore requires numerical treatment. The equations are given in terms of generalized coordinates rather than finite difference approximations to field equations in order to avoid speed limitations imposed by space-time mesh ratio requirements necessary for convergence. The relative speed of the two methods is not known and mesh ratio requirements were not determined. It was felt that the finite difference approach had a higher chance of complete failure by virtue of speed and, therefore, should not be the first approach to be attempted. By virtue of the generalized coordinate approach, shock discontinuities are smoothed over. Also, the degree of approximation to the exact solution for the field equations depends upon the number of generalized coordinates and the choice of basis functions.

Basis functions X_n and Y_n, as given by Equations (H-5) and (H-6),* are defined over the region $r_o \leq r \leq r_1(t)$, $0 \leq \theta \leq \pi/2$ and $0 \leq \phi \leq 2\pi$, where r, θ and ϕ are polar spherical coordinates. The radius is r; θ is the polar angle and ϕ is the meridian angle. The basis functions are independent of ϕ and, consequently, the equations are restricted to the axially symmetric case. The inner radius, r_o, is fixed (i.e., r_o = a constant for any given problem). The outer radius, $r_1(t)$, moves outward with a constant velocity, v. Displacements are expressed as linear combinations of the basis functions as given by

$$u_r = \sum_n g_n(t) X_n \tag{1}$$

*Letter H, where it appears in equation numbers, denotes Appendix H.

$$u_\theta = \sum q_n(t)\, Y_n \tag{2}$$

where coefficients, q_n, become the generalized coordinates.

Substitution of Equations (1) and (2) into the familiar expression for kinetic energy,

$$T = \frac{1}{2}\int_r\int_\theta\int_\phi \rho(\dot{u}_r^2 + \dot{u}_\theta^2)\, r^2 \sin\theta \; dr\, d\theta\, d\phi \tag{3}$$

yields:

$$T = \pi \sum_m \sum_n \left(A_{mn}\dot{q}_m \dot{q}_n + B_{mn}\dot{q}_m q_n + F_{mn} q_m q_n\right) \tag{4}$$

where A_{mn}, B_{mn}, and F_{mn} are time dependent coefficients and ρ is the mass density of the medium. Coefficients A_{mn} are given by:

$$A_{mn} = \int_{r_0}^{r_1}\int_0^{\pi/2} \rho(X_m X_n + Y_m Y_n)\, r^2 \sin\theta \; dr\, d\theta \tag{5}$$

By introducing the variable, ζ, given by:

$$\zeta = \frac{r - r_0}{r_1 - r_0} \tag{6}$$

and by requiring that X_n and Y_n be functions of θ and ζ only, coefficients A_{mn} take on the form given by:

$$\begin{aligned} A_{mn} = {} & r_0^2(r_1 - r_0)\int_0^{\pi/2}\int_0^1 \rho(X_m X_n + Y_m Y_n)\sin\theta \; d\theta\, d\zeta \\ & + 2r_0(r_1 - r_0)^2 \int_0^{\pi/2}\int_0^1 \rho(X_m X_n + Y_m Y_n)\,\zeta \sin\theta \; d\theta\, d\zeta \\ & + (r_1 - r_0)^3 \int_0^{\pi/2}\int_0^1 \rho(X_m X_n + Y_m Y_n)\,\zeta^2 \sin\theta \; d\theta\, d\zeta \end{aligned} \tag{7}$$

The integrals in Equation (7) are independent of time and can be evaluated once for each problem. Similar formulas for B_{mn} and F_{mn} are given by Equations (H-19) and (H-20) of the Appendix.

Displacements are partitioned into elastic and yielded components with primes denoting elastic components and double-primes denoting yielded components. The total displacement, or unprimed quantity, by definition of notation equals the sum of the primed and double-primed displacements. The unprimed, primed and double-primed notation is also extended to generalized coordinates and strains.

Stresses are functions of elastic strains given by the usual elastic relations between stress and strain. Consequently, the elastic strain energy of the medium is a quadratic function of the elastic components of the generalized coordinates as given by:

$$V = \pi \sum_m \sum_n D_{mn} q_m' q_n' \tag{8}$$

Coefficients D_{mn} are functions of time given by Equations (H-27) through (H-30) of the Appendix.

The potential of the external forces is given by:

$$W = \int_0^{2\pi}\int_0^{\pi/2} u_r(0,\theta)\, P(t)\, r_0^2 \sin\theta \; d\phi \, d\theta$$

$$- \int_0^{2\pi}\int_0^{\pi/2} u_\theta\left(\zeta, \frac{\pi}{2}\right) p(t)\, r \sin\frac{\pi}{2} \; d\phi \, dr \tag{9}$$

where P(t) and p(t) are pressures on the spherical surface, $r = r_o$, and on the ground surface respectively. The pressure functions, P(t) and p(t) are simplified to functions of t alone by virtue of the specific problems to be worked. Hydrodynamic computations* indicate that at certain suitable values of initial time, t_o, most of the energy transmission across a suitably chosen inner radius, r_o, will have already occurred and practically no energy transmission will have occurred across a spherical surface of radius twice that of r_o. At the same time, pressures p(r , t) and P(θ, t) will have decreased to more than an order of magnitude less than those midway between r_o and $2r_o$. The air wave front will have traveled ahead of the radius, r_1, and the pressure distribution over the ground surface from r_o to r_1 will be approximately constant at any given time. The pressure over the inner surface will have dropped to the same order of magnitude as the ground surface pressure and, by virtue of its insignificance, can be assumed to be uniformly distributed.

By making suitable substitutions of expressions already developed, Equation (9) becomes:

$$W = 2\pi \sum H_m g_m \quad , \tag{10}$$

where

$$H_m = P(t)\, r_o^2 \int_0^{\pi/2} X_m(0,\theta) \sin\theta \, d\theta$$

$$- p(t)\, r_o (r_1 - r_o) \int_0^1 Y_m(\zeta, \tfrac{\pi}{2})\, d\zeta$$

$$- p(t)\, (r_1 - r_o)^2 \int_0^1 Y_m(\zeta, \tfrac{\pi}{2})\, \zeta \, d\zeta \tag{11}$$

*Brode, H. L. and Bjork, R. L., "Cratering from a Megaton Surface Burst", RM-2600, 1960, The RAND Corporation.

From the familiar form of the Lagrangian equations of motion, or from the equivalent Hamilton's principle, the equations of motion are found to be:

$$\sum_n A_{mn}\ddot{q}_n + \sum_n B_{mn}\dot{q}_n + \sum_n C_{mn}q_n + D_{mn}q'_n = H_m \qquad m = 1, 2 \ldots \tag{12}$$

where coefficients A_{mn}, B_{mn}, C_{mn} and D_{mn} are given in Appendix H. Except in the elastic case, in which $q'_n = q_n$, an auxiliary set of yield equations must be developed for determination of the q''_n.

Suppose we apply Coulomb's equation, which is given by Equation (13), and determine values of yield strains*, ϵ''_{rr}, $\epsilon''_{\theta\theta}$, $\epsilon''_{\phi\phi}$, and $\epsilon''_{r\theta}$, such that, for given relations, the following expression is satisfied:

$$|\tau| \leq c - \sigma \tan\phi \tag{13}$$

where τ is the shearing stress, c is cohesion, σ is the normal stress and ϕ is the angle of internal friction. Let us denote the values of ϵ''_{rr}, $\epsilon''_{\theta\theta}$, $\epsilon''_{\phi\phi}$ and $\epsilon''_{r\theta}$ which have been determined from application of Equation (13) by f_1, f_2, f_3 and f_4 respectively. Then let us seek values of q''_n, n = 1, 2 .... such that yield strains computed from the q''_n approximate the values given by f_1, f_2, f_3 and f_4. By substitution of yield displacements determined from formulas such as Equations (1) and (2) into formulas for strain we obtain:

$$\epsilon''_{rr} = \sum_n q''_n \frac{\partial X_n}{\partial r} \tag{14}$$

---

*The strain notation is fairly obvious. Only the expression for $\epsilon_{r\theta}$ might cause some confusion; it is

$$\epsilon_{r\theta} = \frac{1}{2}\left(\frac{\partial u_\theta}{\partial r} - \frac{1}{r}u_\theta + \frac{1}{r}\frac{\partial u_r}{\partial \theta}\right)$$

$$\epsilon''_{\theta\theta} = \sum_n q''_n \left\{ \frac{1}{r} \right\} \left\{ \frac{\partial Y_n}{\partial \theta} + X_n \right\} \tag{15}$$

$$\epsilon''_{\phi\phi} = \sum_n q''_n \left\{ \frac{1}{r} \right\} \left\{ Y_n \cot\theta + X_n \right\} \tag{16}$$

$$\epsilon''_{r\theta} = \frac{1}{2} \sum q''_n \left\{ \frac{\partial Y_n}{\partial r} - \frac{1}{r} Y_n + \frac{1}{r} \frac{\partial X_n}{\partial \theta} \right\} \tag{17}$$

Then, if we require the following equation to be satisfied for arbitrary variations of stress, $\delta\sigma_r$, $\delta\sigma_\theta$, $\delta\sigma_\phi$ and $\delta\tau_{r\theta}$:

$$2\pi \int_r \int_\theta \Big\{ (\epsilon''_{rr} - f_1)\,\delta\sigma_r + (\epsilon''_{\theta\theta} - f_2)\,\delta\sigma_\theta + (\epsilon''_{\phi\phi} - f_3)\,\delta\sigma_\phi$$

$$+ 2(\epsilon''_{r\theta} - f_4)\,\delta\tau_{r\theta} \Big\} r^2 \sin\theta \, dr \, d\theta = 0, \tag{18}$$

we obtain the following set of simultaneous equations for determination of the q''_n

$$\sum_n D_{mn} \, q''_n = G_m \quad , \tag{19}$$

where G_m is found from:

$$G_m = \int_{r_0}^{r_1} \int_0^{\pi/2} \Big\{ \lambda (f_1 + f_2 + f_3) \left(\frac{\partial X_m}{\partial r} + \frac{2}{r} X_m + \frac{\cot\theta}{r} Y_m + \frac{1}{r} \frac{\partial Y_m}{\partial \theta} \right)$$

$$+ 2\mu (f_1) \left(\frac{\partial X_m}{\partial r} \right) + 2\mu (f_2) \left(\frac{1}{r} \right) \left(\frac{\partial Y_m}{\partial \theta} + X_m \right) \tag{20}$$

$$+ 2\mu (f_3)\left(\frac{1}{r}\right)(Y_m \cot\theta + X_m)$$

$$+ 2\mu (f_4)\left(\frac{\partial Y_m}{\partial r} - \frac{1}{r} Y_m + \frac{1}{r}\frac{\partial X_m}{\partial \theta}\right)\Big\} r^2 \sin\theta \; dr \, d\theta \qquad \text{(20 con't.)}$$

The D_{mn} coefficients in Equation (19) are the same as the D_{mn} coefficients in the equations of motion. Hence the equations of motion become:

$$\sum_n \left\{ A_{mn}\ddot{q}_n + B_{mn}\dot{q}_n + (C_{mn} + D_{mn})\, q_n \right\} = H_m + G_m \qquad (21)$$

In the "simplified theory", for which Equations (21) are the equations of motion, stresses depend only on the instantaneous total strains and not on the past strain history. The more complete theory is contained in Appendix H. In place of Equation (19), the more complete equation, copied from Equation (H-57), is as follows:

$$\sum_n D_{mn}\left\{ q_n''(t) - q_n''(t-\Delta t) \right\} = \sum_n E_{mn}\, q_n''(t-\Delta t) + G_m \;, \qquad (22)$$

Equation (22) has been coded into the existing machine program, but temporary inaccuracies in the E_{mn} matrix render the more complete code inoperative.

It remains to provide formulas for computation of f_1, f_2, f_3 and f_4. In doing so we proceed to sketch the detail contained in the Appendix quite sparsely. Combining the equation of Mohr's circle with Equation (13), we obtain:

$$\frac{S_1 - S_3}{2} \leq c \cot \phi - \left(\frac{S_1 + S_3}{2}\right) \sin \phi \tag{23}$$

$$\frac{S_1 - S_2}{2} \leq c \cot \phi - \left(\frac{S_1 + S_2}{2}\right) \sin \phi \tag{24}$$

$$\frac{S_2 - S_3}{2} \leq c \cot \phi - \left(\frac{S_2 + S_3}{2}\right) \sin \phi \tag{25}$$

where S_1, S_2 and S_3 are principal stresses ordered such that $S_3 \leq S_2 \leq S_1 \leq c \cot \phi$. Equations (23) through (25) are, in reality, only more explicit forms of Coulomb's equation.

We now compute the principal strains which for the simplified theory are given by:

$$\epsilon_1 = \frac{1}{2}\left(\epsilon_{rr} + \epsilon_{\theta\theta}\right) - \sqrt{\frac{1}{4}\left(\epsilon_{rr} - \epsilon_{\theta\theta}\right)^2 + \epsilon_{r\theta}^2} \tag{26}$$

$$\epsilon_2 = \frac{1}{2}\left(\epsilon_{rr} + \epsilon_{\theta\theta}\right) + \sqrt{\frac{1}{4}\left(\epsilon_{rr} - \epsilon_{\theta\theta}\right)^2 + \epsilon_{r\theta}^2} \tag{27}$$

$$\epsilon_3 = \epsilon_{\phi\phi} \tag{28}$$

For the more complete theory, principal strains are given by Equations (H-77) through (H-79).

Next, let

$$\epsilon_1'' = \xi_0\left(\frac{\epsilon_1+\epsilon_2+\epsilon_3}{3}\right) + \xi_1\left(\frac{\epsilon_1-\epsilon_2}{2}\right) - \xi_3\left(\frac{\epsilon_3-\epsilon_1}{2}\right) \tag{29}$$

$$\epsilon_2'' = \xi_0\left(\frac{\epsilon_1+\epsilon_2+\epsilon_3}{3}\right) - \xi_1\left(\frac{\epsilon_1-\epsilon_2}{2}\right) + \xi_2\left(\frac{\epsilon_2-\epsilon_3}{2}\right) \tag{30}$$

$$\epsilon_3'' = \xi_0\left(\frac{\epsilon_1+\epsilon_2+\epsilon_3}{3}\right) - \xi_2\left(\frac{\epsilon_2-\epsilon_3}{2}\right) + \xi_3\left(\frac{\epsilon_3-\epsilon_1}{2}\right) \tag{31}$$

where coefficients ξ_0, ξ_1, ξ_2, and ξ_3 are to be determined such that Equations (26) through (28) are satisfied. It is found that if

$$c\cos\phi \geq \left(\lambda + \tfrac{2}{3}\mu\right)(\epsilon_1+\epsilon_2+\epsilon_3)\sin\phi \tag{32}$$

then

$$\xi_0 = 0 \tag{33}$$

If Equation (32) is not true, then

$$\xi_0 = 1 - \frac{c\cot\phi}{\left(\lambda+\frac{2}{3}\mu\right)(\epsilon_1+\epsilon_2+\epsilon_3)} \tag{34}$$

Having ξ_0, if $\epsilon_1 \leq \epsilon_3 \leq \epsilon_2$, and if

$$2\mu\left(\frac{\epsilon_2-\epsilon_1}{2}\right) \leq c\cos\phi - \sin\phi\left\{\left[\epsilon_1+\epsilon_2+\epsilon_3\right]\left[\lambda-\left(\lambda+\tfrac{2}{3}\mu\right)\xi_0\right] + 2\mu\left(\frac{\epsilon_2+\epsilon_1}{2}\right)\right\} \tag{35}$$

then

$$\xi_1 = \xi_2 = \xi_3 = 0\,. \tag{36}$$

Otherwise, if

$$\xi_3 - \left(\frac{\epsilon_2+\epsilon_1}{2}\right) \geqslant 0 \tag{37}$$

and if

$$2\mu\epsilon_3 - 2\mu\left(\frac{\epsilon_2+\epsilon_1}{2}\right) \leq c\cos\phi - \sin\phi\left\{\left[\epsilon_1+\epsilon_2+\epsilon_3\right]\left[\lambda - \left(\lambda+\tfrac{2}{3}\mu\right)\xi_0\right] + 2\mu\left[\frac{\epsilon_2+\epsilon_1}{2}\right]\right\} \tag{38}$$

then

$$\xi_1 = 1 - \frac{c\cos\phi - \sin\phi\left\{\left[\epsilon_1+\epsilon_2+\epsilon_3\right]\left[\lambda-\left(\lambda+\tfrac{2}{3}\mu\right)\xi_0\right]+2\mu\left[\frac{\epsilon_2+\epsilon_1}{2}\right]\right\}}{2\mu\left(\frac{\epsilon_2-\epsilon_1}{2}\right)} \tag{39}$$

and $\xi_2 = \xi_3 = 0$. The complete set of possibilities includes 8 other cases which are given in the Appendix. Having obtained ϵ_1'', ϵ_2'', and ϵ_3'', a transformation inverse to Equations (26), (27) and (28) gives f_1, f_2, f_3 and f_4 for use in numerical evaluation of G_m, m = 1, 2 .....

The machine program was originally coded from working reports whose contents are essentially the same as given in Appendix H of this report, except for differences in notation and grouping of terms. Coding, formula evolution, and reporting never reached exact coincidence. The code was gradually "de-bugged" and modified in order to eliminate trouble which manifests itself as a violation of the principle of conservation of energy. In addition to correction of coding errors, two modifications had a prounouced effect on the computations.

The first modification concerned the simultaneous integration of the equations of motion, given by Equation (12), and the stepwise advancement of the yield components of the generalized coordinates by use of Equation (22). The program uses a Runge-Kutta integration routine which requires computation of derivatives at times t, t + h/2, t + h/2 and t + h for integration over the interval from t to t + h. Associated with successive derivative computations within an integration cycle, the values of Δt in Equation (22) were originally taken to be 0, h/2, 0, and h/2, corresponding to time intervals from t to t, t to t + h/2, t + h/2 to t + h/2 and t + h/2 to t + h. The original sequence of Δt values in Equation (22) was changed to 0, h/2, h/2 and h, corresponding to time intervals from t to t, t to t + h/2, t to t + h/2 and t to t + h. This change produced physically plausible results for short test runs but energy growth trouble returned when attempts were made to integrate over durations of time suitable for practical problems.

The second modification was made when it was learned that inaccuracies in matrix elements, E_{mn}, were causing the difficulty. The change consists of replacing Equation (22) by Equation (19) and replacing Equations (H-77) through (H-79) by Equations (26) through (28). Errors in the E_{mn} elements are on the order of $(\Delta t)^2$ by virtue of its derivation. This leads to errors in the time-wise advancement of Equation (22) which are not acceptable. This inadequacy can be corrected in the derivation and incorporated into the code, but lack of time prevented doing so in this study.

D. PILOT PROBLEM

A pilot problem has been run which demonstrates the adequacy of the method and correctness of the coded procedure. The problem parameters are as follows:

Number of degrees of freedom	$N = 4$
Lamé's constants	$\lambda = 301$ ksi
	$\mu = 451$ ksi
Density	$\rho = 3.3$ slugs/ft^3
Cohesion	$c = 100$ psi
Dilatational wave velocity	7250 ft/sec
Air pressure parameters for	2 MT burst
Inner radius	$r_o = 250$ ft
Initial outer radius	$r_1(t_o) = 300$ ft
Beginning of computation	22 milliseconds
Initial strain energy	zero
Initial kinetic energy	3.07×10^{14} ft - lbs

Initial conditions were chosen to give a velocity distribution which, qualitatively, had the appearance of the velocity distributions shown in RAND report number RM-2600 by Brode and Bjork. The magnitudes of the velocities were chosen such that the initial kinetic energy was 100 KT (TNT equivalent). The initial strain energy was taken to be zero since code checks had shown a rapid re-apportionment of energy irrespective of the initial assumptions. The initial conditions are as follows:

$$q_1(t_0) = q_2(t_0) = q_3(t_0) = q_4(t_0) = 0$$
$$\dot{q}_1(t_0) = 703 \text{ ft/sec.}$$
$$\dot{q}_2(t_0) = 703 \text{ ft/sec.}$$
$$\dot{q}_3(t_0) = 703 \text{ ft/sec.}$$
$$\dot{q}_4(t_0) = 1406 \text{ ft/sec.}$$

This choice gives a peak initial horizontal velocity at the ground surface of about 2.6 feet per millisecond and a peak initial vertical velocity (not at the same point) at the ground surface of about 1.2 feet per millisecond upward. Directly below the burst, the peak velocity is about 3.5 feet per millisecond at the beginning of computations.

Results obtained from the computer are tabulated at regularly-spaced intervals in time, angle Θ, and coordinate ζ; they are then plotted against radius for fixed values of time and angle Θ. From these plots, quantities can be re-plotted as functions of time or angle Θ.

Figure 158 shows radial stress versus time for various radii along a line which makes an angle of 72 degrees with the vertical axis. Figure 159 shows radial stress versus time for points along the vertical axis. Inversion of stress magnitudes from what one would expect is due to too large a value of $\dot{q}_2(t_0)$ in the initial conditions. The initial velocity distribution for the pilot run simply does not match the intended initial distribution and, as a result, the region below the

crater is rapidly put into tension. The limiting value of tension, which is c cot ϕ, shows up as zero on the scale of Figures 158 and 159. Of course, more appropriate initial conditions can be used.

Results shown in Figure 158 and 159 were so disturbing that hand computations were performed to spot check the machine computation of yield strains. An error was found but it could not possibly have influenced the results appreciably. The error had the effect of limiting the tensile stresses to approximately 600 psi instead of 172 psi, as had been intended. Figure 160, which shows time histories of tangential stress for θ = 72 degrees, is given for comparison with Figure 158. Although the time scales used in Figures 158 and 160 are different, it can be seen that the general curve shapes for both radial and tangential stresses are quite similar. As shown by these figures, tangential stresses apparently begin to attenuate more rapidly than radial stresses beyond a distance of 1,000 feet. No explanation of this phenomenon has been found as yet.

Radial displacements along the vertical axis (θ = 0 degrees) are shown in Figure 161; radial displacements for θ = 72 degrees are shown in Figure 162. These results are not a good representation of the true physical behavior. This occurrence in the computed results can be explained on the basis of a deficiency in the choice of basis functions. Of the basis functions currently contained in the computer program, none has a radial strain component different from zero at $r = r_o$. This deficiency can be corrected relatively easily and such a correction is an obvious necessity before further computations are made.

Figure 163 shows tangential displacements along $\theta = 72$ degrees for various radii. The curves extend to 225 milliseconds. Computations were performed out to 490 milliseconds and the tangential displacements peak at approximately 280 milliseconds. The fact that tangential displacements are large is just another result of the initial velocity pattern which was chosen. Another factor contributing to the large displacements shown in Figures 161, 162 and 163 is the inability of the "simplified theory" to leave behind residual displacements.

The computer results are heartening in that they indicate the readiness of a usable computer code and in that they indicate a high attenuation of stress. However, any conclusion to be drawn from them must, of course, take into account the preliminary nature of the results. These results are intended only as an indication of the possibilities of approaching an extremely difficult and complex problem in a greatly simplified manner. That certain physical conditions have been violated is not at all surprising. Correcting such discrepancies is part of the usual effort in evolving such techniques.

E. CONCLUSIONS AND RECOMMENDATIONS

The following comments summarize the Brooks study of the propagation in soil of an axially symmetric wave generated by a nuclear detonation at the ground surface. The general objective of this analysis is to provide motion and stress values for the directly-transmitted ground shock in the near crater region where plastic disturbances are likely to occur. These comments define the extent of the results obtained thus far and outline the work necessary to carry further the already-developed analytical techniques to the level and range of conditions required for confident engineering design.

The model is that of an elasto-plastic medium bounded by the ground surface plane and two concentric spherical surfaces of radii, r_0 and r_1. The inner surface describes approximately the boundary between the hydrodynamic and the plastic regimes. The outer surface describes the boundary beyond which the medium is undisturbed at any given time. The model is specifically developed to treat the plastic two-dimensional behavior of the ground at the crater periphery. The hydrodynamic inputs are derived from the Brode-Bjork data which were graphically reduced to a more suitable and simple form. For the conditions computed by Brode and Bjork, the radius of the interior sphere is approximately 70 meters or less.

The model is designed to provide displacements, stresses, strains, and, in particular, partitioning of strains into elastic and plastic components. These values are obtainable for any selected net point in time and space for any ground medium described parametrically by the angle of friction ϕ, cohesion c, and Lamé constants λ and μ. The net points are defined at regular time intervals Δt at regular

spatial intervals in spherical coordinates θ and r, where θ is the angle between the vertical axis and radius r going through the burst point.

A computing code is available. The basic formulation uses a generalized coordinate approach rather than a finite difference approach. It incorporates certain simplifications. For instance, shock discontinuities in the region between the hemispherical boundaries have been ignored and smoothed over by means of a series expansion which is the same over the whole region. This simplification does not invalidate the two-dimensional aspect of the model.

In a similar fashion, the air blast pressure over the ground surface at any given time is assumed not to extend beyond the radius of the outer boundary. This simplified assumption does not allow the simultaneous treatment of air-induced and directly-transmitted ground shock but the soil confinement from the air load is properly simulated. The code was developed for the IBM 1604 computer. It can compute the components of stress, elastic and plastic strain, and displacements at net points within the region. At present, the code also incorporates a simplified yield condition in which the stresses depend solely on total strains and Coulomb's equation. Only one pilot problem has been solved using relatively simple soil parameters and weapon inputs. Resulting soil stresses and motions have been computed for only a few space points and time intervals. Because the small number of generalized coordinates used in this pilot problem restricts the detail of the solution, the results do not provide final design data. They do, however, demonstrate the adequacy of the computational approach.

The analysis and computer program developed in this study are now ready for solution of physically significant surface burst problems. At present, the numerical procedure employs stress computation routines which do not depend on the past strain history but only on current strains. Thus the present code does not include the ability to handle residual strains and displacements, but there is no indication that this feature cannot be added.

Preliminary results from the pilot problem used to check the programming indicates that directly transmitted ground shock from a 2 MT burst will be insignificant in a structural design sense beyond a radius of about 2,000 feet.

Further effort toward making the Brooks solution more useful in the definition of underground effects logically divides itself into two sequential phases, the first being concerned with improving the code and the second consisting of parametric solutions.

Improvement of the code has two concurrent objectives. The first is to improve the available code by incorporating a more sophisticated yield condition in which stresses depend upon the past strain history. The second is to enhance the speed of computing operations and thus substantially diminish the burden and cost of the parametric studies of soil response in the plastic region.

The present difference equation form of the yield equations has been found less accurate than the companion differential equation form of the equations of motion. This difference equation can be replaced by a hybrid differential difference formulation which will correct the difficulties inherent in a generalized coordinate

approach. The generalized coordinate system was adopted early in the analysis of the model in order to provide the simplification necessary for solution.

The lack of speed in the computational procedure has been found to be due primarily to recomputation of quantities which could be stored in the computer memory. Therefore, the code should be modified in order to optimize data transfer and use of tape units.

Parametric studies are needed both to indicate the sensitivity of computed results to changes in soil parameters and to provide free-field design inputs for the analysis of structures in the plastic zone. As a basic program to be followed it is suggested that three typical earth materials be chosen for study: a hard rock, a soft clay or other plastic soil, and a soil of characteristics between those of rock and soft clay.

Each of these media can be described by a set of parametric values, (i.e., λ , μ, ϕ, and c). Computed results of stresses, strains, displacements and velocities should be obtained for each set of parametric values rather than for independent variation of soil parameters. The bomb inputs to such analyses are those found in the Brode-Bjork computations of RM-2600 (and subsequent amended and unpublished data using a finer mesh)as well as any later computations by AFSWC. These data provide both initial energy and pressure-versus-time functions, each of which is sufficient for total excitation of the plastic regions. The response of one of the three media to each of these functions should be computed and compared in order to ascertain their compatibility with the general model as well as with the

set of parametric values describing the media.

Thus a first extension of the Brooks study involves a minimum of four sets of computations. It must be understood that the use in the computations of the RAND data automatically involves certain uncertainties and limitations. The influence of the plastic zone behavior on the pressures in the hydrodynamic zone is ignored. This influence, however, has been shown by Newmark to be small and the results of a parametric study will enhance considerably our quantitative understanding of the physical phenomena. Such a study should be primarily aimed toward distinguishing between the environment created by the wave propagation at the surface on one hand and at depths below the crater on the other. The Brooks model, in fact, is not designed to measure small localized variations at minute depth differences; consequently, the rays, (along which information is reported as a function of distance and time) should be limited to a small number. The number of rays and points on each ray will be determined by the requirement for graphical presentation of the results.

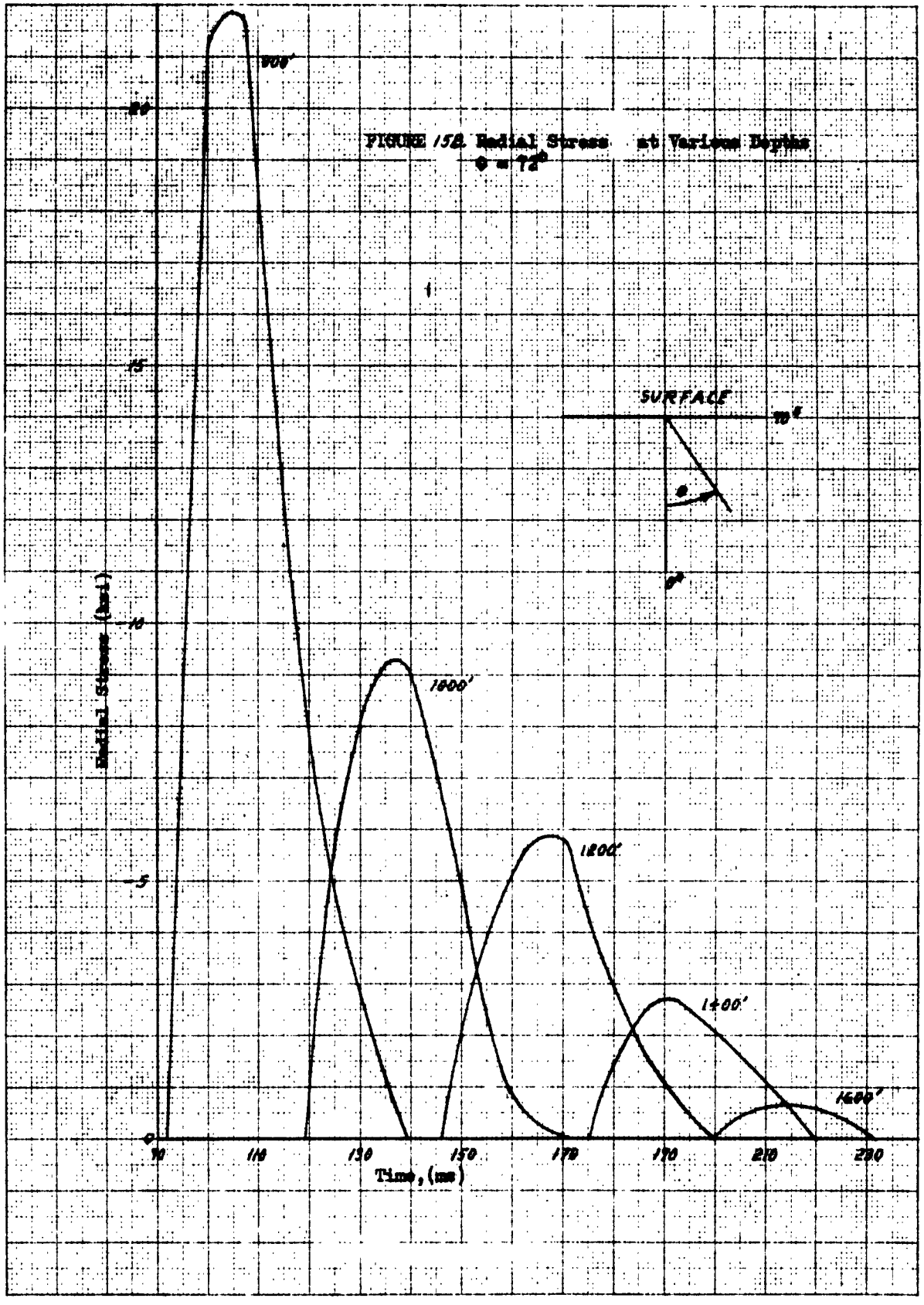

FIGURE 15B. Radial Stress at Various Depths
$\phi = 72^{\circ}$

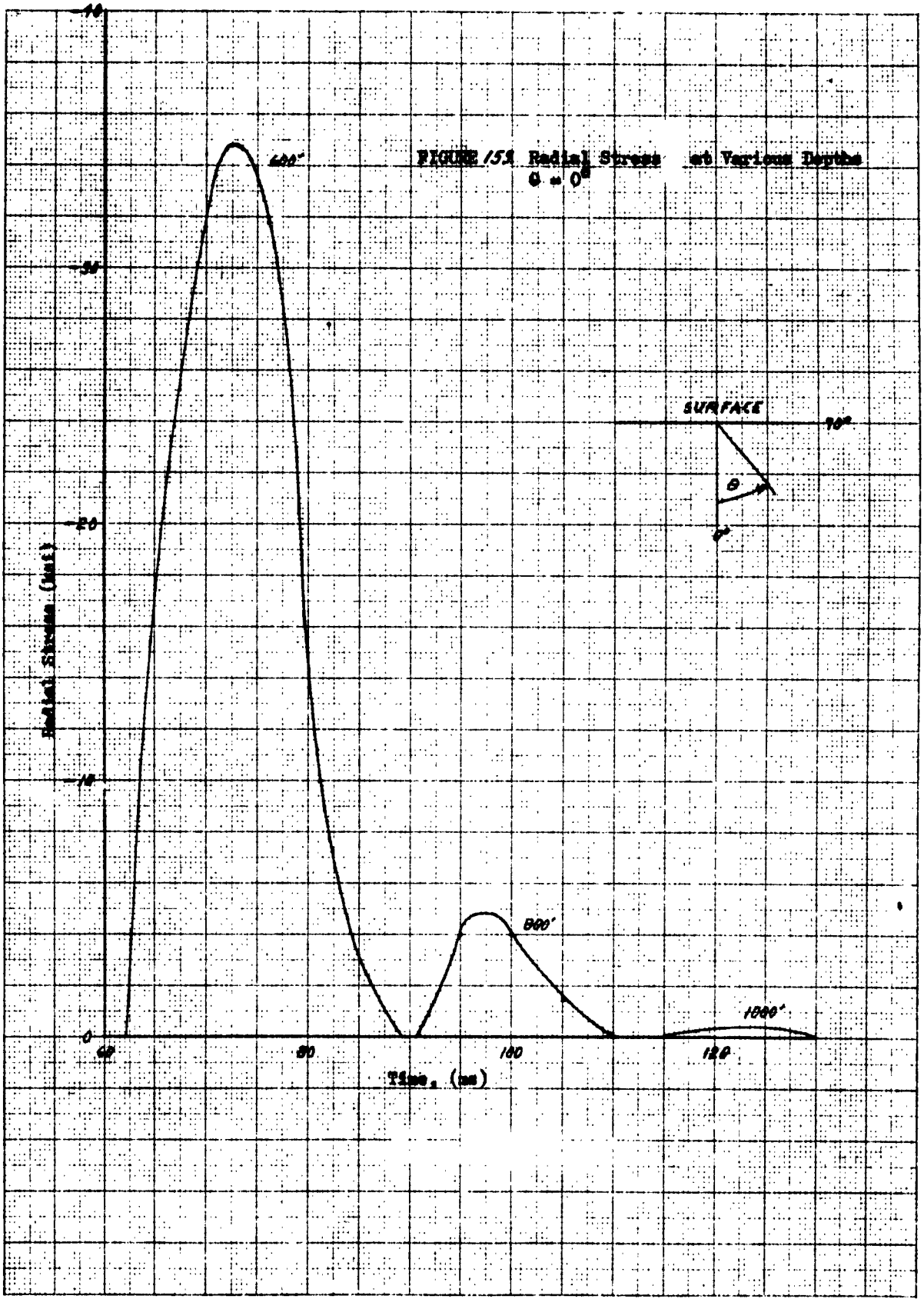
FIGURE 151 Radial Stress at Various Depths
Φ = 0°
400'
800'
1000'
SURFACE
90°
θ
0°
-10
-30
-20
-10
0
Radial Stress (psi)
60
80
100
120
Time, (ms)

10 X 10 TO THE CM. 359F-14G
KEUFFEL & ESSER CO.
ALBANY, N.Y.

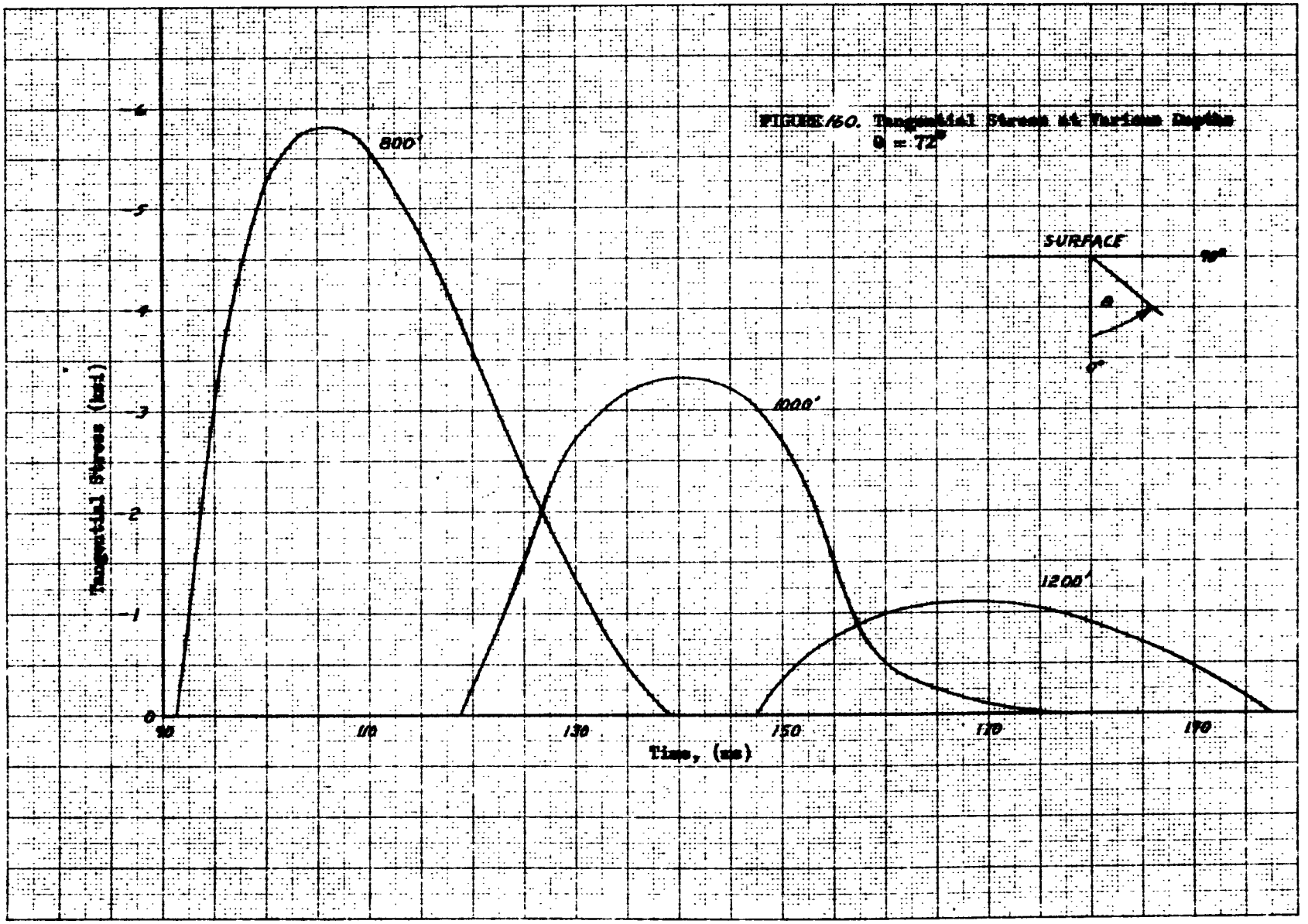

FIGURE 150. Tangential Stress at Various Depths
θ = 72°

10 X 10 TO THE CM. 359T-14G
KEUFFEL & ESSER CO.
ALBANY, N.Y.

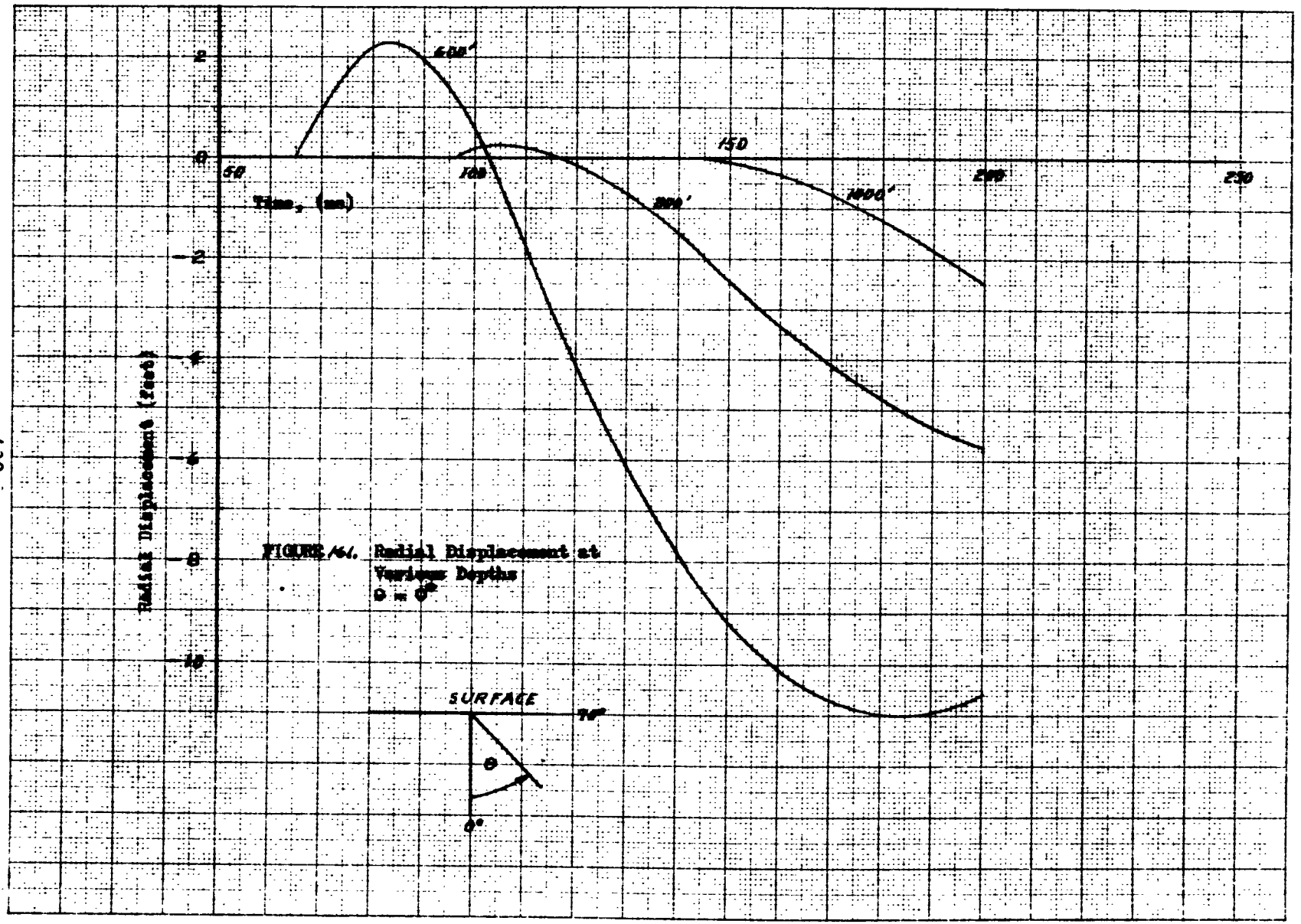

FIGURE 161. Radial Displacement at Various Depths
θ = 0°

10 X 10 TO THE CM. 359T-14G
KEUFFEL & ESSER CO.
ALBANENT X

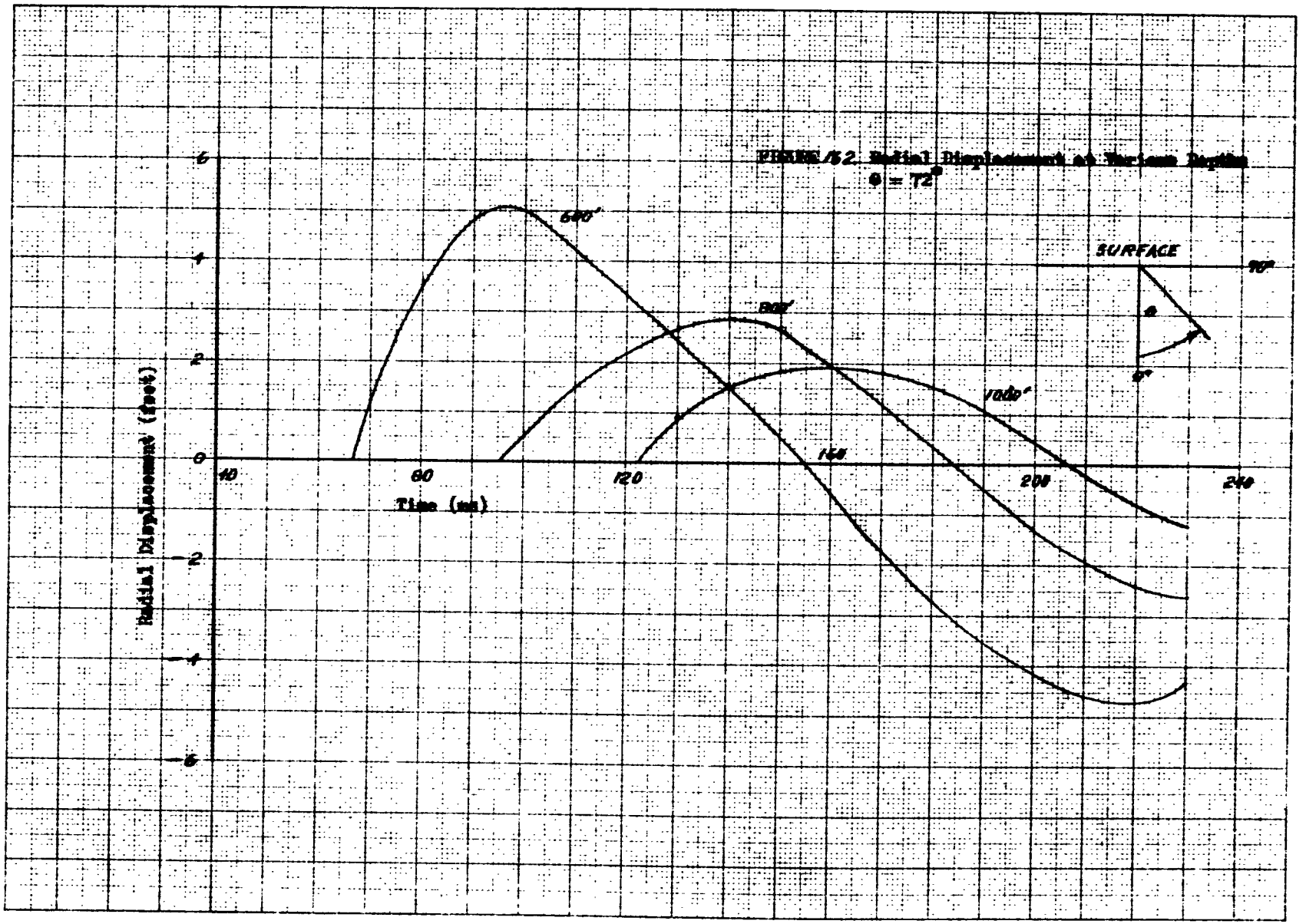

FIGURE 52. Radial Displacement at Various Depths
$\theta = T2^{\theta}$

10 X 10 TO THE CM. 359T-14G
KEUFFEL & ESSER CO.
ALBANY, N.Y.

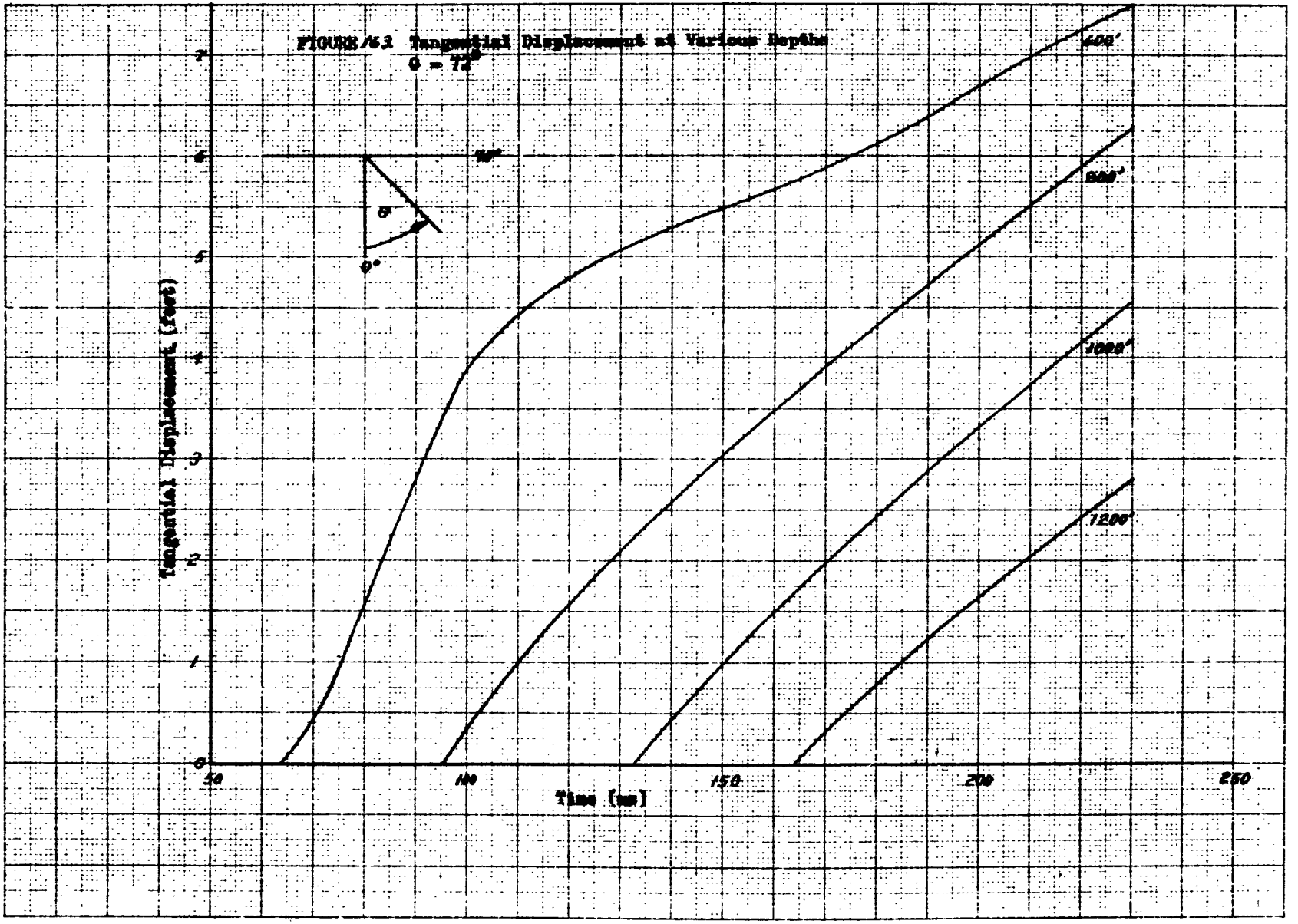

CHAPTER VI

COMBINED EFFECTS

By combined effects is meant primarily the combination of air-induced and directly-transmitted ground effects. Another combined effect, that of the Rayleigh wave, is a result of complex interactions of the dilatational and shear waves and is all air-induced. It has been discussed in Chapter II (Vol. I). Before discussing means of combining air-induced and directly-transmitted effects, it is helpful to summarize briefly the state of the art of determining directly-transmitted effects.

A. STATE OF THE ART -- DIRECTLY-TRANSMITTED EFFECTS

1. Hydrodynamic Analysis

The hydrodynamic cratering analysis of Brode and Bjork has been used as input to both of the analyses of directly-transmitted ground effects; therefore, any uncertainties or approximations in the hydrodynamic analysis will affect the results farther out. Several approximations were made as well as certain assumptions. One of the approximations is the equation of state of the only material considered, Nevada tuff; the approximation is satisfactory for this material but not necessarily for other ground materials. However, one of the results of Newmark's analysis is an indication that the computations are not sensitive to variations in the equation of state. Further effort is required to establish this important conclusion.

Details of the weapon decomposition and other early-time phenomena have been based on assumptions which are based on highly-classified weapon detail information; hence, calling the detonation a 2 MT burst is open to question. Knowledge of the

basis of these assumptions is of little value since the attacker's weapons will remain an unknown quantity. Thus, a major input will always be uncertain, a fact which simply must be accepted. Location of the explosion is also limited at present to the ground surface since the RAND computations were made only for a surface burst. Depth effects should be considered in any further computations undertaken.

The Eulerian approach to the hydrodynamic problem carries with it certain difficulties and has resulted in some smearing of the shock front. This is not a critical difficulty nor does it bring about possible large errors.

In summary it can be stated that the hydrodynamic analysis of Brode and Bjork is highly satisfactory as a means of determining energy partitioning between air and ground-shock. Computations based on this analysis have proven to be adequate as inputs to analyses of the plastic and elastic regions beyond the crater. The chief shortcoming of the computations lies in the limited extent of the results. More materials need to be studied as well as detonations at various depths. Until such results are obtained it is necessary to limit the conclusions which can be drawn from the plastic and elastic analyses of Brooks and Newmark.

2. Elastic Analysis (Newmark)*

Newmark's analysis takes as inputs the hydrodynamic results at a radius of about 650 feet. These are applied directly to an elastic half-space without any consideration of plastic-zone effects, including attenuation of peak stress and change of pulse shape. Neglect of the plastic zone was dictated by available means of obtaining approximations of response. The basic model used by Newmark is a mass-sprung approximation

---

*See Chapter 4, Vol. II

incorporating radial and tangential degrees of freedom. To this model were applied pressure-time inputs based on the hydrodynamic results. An important result of one part of the Newmark study is that the variation of material properties from one side of the hydrodynamic boundary to the other (i.e., from hydrodynamic to elastic in Newmark's analysis) does not cause serious reflections or other difficulties in matching hydrodynamic outputs to elastic inputs. Because Brode's results were for tuff, Newmark's results were limited to a similar material.

Results of these computations are extremely interesting but, as is to be expected with first results of complicated analyses, raise several questions that must be answered before practical use can be made of the results. First, the results show large tensile tangential stresses far beyond the ability of ground materials to resist. Furthermore, results are obtained only for fairly large depths at moderate distances from the burst because the ray nearest the surface emanates from the burst at a 15 degree angle from the horizontal. Also significant for shallow-depth effects is the neglecting of air blast loading on the surface.

In addition to closing the gaps in the results as listed above, results from the Newmark analysis should be extended to layered media and viscoelastic media. The analysis is capable of handling these more complex problems with only moderate changes and additions.

3. Elasto-Plastic Analysis (Brooks)*

The Brooks plastic-region analysis was undertaken precisely to close the gap between the hydrodynamic and elastic regions. Newmark's results extend the elastic region to over 100,000 psi, which is far above the elastic stress-carrying ability of earth materials. The main results which were sought from the plastic analysis are the limits of the plastic zone and the amount of attenuation of energy and stress within this zone.

This analysis employs generalized coordinates and numerical approximations and includes a means of detecting the cessation of inelastic behavior. Further, it eliminates one of the problems encountered in Newmark's results, that of high tensile stresses, by limiting tensile stresses to a level which a ground material can withstand; Coulomb's equation is the basis of the assumed behavior of the ground. Only one pilot problem has been run and the computed results are extremely interesting although inadequate for use as design inputs. Certain necessary assumptions were found to be unrealistically chosen; this caused some inconsistencies. Such occurrences are, of course, the rule for first results from highly complex analyses, and do not affect the validity of the procedure.

The preliminary results, which include the effect of air-blast loading on the surface, show large attenuation of stress and energy in the plastic zone. No results were obtained near the surface, however, because the shallowest ray which was used was at an angle of 18 degrees from the horizontal. The solution is capable of considering shallower rays (even surface rays) and such rays should be included in any extensions of the computations. The most important shortcoming of the computer program, from which these results have been obtained, is

---

*See Chapter 5, Vol. II

its low speed. Another lack is that of a more sophisiticated yield condition than that used thus far. After these problems are corrected, parametric studies should be undertaken to show how sensitive results are to ground material properties. When this has been established, typical earth materials properties should be used in computations which would be suitable for design inputs for structures which might be located in the plastic medium.

In addition, based on Newmark's conclusion that interface discrepancies do not seriously affect the phenomena transmitted across the interface, it will be possible to combine the hydrodynamic, plastic, and elastic analyses in one solution, and, further, to include air-induced effects. This combination will constitute the first complete and unified description of ground effects in the close-in region and beyond Proposed means of accomplishing this are outlined in the following section.

B. PROPOSED METHODS FOR COMBINING EFFECTS.

The Brooks analysis has been shown to be capable of handling the ground stresses and motions associated with the zone of hydrodynamic behavior. The precise boundary at which behavior changes from hydrodynamic to plastic is unknown and, indeed, probably does not exist as a definable interface. Therefore, a suitable radius can be chosen, as was done for the Brooks pilot problem, and inputs to the plastic analysis obtained from the hydrodynamic stresses and motions. In the hydrodynamic region air blast effects are trivial, although the hydrodynamic analysis does include such effects.

The plastic analysis, including air blast effects (which increase in importance with increasing distance from the burst) gives results which can be used to extend the description of the phenomena into the elastic regime. This can be accomplished in three possible ways.

The first method is to continue the elasto-plastic analysis according to the Brooks equation into the elastic zone. This would not result in the most detailed estimates of stresses and strains because the procedure is hindered by the non-linear features of the plastic analysis which are not required for the elastic solution.

The second method is to use the Newmark analysis in which the stress inputs into the elastic zone are obtained from the Brooks plastic analysis. This procedure presents no intractable difficulty and appears rather attractive. The Newmark analysis must, of course, be extended to points nearer the surface at distances of interest and air blast effects must be added to the description.

The last method is to use a half-space solution similar to that of Freeman Gilbert for the Rayleigh wave problem. The procedure would consist of applying to the surface of the elastic solid a point source input which is derived from the energy attenuation factor computed in the plastic analysis. This procedure is feasible because no energy attenuation takes place in an elastic body. The characteristics of the surface input can be varied until a match is obtained between the stresses and motion (at the radius corresponding to the plastic zone limit) in the elastic half-space and those obtained

from the combined hydrodynamic and plastic analyses. It will be necessary to choose the source such that air blast effects are the same as those from a surface burst or, alternatively, to use superposition to combine a solution for an air burst (such as the Gilbert Rayleigh wave pulse) with the surface source. Since the solutions are linear, no difficulties arise. This last approach has certain advantages in dealing with locations near the surface but is not as versatile as Newmark's numerical technique.

DISTRIBUTION LIST FOR

BLAST & SHOCK

R & D REPORTS

Revised 9 Nov. 1962

ADDRESSEE	ARMY	No. of Cys.
Chief of Research and Development, D/A, Washington 25, D. C. Attn: Atomic Division		1
Chief of Engineers, D/A, Washington 25, D. C.		
Attn:	ENGCW-NE	1
	ENGTE-E	1
	ENGMC-E	1
Commanding General, U. S. Army Materiel Command, Washington, D. C. Attn: AMCRD-DE-N		2
Commanding General, U. S. Continental Army Command, Ft. Monroe, Virginia		1
President, U. S. Army Air Defense Board, Ft. Bliss, Texas		1
Commandant, Command & General Staff College, Ft. Leavenworth, Kansas, Attn: Archieves		1
Commandant, U. S. Army Air Defense School, Ft. Bliss, Texas Attn: Command & Staff Dept.		1
Director, Special Weapons Development, Hq, CDC, Ft. Bliss, Texas, Attn: Chester I. Peterson		1
Commanding General, Aberdeen Proving Ground, Aberdeen, Md. Attn: Director, BRL		1
Commanding General, The Engineer Center, Ft. Belvoir, Va. Attn: Asst. Commandant, Engineer School		1
Director, U. S. Army Research and Development Laboratory Ft. Belvoir, Va. Attn: Chief, Tech. Support Branch		1
Commanding Officer, U. S. Army Mobility Command, Center Line, Michigan		1
Commanding Officer, Picatinny Arsenal, Dover, N. J. Attn: ORDBB-TK		1
Commanding Officer, Transportation Research Command, Ft. Eustis, Va., Attn: Chief, Tech. Info. Div.		1

ARMY CONT'D	No. of Cys.
Commanding General, USA Electronic R&D Lab., Ft. Monmouth N. J., Attn: Technical Documents Center, Evans Area	1
Commanding General USA Missile Command, Huntsville, Alabama	1
Commanding General, USA Munitions Command, Dover, New Jersey	1
Commanding Officer, U. S. Army Corps of Engineers, Beach Erosion Board, Washington, D. C.	1
Commanding Officer, U. S. Army Nuclear Defense Laboratory, Edgewood Arsenal, Edgewood, Md., Attn: Tech. Library	1
Director, Waterways Experiment Station, U. S. Army Corps of Engineers, Vicksburg, Mississippi, Attn: Library	1
Director, U. S. Army Corps of Engineers, Nuclear Cratering Group, Livermore, California	1
NAVY	
Chief of Naval Operations, ND, Washington 25, D. C.	
Attn: OP-75	2
Attn: OP-03EG	1
Director of Naval Intelligence, ND, Washington 25, D. C.	
Attn: OP-922V	1
Chief, Bureau of Naval Weapons, ND, Washington 25, D. C.	2
Chief, Bureau of Ships, ND, Washington 25, D. C.	
Attn: Code 372	1
Attn: Code 423	1
Chief, Bureau of Yards and Docks, ND, Washington 25, D. C.	
Attn: Code D-400	1
Attn: Code D-440	1
Chief of Naval Research, ND, Washington 25, D. C.	
Attn: Code 811	1
Commander-in-Chief, U. S. Pacific Fleet, FPO, San Francisco, California	1
Commander-in-Chief, U. S. Atlantic Fleet, U. S. Naval Base, Norfolk 11, Va.	1

NAVY CONT'D	No. of Cys.
Commandant of the Marine Corps, ND, Washington 25, D. C. Attn: Code AO3H	4
President, U. S. Naval War College, Newport, R. I.	1
Superintendent, U. S. Naval Postgraduate School, Monterey, California	1
Commanding Officer, Nuclear Weapons Training Center, Atlantic, Naval Base, Norfolk 11, Va., Attn: Nuclear Warfare Dept.	1
Commanding Officer, U. S. Naval Schools Command, U. S. Naval Station Treasure Island, San Francisco, California	1
Commanding Officer, Nuclear Weapons Training Center, Pacific, Naval Station, North Island, San Diego 35, California	2
Commanding Officer, U. S. Naval Damage Control Training Center, Naval Base, Philadelphia 12, Pa., Attn: ABC Defense Course	1
Commander, U. S. Naval Ordnance Laboratory, Silver Spring 19, Md.	
Attn: EA	1
Attn: EU	1
Attn: E	1
Commander, U. S. Naval Ordnance Test Station, China Lake, Calif.	1
Commanding Officer & Director, U. S. Naval Civil Engineering Laboratory, Port Hueneme, Calif., Attn: Code 131	1
Director, U. S. Naval Research Laboratory, Washington 25, D. C.	1
Commanding Officer & Director, Naval Electronics Laboratory, San Diego 52, California	1
Commanding Officer, U. S. Naval Radiological Defense Laboratory, San Francisco, Calif., Attn: Tech. Info. Division	1
Commanding Officer & Director, David W. Taylor Model Basin, Washington 7, D. C., Attn: Library	1
Underwater Explosions Research Division, DTMB, Norfolk Naval Shipyard, Portsmouth, Virginia	1

AIR FORCE	No. of Cys.
Hq, USAF (AFDRC/NE - Maj. Lowry) Washington 25, D. C.	1
Deputy Chief of Staff, Plans and Programs, HQ USAF Washington 25, D. C., Attn: War Plans Division	1
Director of Research and Development DCS/D, Hq USAF, Washington 25, D. C., Attn: Guidance & Weapons Division	1
Air Force Intelligence Center, Hq USAF, ACS/I (AFCIN-3K2) Washington 25, D. C.	1
Commander-in-Chief, Strategic Air Command, Offutt AFB, Nebraska, Attn OAWS	1
Commander, Tactical Air Command, Langley AFB, Virginia, Attn: Document Security Branch	1
ASD, Wright Patterson AFB, Ohio	1
Commander, Air Force Logistics Command, Wright-Patterson AFB, Ohio	2
AFSC, Andrews Air Force Base, Washington 25, D. C., Attn: RDRWA	1
Director, Air University Library, Maxwell AFB, Alabama	2
AFCRL, L. G. Hanscom Field, Bedford, Massachusetts Attn: CRQST-2	1
AFSWC (SWRS) Kirtland AFB, New Mexico	3
Commandant, Institute of Technology, Wright-Patterson AFB, Ohio, Attn: MCLB-ITRIDL	1
BSD, Norton AFB, California	1
Director, USAF Project RAND, Via: U. S. Air Force Liaison Office, The RAND Corporation, 1700 Main Street, Santa Monica, California	1
Director of Civil Engineering, Hq USAF, Washington 25, D. C. Attn: AFOCE	1

OTHERS	No. of Cys.
Director of Defense Research & Engineering, Washington 25, D. C. Attn: Tech. Library	1
U. S. Documents Officer, Office of the United States National Military Representative-SHAPE, APO-55, New York, N. Y.	1
Commander-in-Chief, Pacific, Fleet Post Office, San Francisco, California	1
Director, Weapons Systems Evaluation Group, OSD, Room 1880, The Pentagon, Washington 25, D. C.	1
Commandant, Armed Forces Staff College, Norfolk 11, Virginia Attn: Library	1
Commander, Field Command, DASA, Sandia Base, Albuquerque, New Mexico	1
Commander, Field Command, DASA, Sandia Base, Albuquerque, New Mexico, Attn: FCWT	1
Attn: FCTG	1
Chief, Defense Atomic Support Agency, Washington 25, D. C.	5
Commandant, Army War College, Carlisle Barracks, Pensylvania Attn: Library	1
Commandant, National War College, Washington 25, D. C. Attn: Class Rec. Library	1
Commandant, The Industrial College of the Armed Forces, Ft. McNair, Washington 25, D. C.	1
Officer-in-Charge, U. S. Naval School, Civil Engineering Corps Officers, U. S. Naval Construction Battalion, Port Hueneme, California	[illegible]
Los Alamos Scientific Laboratory, P. O. Box 1[illegible] C. Graves) New Mexico, Attn: Report Librarian	1
Administrator, National [illegible] Aeros & Space Administration 1512 H Street, N. W. Washington 25, D. C.	[illegible]
[illegible] Research Center, NASA, Langley Field, Hampton, Va. Attn: Mr. Philip Donely	1
Chief, Classified Technical Library, Technical Information Service, U. S. Atomic Energy Commission, Washington 25, D. C., Attn: Mrs. Jean O'Leary (for Dr. Paul C. Fine)	1

OTHERS CONT'D

	No. of Cys.
Chief, Classified Technical Library, Technical Information Service U. S. Atomic Energy Commission, Washington 25, D. C., Attn: Mrs. Jean O'Leary	1
Dr. Walker Bleakney, Forestal Research Center Library, Aeronautical Sciences Bldg., Princeton University Princeton, N. J., Attn: Librarian	1
Manager, Albuquerque Operations Office, U. S. Atomic Energy Commission, P. O. Box 5400, Albuquerque, New Mexico	
Dr. Robert J. Hansen, Division of Industrial Cooperation, Massachusetts Institute of Technology, 77 Massachusetts Avenue, Cambridge, Massachusetts (Send TS to [illegible] Lexington, Mass.)	1
Dr. Bruce G. Johnston [illegible] Engineering Bldg., Research Sec[illegible] Send Top Secret to this addressee) Ann Arbor, [illegible]	1
Sandia Base, Albuquerque, New Mexico Sandia C[illegible] Document Division (for Dr. M. L. Merritt)	1
[illegible]t, Eastern Experiment Station, U. S. Bureau of [illegible]ollege Park, Md., Attn: Dr. Leonard Obert [illegible]round Effects (only)	1
[illegible]athan M. Newmark, University of Illinois, Room 207, Talbot Laboratory, Urbana, Illinois (No Top Secret to this addressee)	1
Commander, ASTIA, Arlington Hall Station, Arlington 12, Virginia, Attn: TIPDR (No Top Secret or Restricted Data to this addressee)	15
Holmes & Narver, Inc., AEC Facilities Division, 849 S. Broadway Los Angeles 14, California, Attn: Mr. Frank Galbreth	1
Professor Robert V. Whitman, Massachusetts Institute of Technology, Room 1-343, Cambridge 39, Massachusetts	1
Professor J. Neils Thompson, University of Texas, Structural Mechanics Research Laboratory, Austin, Texas	1
Mr. Kenneth Kaplan, United Research Services, 1811 Trousdale Drive, Burlingame, California	1
Mr. Fred M. Sauer, Department of Physics, Stanford Research Institute, Menlo Park, California	1